TROISIEME CYCLE DE LA PHYSIQUE

EN SUISSE ROMANDE

DARK MATTER AND DARK ENERGY

Céline Boehm[1] **& Julien Lesgourgues**[1,2]

[1] LAPTH, Annecy-Le-Vieux, France

[2] Theory Division, CERN, Genève

SEMESTRE D'AUTOMNE 2008

Contents

1 Introduction: experimental evidence for dark matter and dark energy (Julien Lesgourgues) 6

1.1 FLRW model . . . 6
1.1.1 Friedmann equation . . . 6
1.1.2 From Friedmann and Lemaître to the ΛCDM model . . . 7
1.2 Curvature of light-rays in the FLRW universe . . . 8
1.2.1 Photon geodesics . . . 8
1.2.2 Redshift . . . 9
1.2.3 Hubble parameter . . . 10
1.2.4 The notion of distance to an object . . . 10
1.2.5 Angular diameter distance – redshift relation . . . 12
1.2.6 Luminosity distance – redshift relation . . . 12
1.3 Astrophysical evidence for dark matter . . . 14
1.3.1 Galaxy rotation curves . . . 14
1.3.2 Motions in galaxy clusters . . . 14
1.3.3 X-ray gas in galaxy clusters . . . 14
1.3.4 Weak lensing around galaxy clusters . . . 15
1.3.5 Microlensing . . . 15
1.4 Cosmological evidence for cold dark matter and for dark energy . . . 16
1.4.1 Cosmological parameters . . . 16
1.4.2 Expansion rate . . . 16
1.4.3 Abundance of primordial elements . . . 17
1.4.4 Age of the universe . . . 18
1.4.5 Luminosity of Type Ia supernovae . . . 19
1.4.6 CMB temperature anisotropies: overview of the theory . . . 22
1.4.7 Structure formation . . . 27
1.4.8 Difference between CDM, HDM and WDM . . . 29
1.4.9 Galaxy correlation function and Lyman-α forests . . . 30
1.4.10 Combining observations: results for dark matter . . . 32
1.4.11 Combining observations: results for dark energy . . . 33

2 Dark matter (Céline Boehm) 37

2.1 Evidence for dark matter . . . 37
2.1.1 Rotation curves of galaxies and density profile . . . 37
2.1.2 Gravitational Lensing . . . 38
2.1.3 primordial Big Bang Nucleosynthesis . . . 39
2.1.4 Silk damping and CMB observations . . . 39
2.2 Dark Matter candidates . . . 41
2.2.1 MACHOs and dark astrophysical objects . . . 41
2.2.2 Modifying gravity . . . 41
2.2.3 New type(s) of particles . . . 43
2.3 Relic density . . . 43
2.4 Exceptions to relic density calculations . . . 47
2.5 Direct detection . . . 48
2.6 Indirect detection . . . 50
2.6.1 “Bare” flux calculations . . . 50
2.6.2 Bare neutrino flux calculations . . . 53
2.6.3 Simplified cosmic ray flux calculations . . . 53
2.6.4 Experimental signatures and results . . . 54
2.7 Structure formation . . . 55
2.8 Conclusion . . . 57

3 Dark energy (Julien Lesgourgues) 58
3.1 Possible theoretical models for Dark Energy . . . 58
3.1.1 Vacuum energy . . . 58
3.1.2 Topological defects . . . 60
3.1.3 Scalar field (quintessence) . . . 61
3.1.4 Scalar field coupled to matter . . . 65
3.1.5 Modifications of gravity . . . 67
3.1.6 Non-linear structure formation . . . 68
3.2 Cosmological tests for DE models . . . 68
3.2.1 Current measurements of $\Omega_{DE}(z)$ . . . 69
3.2.2 Future measurements of $\Omega_{DE}(z)$ . . . 70
3.3 Conclusion . . . 71

1 Introduction: experimental evidence for dark matter and dark energy (Julien Lesgourgues)

1.1 FLRW model

In the standard cosmological model and at the level of background quantities (i.e., averaging over spatial fluctuations), the universe is described by the Friedmann-Lemaître-Robertson-Walker metric

$$ds^2 = dt^2 - a(t)^2 \left[\frac{dr^2}{1 - k\,r^2} + r^2 (d\theta^2 + \sin^2\theta d\varphi^2) \right] \tag{1}$$

where k is a constant related to the spatial curvature (positive for closed models, negative for open ones, zero for a flat universe) and t is the proper time measured by a free-falling observer, that we will call *cosmological time*. Throughout this course, we adopt units such that $c = \hbar = 1$. The value of the scale factor at a given time, $a(t)$, does not have an intrinsic physical meaning; it is only the *variation* of $a(t)$ which matters. It is always possible to redefine $a(t)$ by a constant factor for convenience. For instance, it is often convenient to us a normalization such that today, $a(t_0) = 1$.

1.1.1 Friedmann equation

The Einstein equation relates curvature to matter. In the case of a homogeneous, isotropic universe, described by the Friedmann metric, the Einstein equation yields the Friedmann equation, which relates the total energy density ρ to the space-time curvature: on the one hand, the spatial curvature radius $R_k \equiv a\,|k|^{-1/2}$, and on the other hand the Hubble radius $R_H \equiv H^{-1} = a/\dot{a}$. The Friedmann equation reads

$$\frac{3}{R_H^2} \pm \frac{3}{R_k^2} = 8\pi\mathcal{G}\rho \tag{2}$$

where $\mathcal{G}$ is the Newton constant. The Friedmann equation is more commonly written as

$$\left(\frac{\dot{a}}{a}\right)^2 + \frac{k}{a^2} = \frac{8\pi\mathcal{G}}{3}\rho\ . \tag{3}$$

When $k \neq 0$, it is convenient to renormalize the scale factor and the comoving coordinate r in such way that k takes the value +1 in a closed universe (instead of any positive value), or -1 in an open universe (instead of any negative value). This redefinition can be done without any loss of generality. So, for simplicity, in what follows, we will consider that k takes one of the following values: -1, 0 or +1.

The Einstein equations also lead, through Bianchi identities, to the energy conservation equation

$$\dot{\rho} = -3\frac{\dot{a}}{a}(\rho + p) \tag{4}$$

which applies to the total cosmological density ρ and pressure p (actually, this conservation equation can be derived by variation of the action for each individual homogeneous component in the universe).

Non-relativistic matter has vanishing pressure and gets diluted according to $\rho_m \propto a^{-3}$, while ultra-relativistic matter has $p_r = \frac{1}{3}\rho_r$ and follows $\rho_r \propto a^{-4}$. These dilution laws can be derived more intuitively by considering a comoving sphere of fixed comoving radius. The number of particles (ultra-relativistic or non-relativistic) is conserved inside the sphere (although non-relativistic particles are still in the comoving coordinate frame, while ultra-relativistic particles flow in and out). The individual energy $E \simeq m$ of a non-relativistic particle is independent of the expansion. Instead the energy of a photon is inversely proportional to its wavelength and is redshifted like a^{-1}. The volume of the sphere scales like a^3. Altogether these arguments lead to the above dilution laws. The curvature of the universe contributes to the expansion in the same way as an *effective curvature density*

$$\rho_k^{\mathrm{e}ff} \equiv -\frac{3}{8\pi\mathcal{G}}\frac{k}{a^2} \tag{5}$$

which scales like a^{-2}. Finally, the vacuum energy can never dilute, $\dot{\rho}_v = 0$ and $p_v = -\rho_v$. This is valid for the energy of a quantum scalar field in its fundamental state, as well as for a classical field in a state of equilibrium (its energy density density ρ_v is then given by the scalar potential $V(\varphi)$ at the equilibrium point). The vacuum energy is formally equivalent to a cosmological constant Λ which can be added to the Einstein equation without altering the covariance of the theory,

$$G^{\nu}_{\mu} + \Lambda \delta^{\nu}_{\mu} = 8\pi \mathcal{G} T^{\nu}_{\mu} \ , \tag{6}$$

with the identification $\rho_v = -p_v = \Lambda/(8\pi\mathcal{G})$. The critical density is defined for any given value of the Hubble parameter $H = \dot{a}/a$ as the total energy density that would be present in the universe if the spatial curvature was null,

$$H^2 = \frac{8\pi\mathcal{G}}{3}\rho_{crit} \ . \tag{7}$$

With such a definition, the Friedmann equation reads

$$\rho_{crit} - \rho_k^{eff} = \rho_{\rm tot} \ . \tag{8}$$

The contribution of spatial curvature to the expansion of the universe is parametrized by

$$\Omega_k \equiv \frac{\rho_k^{eff}}{\rho_{crit}} = -\frac{k}{(aH)^2} = \frac{R_H^2}{R_k^2} \ . \tag{9}$$

Whenever $|\Omega_k| \ll 1$, the universe can be seen as effectively flat. The contribution of any other component "i" to the expansion can be parametrized in the same way:

$$\Omega_i \equiv \frac{\rho_i}{\rho_{crit}} \tag{10}$$

For instance, Ω_m stands for the (non-relativistic) matter fraction, Ω_r for the (relativistic) radiation fraction, Ω_Λ for the cosmological contant fraction. Hence, after division by ρ_{crit}, the Friedmann equation gives the so-called "Universe budget equation"

$$\sum_i \Omega_i = 1 + \Omega_k \ . \tag{11}$$

In total, we have seen four instructive ways of writing the Friedmann relation, in eqs.(2), (3), (8) and (11). Finally, note that the parameter Ω_i is proportonal both to ρ_i and to H_0^{-2}, or to h^{-2} where h is the reduced Hubble parameter defined through $H_0 \equiv 100h$ km/s/Mpc. Hence, ρ_i is in turn proportional to Ω_i and h^2. Actually, the product $\Omega_i h^2$ is a very convenient way of parametrizing the physical density ρ_i, because it is a dimensionless number (in fact, it is a commonly used choice of units). In what follows, physical densities will usually be parametrized with $\omega_i \equiv \Omega_i h^2$.

1.1.2 From Friedmann and Lemaître to the ΛCDM model

Let us summarize very briefly how the current "standard cosmological model" was built step by step:

- Einstein first proposed a solution for a static universe with $R_H = 0$, based on a non-zero cosmological constant, which was proved later to be unstable. The idea of a static (or even stationary) universe was then abandoned in favor of a nearly homogeneous, isotropic, expanding universe, corresponding in first approximation to the Friedmann-Lemaître-Robertson-Walker metric. This picture was sustained by the discovery of the homogeneous expansion by Hubble in 1929.

- the minimal assumption concerning the composition of the universe is that its energy density is dominated by the components of visible objects like stars, planets and inter-galactic gas: namely, non-relativistic matter. This is the Cold Big Bang scenario, in which the Friedmann equation

$$H^2 = \frac{8\pi\mathcal{G}}{3}\rho_{\rm m} \propto a^{-3} \tag{12}$$

  describes the expansion between some initial singularity ($a \rightarrow 0$) and now, caused by non-relativistic, pressureless matter ("cold matter") at a rate $a \propto t^{2/3}$. Gamow, Zel'dovitch, Peebles and others worked on scenarios for Nucleosynthesis in the Cold Big Bang scenario, and concluded that it was ruled out by the fact that the universe contains a significant amount of hydrogen.

- the next level of complexity is to assume that a radiation component (ultra-relativistic photons and neutrinos) dominated the universe expansion at early times. Nucleosynthesis taking place during radiation domination, when $a \propto t^{1/2}$, is in agreement with observations. Structure formation started after the time of equality between radiation and matter, when $\rho_r = \rho_m$. The detection of the Cosmic microwave background by Penzias and Wilson in the late 60's beautifully confirmed this scenario called the Hot Big Bang, due to the role of ultra-relativistic matter ("hot matter") after the initial singularity.

- later, it was realized that all the non-relativistic matter cannot be formed of usual "baryonic" matter. The Dark Matter hypothesis was formulated by Zwicky in 1933 and confirmed since then in many ways. If dark matter is made of particles with a given average velocity, these particles could be deeply relativistic (Cold Dark Matter) or just slightly non-relativistic (Hot Dark Matter). It is one of the two purposes of this course to introduce the various experimental evidences available now in favor of Cold Dark Matter (CDM), and to give some hints of what it could consist of. The Hot Big Bang model completed by the presence of CDM was called the "standard Cold Dark Matter" (sCDM) model in the 80's and 90's, when it was considered as the simplest viable scenario.

- for many years, people wondered whether this scenario should be completed with a recent stage of curvature and/or vacuum domination, starting after most structure have formed. In that case the cosmological model could be of the type of Open CDM (OCDM) in the case $k < 0$, closed CDM in the case $k > 0$, or ΛCDM in the case $k = 0$, $\Lambda \neq 0$. In the 90's, there was some growing evidence that the universe would have $k < 0$ and/or $\Lambda \neq 0$. The second purpose of this course is to introduce the various reasons for which the simplest viable scenario is now thought to be ΛCDM (with $\Omega_v \equiv \rho_v/\rho_{crit} \simeq \rho_v/(\rho_v + \rho_m)$ close to 0.7) and to propose possible explanations for the origin of this cosmological constant (or more generally, of a Dark Energy component which would have roughly the same properties as a cosmological constant).

- independently of the issue of curvature and dark energy, some pioneers like Starobinsky and Guth suggested around 1979 that this scenario should be completed with a stage of early vacuum domination taking place much before Nucleosynthesis. After some time, this vacuum would decay mainly into ultra-relativistic particles, and the universe would enter into the radiation dominated phase. The large-scale quantum fluctuations of this vaccuum would remain imprinted in the metric, seeding the large-scale density perturbations that we observe today in the form of galaxies and clusters. The existence of inflation is established nowadays on a rather firm basis; inflation can be considered as the theory providing correct initial conditions to the perturbed ΛCDM model.

1.2 Curvature of light-rays in the FLRW universe

Our goal in this section is to understand the concrete consequences of the universe expansion for observers looking at the sky. Hence, we need to understand how light rays propagate in the universe.

1.2.1 Photon geodesics

Photon propagate in the vacuum at the speed of light along geodesics. Hence, over an infinitesimal time interval dt, they run over a distance $dl^2 = dt^2$ (since we use units such that $c = 1$). On macroscopic scales, the relation between distance and time is given by integrating $dl = \pm dt$ over the geodesics.

By definition, we are only interested in photons reaching us at some point, and allowing us to observe an object. Lets us consider that we are a comoving observer and choose the origin of spherical comoving coordinates to coincide with us (this choice is only made for getting simple calculations; it doesn't imply at all that we occupy some privileged point in space or anything like that). In the FLRW universe, a photon reaching us with a momentum aligned with a given direction (θ_0, ϕ_0) must have traveled along a straight line in space, starting from an unknown emission point (r_e, θ_0, ϕ_0). If its spatial trajectory was not a straight line, there would be a contradiction with the assumption of isotropy of the universe with respect to the observer. However the photon trajectory in space-time is curved, as can be checked by integrating over the infinitesimal distance between the emission point $(t_e, r_e, \theta_0, \phi_0)$ and a later point (t, r, θ_0, ϕ_0) with $t > t_e$, $r < r_e$:

$$\int_{r_1}^{r} -\frac{dr}{\sqrt{1-kr^2}} = \int_{t_e}^{t} \frac{dt}{a(t)} \tag{13}$$

On can check that this trajectory is indeed a solution of the geodesic equations, and that it corresponds to a curved trajectory in space-time: if we draw this trajectory in two-dimensional (t, r) space, we see that the slope $dr/dt = -\sqrt{1-kr^2}/a(t)$ changes along the trajectory. The photon is seen by the observer (at the origin of coordinates) at a reception time t_r which can be deduced from r_e and t_e in a given metric through the implicit relation:

$$\int_{r_e}^{0} -\frac{dr}{\sqrt{1-kr^2}} = \int_{t_e}^{t_r} \frac{dt}{a(t)} \ . \tag{14}$$

The ensemble of all points $(t_e, r_e, \theta_0, \phi_0)$ defines our past light-cone, as illustrated in figure 1.

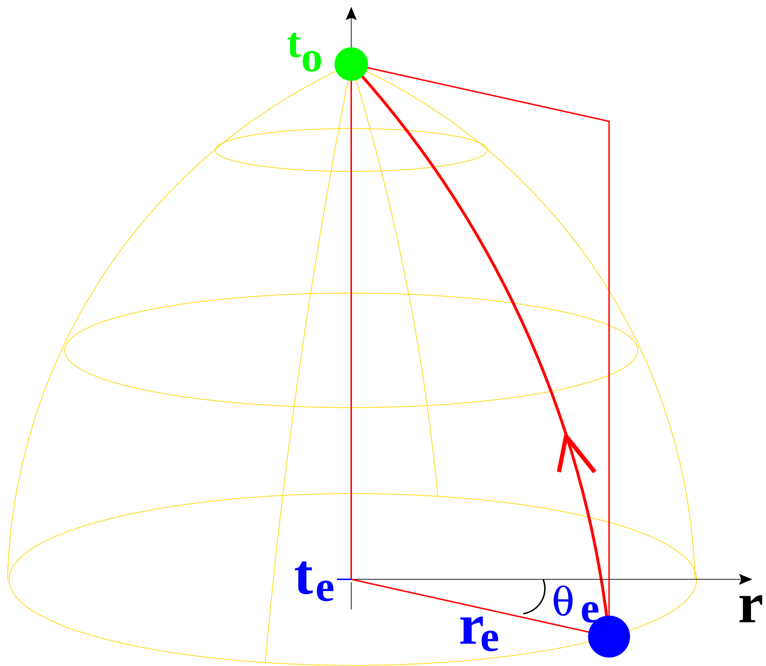

Figure 1: An illustration of the propagation of photons in our universe. The dimensions shown here are (t, r, θ): we skip ϕ for the purpose of representation. We are sitting at the origin, and at a time t_0, we can see a the light of a galaxy emitted at (t_e, r_e, θ_e). Before reaching us, the light from this galaxy has traveled over a curved trajectory. In any point, the slope dr/dt is given by equation (13). So, the relation between r_e and $(t_0 - t_e)$ depends on the spatial curvature and on the scale factor evolution. The trajectory would be a straight line in space-time only if $k = 0$ and $a = constant$, i.e., in the limit of Newtonian mechanics in Euclidean space. The ensemble of all possible photon trajectories crossing $r = 0$ at $t = t_0$ is called our "past light cone", visible here in orange. Asymptotically, near the origin, it can be approximated by a linear cone with $dl = cdt$, showing that at small distance, the physics is approximately Newtonian.

The equation (13) describing the propagation of light (more precisely, of radial incoming photons) is extremely useful - probably, one of the two most useful equations of cosmology, together with the Friedmann equation. It is on the basis of this equation that we are able today to measure the curvature of the universe, its age, its acceleration, and other fundamental quantities.

1.2.2 Redshift

First, a simple calculation based on equation (13) gives the redshift associated with a given source of light. Let's still play the role of a comoving observer sitting at the origin of coordinates. We observe a galaxy located at (r_e, θ_0, ϕ_0), emitting light at a given frequency λ_e. The corresponding wave crests are emitted by the galaxy at a frequency $\nu_e = 1/dt_e = 1/\lambda_e$. Each wave crests follows the trajectory described by Eq. (13). We see the light signal under a frequency $\nu_r = 1/dt_r = 1/\lambda_r$ such that

$$\int_{r_e}^{0} -\frac{dr}{\sqrt{1-kr^2}} = \int_{t_e}^{t_r} \frac{dt}{a(t)} = \int_{t_e+dt_e}^{t_r+dt_r} \frac{dt}{a(t)} \ . \tag{15}$$

The second equality gives:

$$\int_{t_e}^{t_e+dt_e} \frac{dt}{a(t)} = \int_{t_r}^{t_r+dt_r} \frac{dt}{a(t)} \ . \tag{16}$$

Hence in very good approximation:

$$\frac{dt_e}{a(t_e)} = \frac{dt_r}{a(t_r)}. \tag{17}$$

We infer a simple relation between the emission and reception wavelengths:

$$\frac{\lambda_r}{\lambda_e} = \frac{dt_r}{dt_e} = \frac{a(t_r)}{a(t_e)} \tag{18}$$

This result could have been easily guessed: a wavelength is a distance, subject to the same stretching as all physical distances when the scale factor increases. Hence, in the FLRW universe, redshift is given by

$$z = \frac{\Delta\lambda}{\lambda} = \frac{\lambda_r - \lambda_e}{\lambda_e} = \frac{a(t_r)}{a(t_e)} - 1 \ . \tag{19}$$

This is a crucial difference with respect to Newtonian mechanics, in which the redshift follows from the Doppler effect in the expanding universe (where typical galaxies have a bulk motion $\vec{v} = H\vec{r}$). In that case, the redshift reads $z = v/c$ (in units with $c = 1$, $z = v$) and seems to be limited to $|z| < 1$. The true GR expression doesn't have such limitations, since the ratio of the scale factors can be arbitrarily large without violating any fundamental principle. And indeed, observations do show many objects - like quasars - at redshifts of $z \sim 4$ or even bigger. We'll see later that we also observe the Cosmic Microwave Background at a redshift of approximately $z = 1100$! Note finally that in the real perturbed universe, the gravitational redshift due to the variation of the scale factor (and also possibly to that of local metric inhomogeneities) would sum up with the usual Doppler effect given by the peculiar velocity of the object.

1.2.3 Hubble parameter

Hubble's parameter was first introduced as the coefficient relating the bulk velocity of typical galaxies to their distance, in a newtonian interpretation of the Universe expansion. In the limit of small redshift, we expect to recover the Newtonian results, and to find a relation similar to $z = v = Hr$. To show this, let's assume again that t_0 is the present time, and that we are a comoving observer at $r = 0$. We want to compute the redshift of a nearby galaxy, which emitted the light that we receive today at a time $t_0 - dt$. In the limit of small dt, the equation of propagation of light shows that the physical distance L between the galaxy and us is simply

$$L \simeq dl = dt \tag{20}$$

while the redshift of the galaxy is

$$z = \frac{a(t_0)}{a(t_0 - dt)} - 1 \simeq \frac{a(t_0)}{a(t_0) - \dot{a}(t_0)dt} - 1 = \frac{1}{1 - \frac{\dot{a}(t_0)}{a(t_0)}dt} - 1 \simeq \frac{\dot{a}(t_0)}{a(t_0)}dt \ . \tag{21}$$

By combining these two relations we obtain

$$z \simeq \frac{\dot{a}(t_0)}{a(t_0)}L \ . \tag{22}$$

So, at small redshift, we recover the Hubble law, and the role of the Hubble parameter is played by $\dot{a}(t_0)/a(t_0)$. In the Friedmann universe, we will directly define the Hubble parameter as the expansion rate of the scale factor:

$$H(t) = \frac{\dot{a}(t)}{a(t)} \ . \tag{23}$$

The current value of the Hubble parameter (the one measured by Hubble himself) will be noted as H_0.

We have proved that in the FLRW universe, the proportionality between distance and velocity (or redshift) is recovered for small distances and redshifts. What happens at larger distance? This question actually raises a non-trivial problem: the definition of distances for objects which are far enough for the (Euclidean) approximation $L = dl = dt$ to become inaccurate.

1.2.4 The notion of distance to an object

Let's assume again that sitting at $(t_0, 0, 0, 0)$, we observe a remote comoving object emitting light from (t_e, r, θ, ϕ). What is the physical distance to the object? This question is ambiguous. Distances are usually measured using rules, but in the expanding universe, the rules itself do not have a fixed size, they stretch proportionally to the scale factor. Are we asking about the distance in units of today, i.e. the distance between us and the object today (if it is a comoving object, it should be at (t_0, r, θ, ϕ) now)? Then, the distance would be

$$d = \int_0^r dl = a(t_0) \int_0^r \frac{dr}{\sqrt{1 - kr^2}} \ . \tag{24}$$

Very often, the scale factor is defined in such way that $a(t_0) = 1$, and the above distance coincides with the *comoving distance* $\chi(r)$:

$$\chi(r) \equiv \int_0^r \frac{dr}{\sqrt{1 - kr^2}} \ , \tag{25}$$

which can be integrated to

$$\chi(r) = \begin{cases} \sin^{-1}(r) & \text{if} \quad k = 1, \\ r & \text{if} \quad k = 0, \\ \sinh^{-1}(r) & \text{if} \quad k = -1. \end{cases} \tag{26}$$

Hence, it is useful to define

$$f_k(x) \equiv \begin{cases} \sin(x) & \text{if} \quad k = 1, \\ x & \text{if} \quad k = 0, \\ \sinh(x) & \text{if} \quad k = -1, \end{cases} \tag{27}$$

so that $r = f_k(\chi)$.

Comoving distances are well-defined quantities, used by observers in many circumstances. They do not depend on time: two comoving objects are always separated by the same comoving distance, regardless of the universe expansion. However, this is a rather artificial definition, since we can't see the object today - it might even have disappeared. Anyway, instead of arguing about the definition of distance, we should concentrate on the various ways to probe it experimentally, and derive the corresponding phenomenological quantities.

In astrophysics, distances are usually measured in three ways:

- *From the redshift.* In principle the observed redshift measures the ratio $a(t_r)/a(t_e)$ plus corrections due to the local effects of small-scale inhomogeneities (peculiar motion of the object, local gravitational potential). On very large distances, we could neglect the impact of inhomogeneities and assume in first approximation that the observed redshift is really equal to $a(t_r)/a(t_e) - 1$. Then, if we know precisely the evolution of the function $a(t)$, we can identify the time t_e and infer the comoving coordinate r_e through Eq. (14). Finally, if k is also known, we can use the above definition of comoving distance. This method is (in first approximation) the one used by observers trying to infer the spatial distribution of galaxies from *galaxy redshift surveys*. The distance reported in pictures showing the distribution of galaxies in slices of our universe is obtained in that way. However, it assumes a very good knowledge of k and of the function $a(t)$. In many cases, these quantities are precisely what one would like to measure.

- *From the angular diameter of standard rulers.* Surprisingly, there exist a few objects in astrophysics and cosmology which physical size can be known in advance, given some physical properties of these objects. They are called *standard rulers*. In the next chapters we will introduce one example of standard ruler: the sound horizon at decoupling, "observed" in CMB anisotropies. In Euclidean space, the distance to an object can be inferred from its physical size dl and angular diameter $d\theta$ through $d = dl/d\theta$. In FLRW cosmology, although the geometry is not Euclidean, we will adopt exactly this relation as one of the possible definitions of distance. The corresponding quantity is called the angular diameter distance d_A,

$$d_A \equiv \frac{dl}{d\theta} . \tag{28}$$

  In Euclidean space, d_A would be proportional to the usual Euclidean distance to the object and therefore to its redshift. In the FLRW universe, the relation between the angular diameter distance and the redshift is non-trivial and depends on the spacetime curvature, as we shall see in the next subsection.

- *From the luminosity of standard candles.* There exist also objects called *standard candles* for which the absolute luminosity (i.e. the total luminous flux emitted per unit of time) can be estimated independently of its distance and apparent luminosity (for instance, variable stars called cepheids, for which the luminosity can be inferred from the period; they were used by Hubble for proving the Universe expansion). In Euclidean space, the distance could be inferred from the absolute luminosity L and apparent one l through $l = L/(4\pi d^2)$. In cosmology, although the geometry is not Euclidean, we will adopt exactly this relation as one of the possible definitions of distance. The corresponding quantity is called the luminosity distance d_L,

$$d_L \equiv \sqrt{\frac{L}{4\pi l}} . \tag{29}$$

  In Euclidean space, d_L would be again proportional to the usual Euclidean distance to the object and therefore to its redshift, while in the FLRW universe the relation between the luminosity distance and the redshift is as subtle as for the angular diameter distance.

1.2.5 Angular diameter distance – redshift relation

Recalling that in Euclidean space with Newtonian gravity and homogeneous (linear) expansion, one has $z = v$ and $v = Hd$, we easily find a trivial angular diameter distance – redshift relation:

$$d_L = z/H. \tag{30}$$

In General Relativity, because of the bending of light-rays by gravity, the steps of the calculation are different. Using the FLRW metric, we see that the physical size dl of an object orthogonal to the line of sight is related to its angular diameter $d\theta$ through

$$dl = a(t_e)\; r_e\; d\theta \tag{31}$$

where t_e is the time at which the galaxy emitted the light ray that we observe today on Earth, and r_e is the comoving coordinate of the object. Hence

$$d_A = a(t_e)\; r_e = a(t_0)\frac{r_e}{1+z_e}\;. \tag{32}$$

The equation of motion of photons gives a relation between r_e and t_e:

$$\int_{r_e}^{0} \frac{-dr}{\sqrt{1-kr^2}} = \int_{t_e}^{t_0} \frac{dt}{a(t)} = \chi(r_e)\;. \tag{33}$$

where t_0 is the time today. So, the relation between r_e and t_e depends on $a(t)$ and k. If we knew the function $a(t)$ and the value of k, we could integrate (33) explicitly and obtain some function $r_e(t_e)$. We would also know the relation $t_e(z)$ between redshift and time of emission. So, we could obtain a relation of the type $d_A = a(t_0)r_e(z)/(1+z)$. This relation is called the angular diameter distance – redshift relation.

In fact, we can write this relation explicitely by making use of Eqs. (25) - (27):

$$\begin{aligned} d_A &= \frac{a(t_0)}{1+z_e}\; f_k(\chi) && (34)\\ &= \frac{a(t_0)}{1+z_e}\; f_k\left(\int_{t_e}^{t_0}\frac{dt}{a(t)}\right) && (35)\end{aligned}$$

Using $H = \frac{da}{a\,dt}$, we can also write this result as:

$$d_A = \frac{a(t_0)}{1+z_e}\; f_k\left(\int_{a_e}^{a_0}\frac{da}{a^2 H(a)}\right) \tag{36}$$

Finally, using $z = [a(t_0)/a(t_e) - 1]$ and hence $dz = -a(t_0)da/a^2$, we can also reformulate the angular diameter distance as:

$$d_A = \frac{a(t_0)}{1+z_e}\; f_k\left(\int_{0}^{z_e}\frac{dz}{a(t_0)H(z)}\right) \tag{37}$$

A generic consequence is that in the Friedmann universe, for an object of fixed size and redshift, the angular diameter depends on the curvature - as illustrated graphically in figure 2. Therefore, if we know in advance the physical size of an object, we can simply measure its redshift, its angular diameter, and immediately obtain some informations on the geometry of the universe.

1.2.6 Luminosity distance – redshift relation

In absence of expansion and curvature, d_L would simply correspond to the Euclidean distance to the source. On the other hand, in general relativity, it is easy to understand that the apparent luminosity is given by

$$l = \frac{L}{4\pi\, a^2(t_0)\, r_e^2 (1+z_e)^2} \tag{38}$$

leading to

$$d_L = a(t_0)\, r_e (1+z_e)\;. \tag{39}$$

Let us explain this result. First, the reason for the presence of the factor $[4\pi\, a^2(t_0)\, r_e^2]$ in equation (38) is obvious. The photons emitted at a comoving coordinate r_e are distributed today on a sphere of comoving

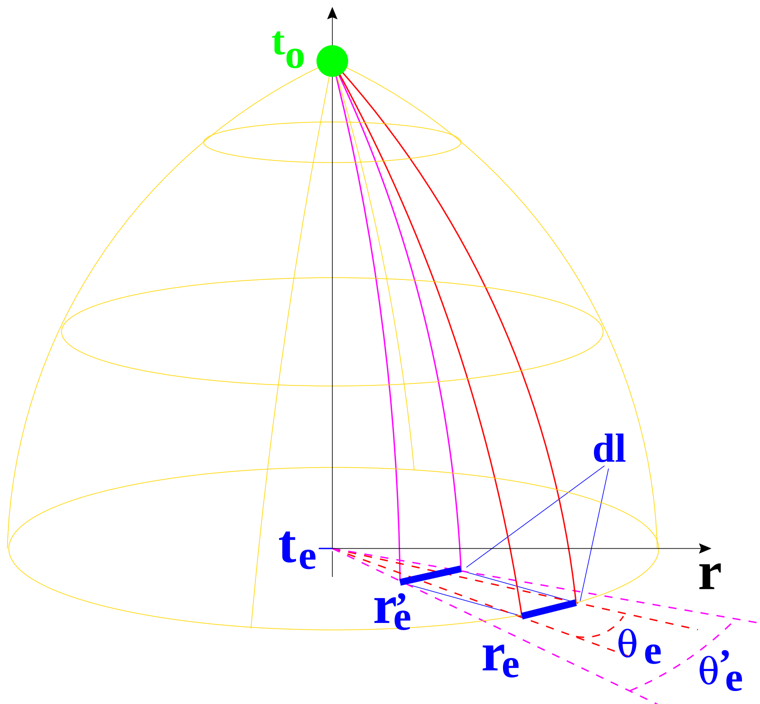

Figure 2: Angular diameter – redshift relation. We consider an object of fixed size dl and fixed redshift, sending a light signal at time t_e that we receive at present time t_0. All photons travel by definition with θ =constant. However, the bending of their trajectories in the (t, r) plane depends on the spatial curvature and on the scale factor evolution. So, for fixed t_e, the comoving coordinate of the object, r_e, depends on curvature. The red lines are supposed to illustrate the trajectory of light in a flat universe with $k = 0$. If we keep dl, $a(t)$ and t_e fixed, but choose a positive value $k > 0$, we know from equation (33) that the new coordinate $r_e{}'$ has to be smaller. But dl is fixed, so the new angle $d\theta'$ has to be bigger, as easily seen on the figure for the purple lines. So, in a closed universe, objects are seen under a larger angle. Conversely, in an open universe, they are seen under a smaller angle.

radius r_e surrounding the source. According to the FLRW metric, the physical surface of this sphere is obtained by integrating over the infinitesimal surface element $dS^2 = a^2(t_0)\, r_e^2 \sin\theta\, d\theta\, d\phi$, which gives precisely $4\pi\, a^2(t_0)\, r_e^2$. In addition, we should keep in mind that L is a flux (i.e., an energy by unit of time) and l a flux density (energy per unit of time and surface). But the energy carried by each photon is inversely proportional to its physical wavelength, and therefore to $a(t)$. This implies that the energy of each photon has been divided by $(1+z)$ between the time of emission and now, and explains one of the two factors $(1+z)$ in (38). The other factor comes from the change in the rate at which photons are emitted and received (we have already seen in section 1.2.2 that since λ scales like $(1+z)$, both the energy and the frequence scale like $(1+z)^{-1}$).

By comparing expressions (32) and (39), we see that the luminosity distance is equal to the angular diameter distance multiplied by $(1+z_e)$. So, using the result obtained in eq. (37):

$$d_L = a(t_0)(1+z_e)\ f_k \left(\int_0^{z_e} \frac{dz}{a(t_0)H(z)} \right) \tag{40}$$

If for several objects we can measure independently the absolute luminosity, the apparent luminosity and the redshift, we can plot a luminosity distance versus redshift diagram.

In the limit $z \longrightarrow 0$, the three definition of distances given in the past sections (namely: $a(t_0)\chi$, d_A and d_L) are all equal and reduce to the usual definition of distance d in Euclidean space, related to the redshift through $d = z/H_0$. Hence, the measurement of $d_A(z)$ and $d_L(z)$ at small redshift does not bring new information with respect to a Hubble diagram (i.e., it only allows to measure one number H_0), while measurements at high redshift depend on the spatial curvature and the dynamics of expansion. We will see in the next chapter that $d_L(z)$ has been measured for many supernovae of type Ia till roughly $z \sim 2$, leading to one of the most intriguing discovery of the past years.

1.3 Astrophysical evidence for dark matter

1.3.1 Galaxy rotation curves

Inside galaxies, the stars orbit around the center. If we can measure the redshift in different points inside a given galaxy, we can reconstruct the distribution of velocity $v(r)$ as a function of the distance r to the center. It is also possible to measure the distribution of luminosity $I(r)$ in the same galaxy. What is not directly observable is the mass distribution $\rho(r)$. However, it is reasonable to assume that the mass distribution of the *observed luminous matter* is proportional to the luminosity distribution: $\rho_{\rm lum}(r) = b\ I(r)$, where b is an unknown coefficient of proportionality called the bias. From this, we can compute the gravitational potential Φ and the corresponding orbital velocity given by ordinary Newtonian mechanics (Poisson equation and fondamental law of dynamics):

$$\Delta\Phi(r) = \frac{1}{r^2}\frac{\partial}{\partial r}\left(r^2\frac{\partial}{\partial r}\Phi\right) = 4\pi\mathcal{G}\ \rho(r), \tag{41}$$

$$\frac{v^2(r)}{r} = \frac{\partial}{\partial r}\Phi(r). \tag{42}$$

So, assuming that $\rho_{\rm lum}(r) = \rho(r)$, $v(r)$ is known up to an arbitrary normalization factor $\sqrt{b}$. The fact that the total density of the galaxy is finite means that beyond the radius of the object, the total mass inside this radius $M(r) = \int dx^3\rho(\mathbf{x}) = 4\pi\int r^2 dr\rho(r)$ goes to a constant; hence $\rho(r)$ must decreases faster than r^{-3} above this radius. For $\rho \propto r^{-3}$, one would get $\Phi \propto r^{-1}$ and $v \propto r^{-1/2}$: this is the famous Keplerian decrease of orbital velocities. Using the above equations it is even trivial to express v as a function of the mass contained in the radius r:

$$v^2 = \frac{GM(r)}{r}\ . \tag{43}$$

In practise, the velocity and luminosity distribution has been measured for many galaxies (typical velocities are of the order of a few hundreds of kilometer per second). However, even by varying b, it is impossible to obtain a rough agreement between the velocity $v(r)$ infered from redshift, and the luminous velocity $v_{\rm lum}(r)$ infered from the luminosity distribution using the above equations (see the sketchy figure 2.3). The stars rotate faster than expected at large radius. Beyond the optical radius, the velocity tend to remain constant instead of obeying to a Keplerian decrease. The conclusion is that either the laws of Newtonian gravitation (and of general relativity) do not apply to galaxies; or that there is some non–luminous matter, which deepens the potential well of the galaxy.

1.3.2 Motions in galaxy clusters

Approximately 30% of galaxies are found in groups (10-100 galaxies) and clusters (100-10000 galaxies). In these objects (let's call all of them clusters) the motions are more complicated than in a galaxy: since objects do not follow nearly circular orbits, the relation (43) does not apply to individual objects, but one can derive a statistical version of it. Indeed, if the radius r containts N objects labeled with their velocity v_i and distance to the center r_i, summing up to a mass $M(r)$, it is possible to show that the velocity dispersion obeys to

$$\langle v_i^2\rangle = GM(r)\langle 1/r_i\rangle\ . \tag{44}$$

If a cluster is observed with good resolution, individual position and redshift give r_i, and the velocity dispersion can be infered from the redshift dispersion. The shape of the mass function $M(r)$ can be obtained e.g. by assuming a common light-to-mass bias b for all galaxies and measuring their individual luminosity (there are other techniques which will not be described here).

Such studies lead to the same conclusion than for galaxy rotation curves: the velocity dispersion does not decrease as expected for distances comparable to the the radius of the cluster, suggesting that most of the cluster mass comes from a smooth dark matter distribution, forming a dark halo bigger than the observable part of the cluster. This argument led Zwicky to formulate the hypothesis of dark matter in for the first time in 1933, based on observations of the Coma cluster. Similar conclusions hold for most clusters studied so far.

1.3.3 X-ray gas in galaxy clusters

In many clusters of galaxy, it is possible to observe in the X-ray band a distribution of hot gas which seems to be in hydrodynamical equilibrium. For this gas, one can derive a relation analogous to eq. (43), altough

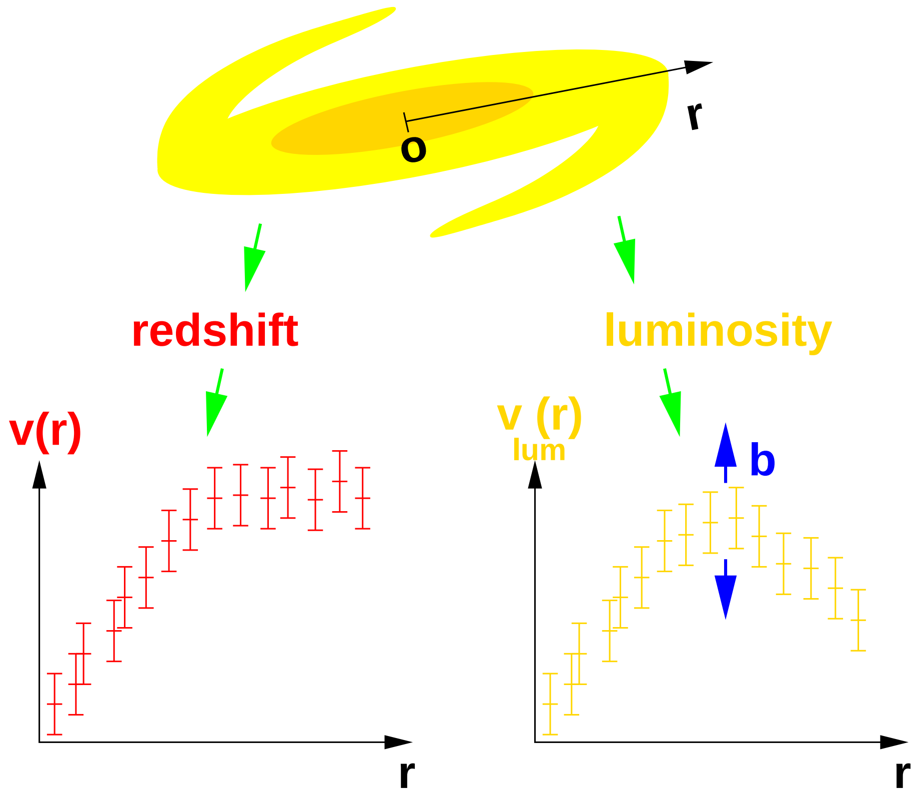

Figure 3: A sketchy view of the galaxy rotation curve issue. The genuine orbital velocity of the stars is measured directly from the redshift. From the luminosity distribution, we can reconstruct the orbital velocity under the assumption that all the mass in the galaxy arises form of the observed luminous matter. Even by varying the unknown normalization parameter b, it is impossible to obtain an agreement between the two curves: their shapes are different, with the reconstructed velocity decreasing faster with r than the genuine velocity. So, there has to be some non–luminous matter around, deepening the potential well of the galaxy.

it relates the temperature distribution $T(r)$ to the mass distribution $\rho(r)$ (i.e., the gas temperature now plays the role of the galaxy velocity dispersion). Again, observations strongly suggest a mismatch between the density reconstructed from the luminosity function and that obtained from $T(r)$, suggesting that most of the cluster mass is in the form of a dark component. This method provide accurate estimates of the visible-to-total mass ratio inside clusters, which is roughly of the order of 10%.

1.3.4 Weak lensing around galaxy clusters

The total mass distribution of a cluster can be estimated from the average deformation of source galaxies located far behind the cluster. In the 90's this techniques has been used to derive estimates of the total mass of the cluster, again found to be much bigger than the plausible mass of observed galaxies and gas. In the last decades, these observation have improved a lot and lead to a rather detailed mapping of the mass distribution, proving this existence of very extended dark halos around visible clusters.

1.3.5 Microlensing

The four types of observations described above suggest the existence of a dark matter component, which just needs to be non-luminous. At this stage, dark matter could still be made of baryons. In the 90's, people studied very seriously the hypothesis of Massive Astrophysical Compact Halo Objects (MACHO's) with mass smaller than the sun mass, and tried to detect them with microlensing. The idea is to monitor the luminosity of a large number of distant stars in the Milky Way, and to detect a possible light variation (over a few days) caused by the travel of a lens close to the line-of-sight. Such events can indeed be observed, possibly due to white dwarfs or small black holes; however, the experiment EROS has proved that MACHOs in the range $10^{-6} < M/M_{\rm sun} < 10$ can only account for a negligible fraction of the halo. Actually, we will see that cosmological observations described in the next section do require non-interacting, non-baryonic dark matter, which is not expected to form small compact objects such as MACHOs.

1.4 Cosmological evidence for cold dark matter and for dark energy

1.4.1 Cosmological parameters

According to the previous section, it is reasonable to assume that the cosmological scenario can be parametrized by:

- the total matter density ω_m and the baryon density ω_b (the dark matter density is then given by $\omega_d = \omega_m - \omega_b$).
- a possible cosmological constant density fraction Ω_Λ and spatial curvature density fraction Ω_k.

The total radiation density is not a free parameter, since the photon density is fixed by the CMB temperature today:

$$
\begin{aligned}
\omega_\gamma &\equiv \Omega_\gamma h^2 \\
&= \frac{\bar{\rho}_\gamma^0}{\bar{\rho}_c^0} h^2 \\
&= \left(\frac{\pi^2}{15} T_0^4\right) \left(\frac{8\pi G}{3H_0^2}\right) h^2 \\
&= \frac{8\pi^3 T_0^4}{45 (H_0/h)^2 M_P^2} \, .
\end{aligned} \tag{45}
$$

In addition, a study of thermodynamical and chemical equilibrium in the early universe shows that when the unverse density is smaller than approximately $(1\mathrm{MeV})^4$, the neutrino density relative to that of photons is fixed by

$$
\omega_\nu = 3 \times \frac{7}{8} \times \left(\frac{4}{11}\right)^{4/3} \omega_\gamma \tag{46}
$$

(it is much beyond the scope of this course to show this). In total the radiation density is equal to

$$
\begin{aligned}
\omega_r &\equiv \omega_\gamma + \omega_\nu \\
&= \left[\frac{\pi^2}{15} T_0^4 + 3 \times \frac{7}{8} \times \frac{\pi^2}{15} T_{\nu 0}^4\right] \left(\frac{8\pi G}{3H_0^2}\right) h^2 \\
&= \left[1 + 3 \times \frac{7}{8} \times \left(\frac{4}{11}\right)^{4/3}\right] \omega_\gamma \\
&\sim 4 \times 10^{-5} \qquad \text{for} \;\; T_0 = 2.726 \text{ K} \, .
\end{aligned} \tag{47}
$$

This model is usually called ΛCDM, since besides baryons and radiation it contains two major ingredients: cold dark matter (CDM) and a cosmological constant Λ. The questions to address now are: is this ΛCDM model able to explain all cosmological observations? If yes, does the data provide a measurement of all the above parameters? If not, what kind of new physical ingredient is needed? We will review here the main cosmological observations and their implications for cosmological parameters. The order of the next sections corresponds more or less to the order in which each observations started to play a crucial role for measuring cosmological parameters over the last twenty years.

1.4.2 Expansion rate

The expansion rate today (i.e., the Hubble parameter $H_0 = 100\, h$ km/s/Mpc) is measured with diagrams of the same type as the one obtained by Hubble in the 1920's. For various standard candles like cepheids and Type IA Supernovae, astronomers measure the redshift and the distance. These objects should be located not too far from us ($z \leq 0.1$), so that the notion of distance coincides with the usual one in euclidian space: for $z \leq 0.1$, corrections from general relavity (spatial curvature, universe expansion) remain subdominant. The distance is inferred from the comparision between the apparent and absolute luminosity (using the period of the cepheid or the extinction time of supernovae): $d = d_L = \sqrt{L/(4\pi l)}$). In a diagram of z versus d with $z \leq 0.1$, the slope corresponds to H_0/c. The most precise experiment of this type (Hubble Space Key Project) gives $H_0 = 72 \pm 8$ km/s/Mpc, i.e. $h = 0.72 \pm 0.08$ (see figure 4).

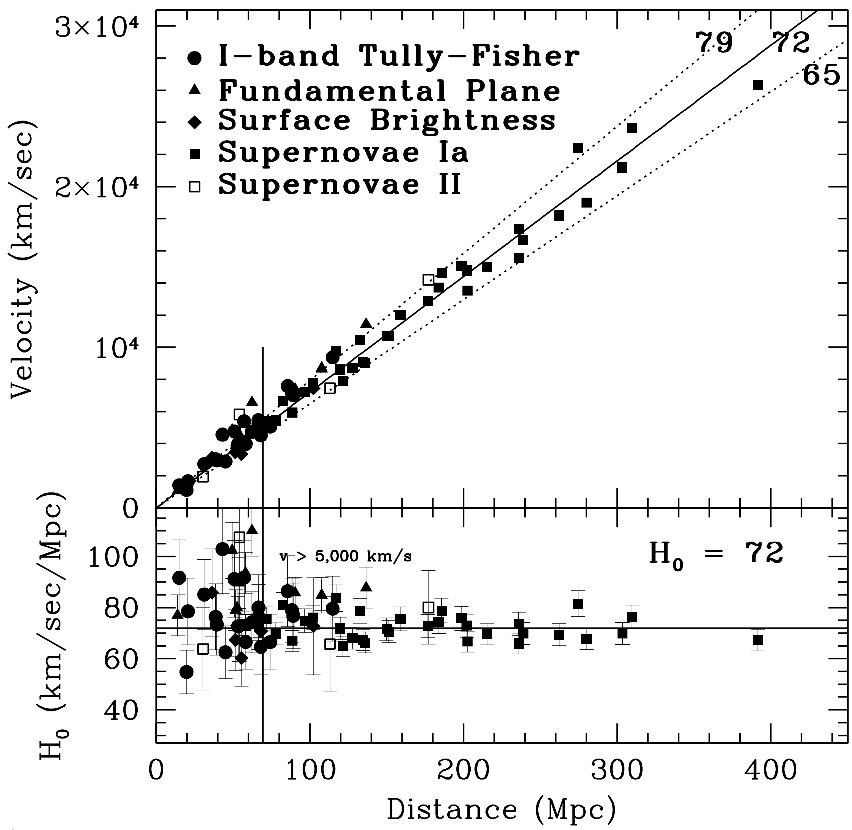

Figure 4: *(Top)* A modern Hubble diagram. The axes correspond to the distance in Mpc, and the velocity $v = z/c$ in km/s. The slope of the curve gives the coefficient H_0 in km/s/Mpc. Note that the distances go up to 400 Mpc in this diagram, while the original diagram published by Hubble reached 2 Mpc only. The velocities reach 3×10^4 km/s, which corresponds to $z = 0.1$.*(Bottom)* corresponding estimate of H_0 for each object. *Plot taken from Astrophys.J. 553 (2001) 47-72 [astro-ph/0012376] by the HST Collaboration (W.L. Freedman et al.).*

1.4.3 Abundance of primordial elements

The theory of nucleosynthesis can predict the abundance of light elements formed in the early universe, when the energy density was of order $\rho \sim (1\,\mathrm{MeV})^4$ and all weak interactions froze out. After nucleosynthesis, there are no more nuclear reactions in the universe, excepted in the core of stars. So, today, in regions of the universe which were never filled by matter ejected from stars, the proportion of light elements is still the same as it was just after nucleosynthesis. Fortunately, the universe contains clouds of gas fullfilling this criteria, and the abundance of deuterium, helium, etc. can be measured in such regions (e.g. by spectroscopy). The results can be directly compared with theoretical predictions.

Numerical simulation of nucleosynthesis accurately predict all relative abundances as a function of the only free parameter in the theory, the baryon density (which fixes the freeze-out temperature of important interactions). Figure 5 shows the dependence of the abundance of ^{4}He, D, ^{3}He and ^{7}Li as a function of $\eta_b \equiv 5.5 \times 10^{-10}(\omega_b/0.020)$.

Current observations (mainly of ^{4}He and D) show that

$$\omega_b \equiv \Omega_b h^2 = 0.020 \pm 0.002. \tag{48}$$

Hence, for $h = 0.7$, the baryon fraction is of the order of $\Omega_b \sim 0.04$: approximately four percent of the universe density is due to ordinary matter. This is already more than the sum of all luminous matter, which represents one per cent: so, 75% of ordinary matter is not even visible.

Note that if ω_r was a free parameter, the outcome of nucleosynthesis would also depend crucially on ω_r. So, nucleosynthesis can also be used as a tool for testing the fact that Eq. (47) is correct. It turns out to be the case: primordial element abundances provide a measurement of ω_r precise at the 10% level, and perfectly compatible with Eq. (47).

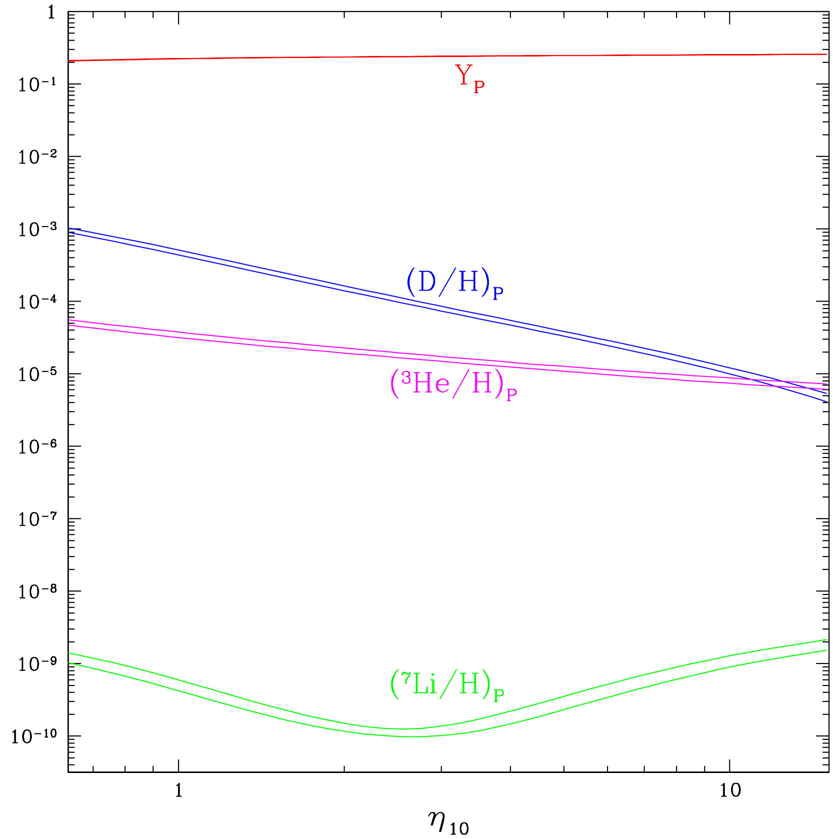

Figure 5: The nucleosynthesis-predicted primordial abundances of D, ^{3}He, ^{7}Li (relative to hydrogen by number), and the ^{4}He mass fraction (Y_P), as functions of the baryon abundance parameter $\eta_{10} \equiv 10^{10}\eta_b$. The widths of the bands reflect the uncertainties in the nuclear and weak interaction rates. *Plot taken from Int.J.Mod.Phys. E15 (2006) 1-36 [arXiv:astro-ph/0511534v1] by Gary Steigman.*

1.4.4 Age of the universe

The age of the universe can be conveniently computed once the function $H(a)/H_0$ or $H(z)/H_0$ is known. This function follows from the Friedmann equation divided by H_0^2:

$$\begin{aligned}\frac{H^2}{H_0^2} &= \frac{\bar\rho_{tot}}{\bar\rho_c} - \frac{k}{a^2 H_0^2} \\ &= \Omega_r\left(\frac{a_0}{a}\right)^4 + \Omega_m\left(\frac{a_0}{a}\right)^3 - \Omega_k\left(\frac{a_0}{a}\right)^2 + \Omega_\Lambda \qquad (49) \\ &= \Omega_r(1+z)^4 + \Omega_m(1+z)^3 - \Omega_k(1+z)^2 + \Omega_\Lambda\ , \qquad (50)\end{aligned}$$

with the constraint that $\Omega_r + \Omega_m - \Omega_k + \Omega_\Lambda = 1$ by construction. Since $H = da/(adt)$, we can write:

$$dt = \frac{da}{aH} = -\frac{dz}{(1+z)H}\ . \qquad (51)$$

Hence, the age of the universe can be computed from the integral

$$t = \int_0^{a_0} \frac{da}{aH} = H_0^{-1}\int_0^{a_0}\frac{da}{a}\left(\frac{H_0}{H(a)}\right)\ , \qquad (52)$$

or equivalently from

$$t = \int_0^{\infty}\frac{dz}{(1+z)H} = H_0^{-1}\int_0^{\infty}\frac{dz}{1+z}\left(\frac{H_0}{H(z)}\right)\ . \qquad (53)$$

This integral converges with respect to the boundary corresponding to the initial singularity, $a \longrightarrow 0$ or $z \longrightarrow \infty$. Actually, it is easy to show that the radiation dominated period gives a negligible contribution to the age of the universe, hence the term proportional to Ω_r can be omitted in the integral. If the universe is matter-dominated today ($\Omega_\Lambda = \Omega_k = 0$), then $\Omega_m = 1$ and the age of the universe is simply given by:

$$t = H_0^{-1} \int_0^\infty dz\, (1+z)^{-5/2} = \frac{2}{3H_0} = 6.52 h^{-1}\text{Gyr} \;, \tag{54}$$

where 1 Gyr $\equiv$ 1 billion years. If $\Omega_\Lambda > 0$ and/or $\Omega_k < 0$ (open universe), the ratio $H(z)/H_0$ decreases with respect to the $\Omega_\Lambda = \Omega_k = 0$ case for all values of z corresponding to Λ or curvature domination. For $\Omega_k > 0$ (closed universe), it increases. Hence, the age of the universe increases with respect to $6.52h^{-1}$Gyr if $\Omega_\Lambda > 0$ and/or $\Omega_k < 0$, and decreases if $\Omega_k > 0$.

The age of of a few specific object in the universe can be evaluated with a number of techniques, e.g. by nucleochronology (studying the radioactive decay of isotopes inside an object, exactly like in the ^{14}C method used in archeology); or by measuring the cooling of stars in their final state, called "white dwarfs", and comparing with the mean evolution curve of white dwarfs; etc. If the age of an object is found to be extremely large, it provides a lower bound on the age of the universe itself. Current observations can set a reliable lower bound on the age of the universe: $t >$ 11Gyr. This is incompatible with the matter-dominated universe of Eq. (54) unless $h < 0.59$, while observations of the Hubble flow prefer $h \sim 0.7$. Hence, these observations provide a strong hint that that the universe is either open or Λ–dominated today. This "age problem" was already known in the 90's.

1.4.5 Luminosity of Type Ia supernovae

The evidence for a non–flat universe and/or a non–zero cosmological constant has increased considerably in 1998, when two independent groups studied the apparent luminosity of distant type Ia supernovae (SNIa). For this type of supernovae, astronomers believe that there is a simple relation between the absolute magnitude and the luminosity decay rate. In other words, by studying the rise and fall of the luminosity curve during a few weeks, one can deduce the absolute magnitude of a given SNIa. Therefore, it can be used in the same way as cepheids, as a probe of the luminosity distance – redshift relation. In addition, supernovae are much brighter that cepheids, and can be observed at much larger distances (until redshifts of order one or two). While observable cepheids only probe short distances, where the luminosity distance – redshift relation only gives the Hubble law (the proportionality between distance and redshift), the most distant observable SNIa's are in the region where general relativity corrections are important: so, they can provide a measurement of the scale factor evolution (see section 1.2.2).

In a ΛCDM Universe with possible spatial curvature, the luminosity distance is given by a combination of equations (40) and (50):

$$\begin{aligned} d_L(z) &= a(t_0)(1+z)\; f_k \left(\int_0^z \frac{dz}{a(t_0)H_0} \frac{H_0}{H(z)} \right) & (55)\\ &= a(t_0)(1+z)\; f_k \left(\int_0^z \frac{dz}{a(t_0)H_0} \left[\Omega_r\,(1+z)^4 + \Omega_m\,(1+z)^3 - \Omega_k\,(1+z)^2 + \Omega_\Lambda \right]^{-1/2} \right) & (56)\end{aligned}$$

Redshifts of interest here correspond to times at which the radiation component was subdominent (a long time after matter/radiation equality), so the above expression can be simplified neglecting the radiation term, and using the relation $\Omega_m + \Omega_\Lambda = 1 - \Omega_k$:

$$d_L(z) = a(t_0)(1+z)\; f_k \left(\int_0^z \frac{dz}{a(t_0)H_0} \left[\Omega_m\,(1+z)^3 + (\Omega_m + \Omega_\Lambda - 1)\,(1+z)^2 + \Omega_\Lambda \right]^{-1/2} \right) \tag{57}$$

A detailed numerical investigation of this equation would show that this function is very sensitive to variations of $\Omega_m - \Omega_\Lambda$, and not very sensitive to variations of $\Omega_m + \Omega_\Lambda$.

On figure 6, the various curves represent the effective magnitude–redshift relation, computed for various choices of Ω_M and Ω_Λ. The effective magnitude m_B plotted here is essentially equivalent to the luminosity distance d_L, since it is proportional to $\log[d_L]$ plus a constant. For a given value of H_0, all the curves are asymptotically equal at short distance. Significant differences show up only at redshifts $z > 0.2$. Each red data point corresponds to a single supernovae in the first precise data set: that of the "Supernovae Cosmology Project", released in 1998. Even if it is not very clear visually from the figure, a detailed statistical analysis of this data revealed that a flat matter–dominated universe (with $\Omega_m = 1$, $\Omega_\Lambda = 0$) was excluded. This result has been confirmed by various more recent data sets. The top panel of figure 7 shows the luminosity distance – redshift diagram for the SNLS data set released in 2005. The corresponding constraints on Ω_m and Ω_Λ are displayed in Figure 8, and summarized by:

$$(\Omega_m - \Omega_\Lambda, \Omega_m + \Omega_\Lambda) = (-0.49 \pm 0.12, 1.11 \pm 0.52) \;. \tag{58}$$

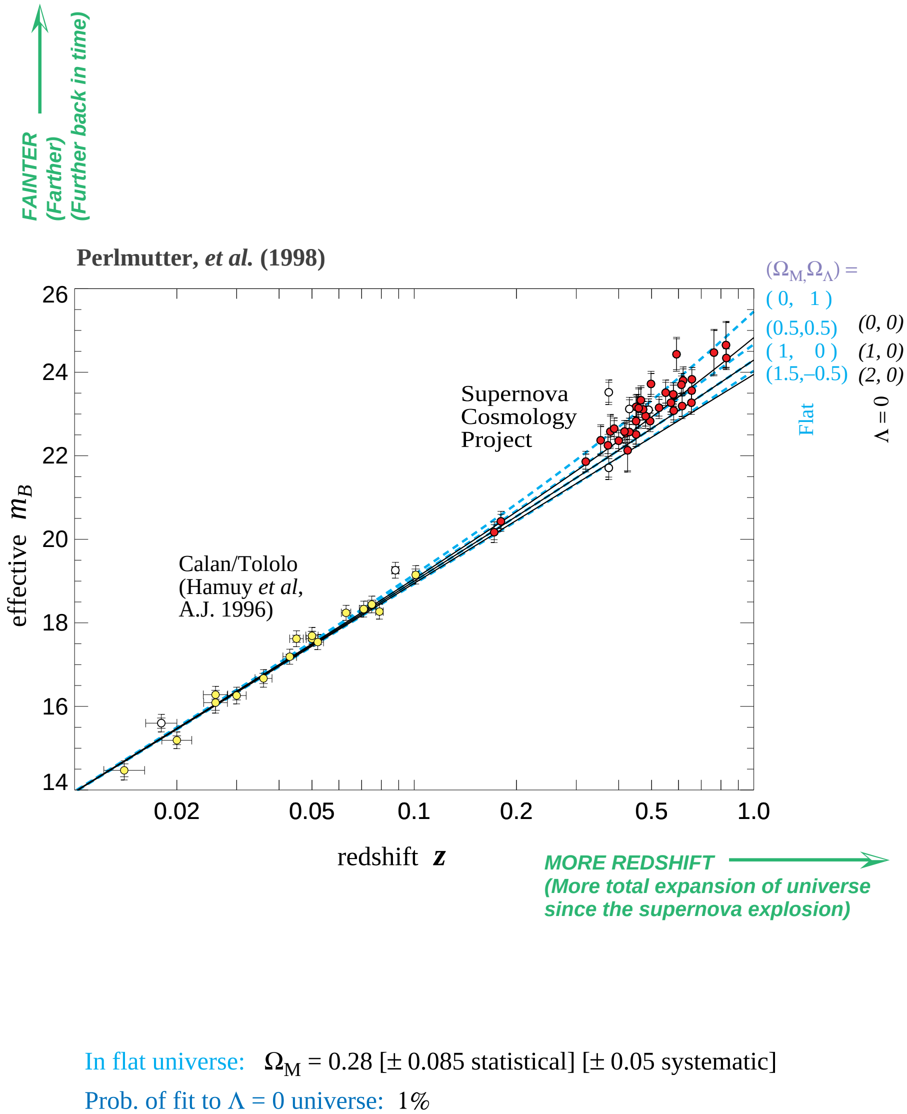

Figure 6: The results published by the "Supernovae Cosmology Project" in 1998 (see Perlmutter et al., Astrophys.J. 517 (1999) 565-586). The various curves represent the effective magnitude–redshift relation, computed for various choices of Ω_m and Ω_Λ. This plot is equivalent to a luminosity distance – redshift relation (effective magnitude and luminosity distance can be related in a straightforward way: $m_B \propto (\log[d_L] + \text{cst})$). The solid black curves account for three examples of a closed/flat/open universe with no cosmological constant. The dashed blue curves correspond to three spatially flat universes with different values of Ω_Λ. For a given value of H_0, all the curves are asymptotically equal at short distance, probing only the Hubble law. The yellow points are short–distance SNIa's: we can check that they are approximately aligned. The red points, at redshifts between 0.2 and 0.9, show that distant supernovae are too faint to be compatible with a flat matter–dominated universe $(\Omega_m, \Omega_\Lambda)$ =(1,0).

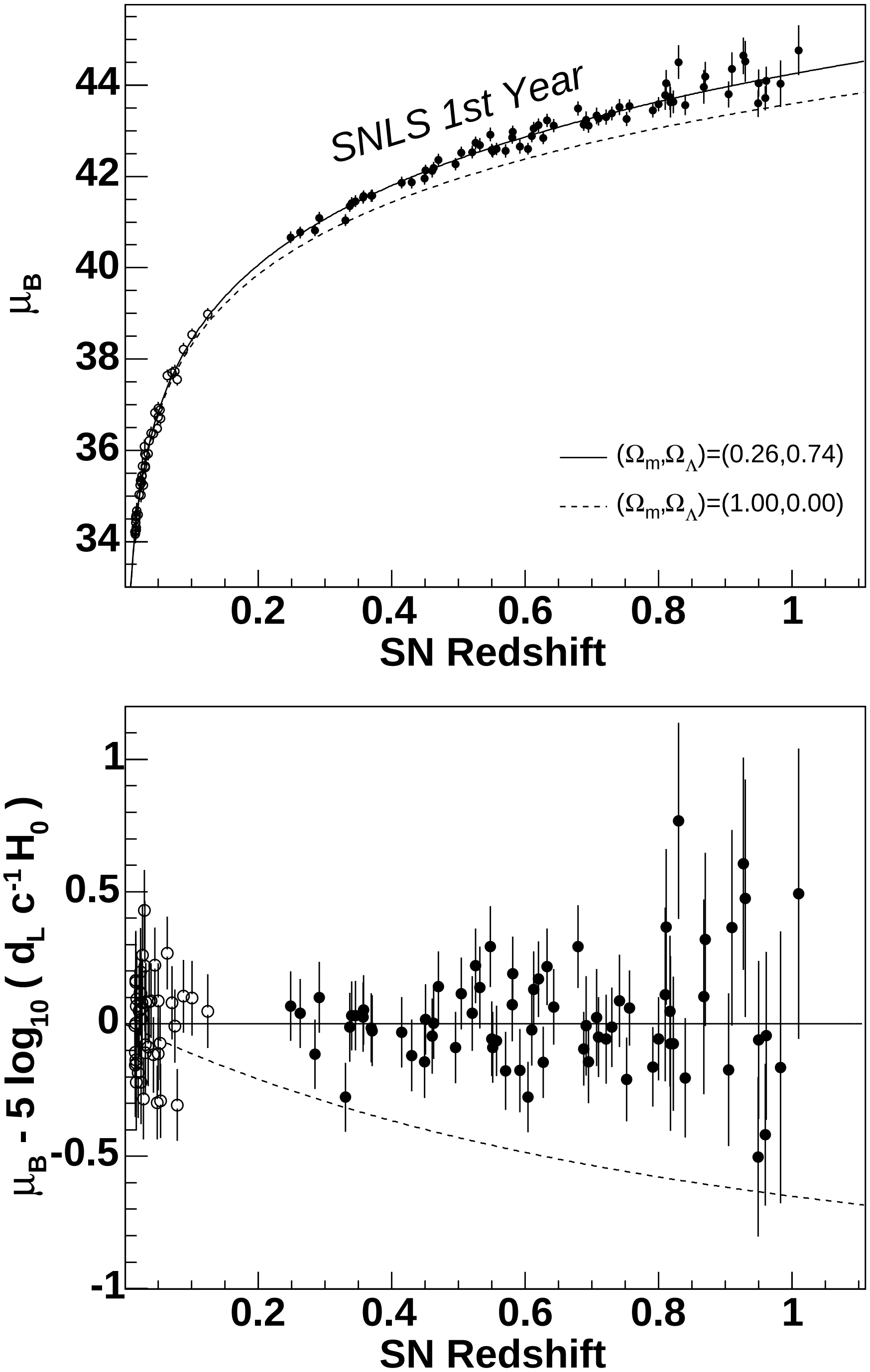

Figure 7: (Top panel) Same kind of luminosity distance – redshift diagram as in the previous figure, but for more recent data published by the SNLS collaboration in 2005. (Lower panel) Same data points and errors, divided by the theoretical prediction for the best fit ΛCDM model. *Plot taken from Astronomy and Astrophysics 447: 31-48, 2006 [e-Print: astro-ph/0510447] by Pierre Astier et al.*

Some even more recent results are shown in figure 18. Hence, supernovae data strongly suggest the existence of a cosmological constant today ($\Omega_\Lambda > 0$). In fact, the small luminosity of high-redshift supernovae suggests that the universe is currently in accelerated expansion. The supernovae data does not say whether the parameter Ω_k is negligible, positive or negative.

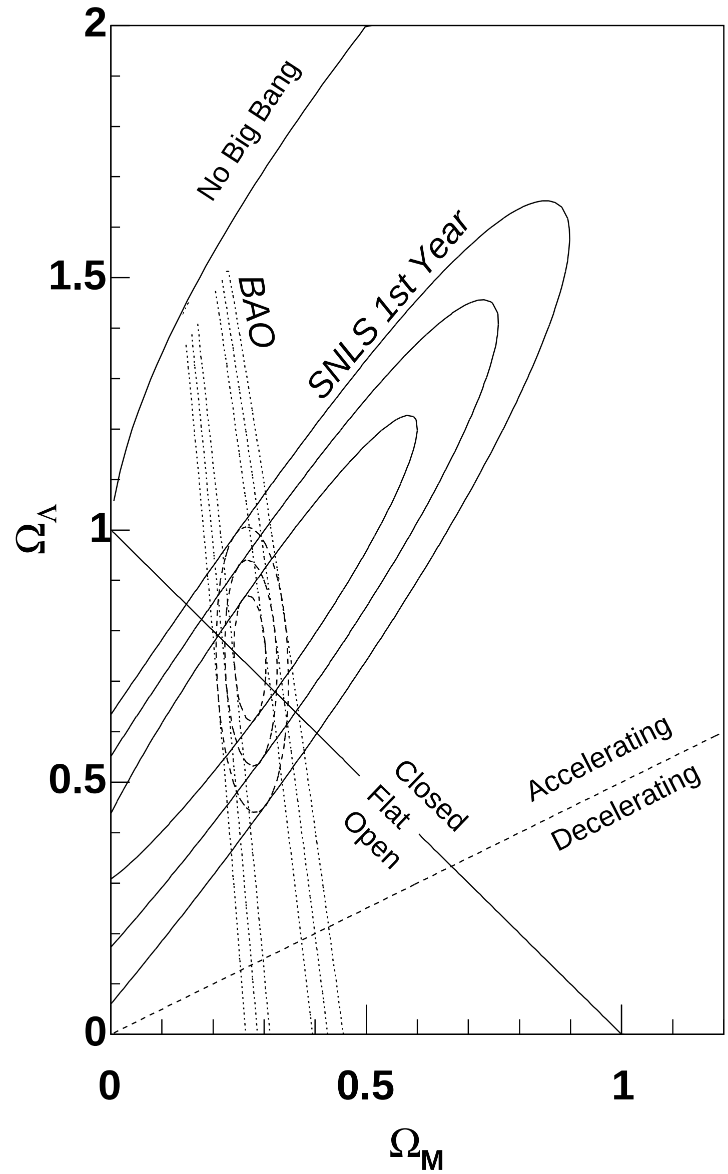

Figure 8: Contours at 68.3%, 95.5% and 99.7% confidence levels in the (Ω_m, Ω_Λ) plane from the SNLS supernovae data (solid contours), the SDSS baryon acoustic oscillations (see section 1.4.9, dotted lines), and the joint confidence contours (dashed lines). These plots are all assuming a ΛCDM cosmology, as we are doing in this chapter. *Plot taken from Astronomy and Astrophysics 447: 31-48, 2006 [e-Print: astro-ph/0510447] by Pierre Astier et al.*

1.4.6 CMB temperature anisotropies: overview of the theory

In the early Universe, photons, electrons and nuclei were tightly coupled through electromagnetic interactions. Hence the universe was opaque. At temperature of the order of 3000 K, the scattering rate became too small for electromagnetic interactions to keep the system in equilibrium. Electrons recombined with nuclei, while photons decoupled from the rest of matter, and started to free-stream in the Universe. Hence, the Universe became transparent around that time. The photons originating from the primordial plasma that we detect today had their last interaction also around that time. This means that observing these photons (forming the so-called Comic Microwave background or CMB) gives an image of a sphere, centered on us, corresponding to a redshift of $z \sim 1100$, and an age of $t \sim 380000$ years after the Big Bang. This sphere is called the last scattering surface. Note that decoupling takes place after the time of equality between radiation and matter ($z_{eq} \sim 10^4$): so, the CMB photons offer a picture of the Universe at the beginning of the matter dominated era.

Before photon decoupling, photons were in thermal equilibrium, with a Planck spectrum (also called blackbody or thermal spectrum). After the last interactions at $t \sim 380000$ years, this distribution is frozen and remains planckian, although the photons are not kept anymore in equilibrium by whatever mechanism; but non-interacting photons can only be redshifted by the expansion; hence the spectrum keeps exactly the same form, but the temperature is shifted like the energy of each photon, i.e. proportionally to a^{-1}; today this temperature reaches $T = 2.726$ K. In terms of wavelength, this gives $\langle \lambda \rangle \sim$ mm, which explains the name of *microwave* background. As mentioned in section 1.1.2, these photons were first detected by Penzias and Wilson in the 60's.

But the most interesting aspect of the CMB is the study of temperature fluctuations observed in various directions (i.e., temperature anisotropies), which are expected to reflect the temperature and density fluctuations of the primordial plasma on the last scattering surface. These anisotropies were first detected by the NASA satellite COBE DMR which produced its final results in 1994. They are of the order of $\delta T/T \sim 10^{-5}$, meaning that in the early universe all perturbations (of the temperature but also of density, pressure and metric) were of the order of 10^{-5}. This had been predicted before COBE's observations, because it is exactly the order of magnitude expected in order to from the observed large scale structures (galaxies, clusters of galaxies, etc.). Indeed, perturbations in the primordial plasma can be considered as *seeds* for these structures: galaxies and clusters formed through a simple mechanism of gravitational clustering, starting from tiny primordial perturbations.

Here we will give a very simplified overview of the evolution of perturbations in the universe, in order to understand qualitatively which type of information is encoded in the map of CMB anisotropies. We will start with a brief qualitative description of what happens in real space, and then in Fourier space. Indeed, the perturbations can be expanded in Fourier modes with respect to comoving coordinates. If their comoving wavenumber is k, their physical wavelength grows with the Universe expansion, like $\lambda(t) = a(t) \times [k/(2\pi)]$.

The most interesting phenomenon occurring before photon decoupling is that of acoustic oscillations. Before decoupling, the tightly coupled photon-electron-baryon fluid experiences two antagonist forces: gravity (mainly due to the baryon mass) and quantum pressure (due to the photons, which resist to compression with a pressure $p = \rho/3$). Hence, the conditions are gathered for the propagation of density waves ($\Leftrightarrow$ acoustic waves $\Leftrightarrow$ sound waves). These waves can exist provided that there is some initial stress; this stress corresponds to primordial perturbations in the very early universe. At very high redshift, we expect that the thermal plasma contains some initial perturbations, presumably inherited from the stage of cosmological inflation. These primordial perturbations set the thermal plasma locally out-of-equilibrium. We can expand the plasma overdensity $\delta\rho/\rho$ in Fourier space, and treat each Fourier mode like a harmonic oscillator, with initial out-of-equilibrium conditions.

In order to understand qualitatively the evolution of perturbations in real or Fourier space, it is crucial to know the behavior of a quantity called the sound horizon, which is simply equal to the distance over which a sound wave can travel between the early universe and a given time t. This quantity is similar to the causal horizon, excepted that sound waves travel at a velocity $c_s \simeq c/\sqrt{3}$ rather than c (because the sound speed is given by $c_s^2 = c^2 \delta p/\delta\rho \simeq c^2(p/\rho) \simeq c^2/3$). The distance travelled by a radial sound wave between a time t_1 and a time t_2, evaluated at time t_2, is given by integrating over dl at $t = t_2$:

$$d_{\mathrm{sound}} = \int_{r_1}^{r_2} a(t_2) \frac{c_s dr}{\sqrt{1 - kr^2}} \ , \tag{59}$$

where r_1 and r_2 are the radial coordinates of the wave at time t_1 and t_2. By analogy with the propagation of light, we know that the wave travels with an infinitesimal relation $dl = \frac{c}{\sqrt{3}} dt = a(t) \frac{dr}{\sqrt{1-kr^2}}$. Hence the sound horizon is given by

$$d_{\mathrm{sound}}(t_1, t_2) = a(t_2) \int_{t_1}^{t_2} \frac{c_s dt}{\sqrt{3} a(t)} \tag{60}$$

Even more interesting is the comoving sound horizon, evaluated in the space of comoving coordinates:

$$d_{\mathrm{sound}}^{\mathrm{comoving}}(t_1, t_2) = \frac{d_{\mathrm{sound}}(t_1, t_2)}{a(t_2)} = \int_{t_1}^{t_2} \frac{c_s dt}{\sqrt{3} a(t)} \ . \tag{61}$$

This quantity is easy to compute. It depends by a negligible amount on the choice of t_1, provided that $t_1 \ll t_2$: hence t_1 can be sent to the initial singularity, or say to the beginning of radiation domination, and does not impact the result. One finds e.g. $d_{\mathrm{sound}}^{\mathrm{comoving}} \propto t_2^{1/2}$ during radiation domination, or $d_{\mathrm{sound}}^{\mathrm{comoving}} \propto t_2^{1/3}$ during matter domination.

Let's now imagine what happens with density perturbations (equivalent to temperature perturbations) in real space, before photon decoupling. Since sound waves cannot travel by more than $d_{\rm sound}^{\rm comoving}$ in real comoving space, the situation can be summarized as follows: we have initially a random distribution of overdensity/underdensity patterns of all sizes. As long as its size is larger than the sound horizon, a given pattern remains frozen; on smaller scales, the patterns evolve simply because of diffusion: i.e., each overdensity diffuses around, and is stretched to a size equal to $d_{\rm sound}^{\rm comoving}$. This is like the propagation of waves on a lake after throwing a rock, with the diameter of the wave being the comoving sound horizon; however, in the case of a the lake surface, a single impact causes several concentric wavefronts, while in the primordial plasma there is only a single wavefront for each initial overdensity.

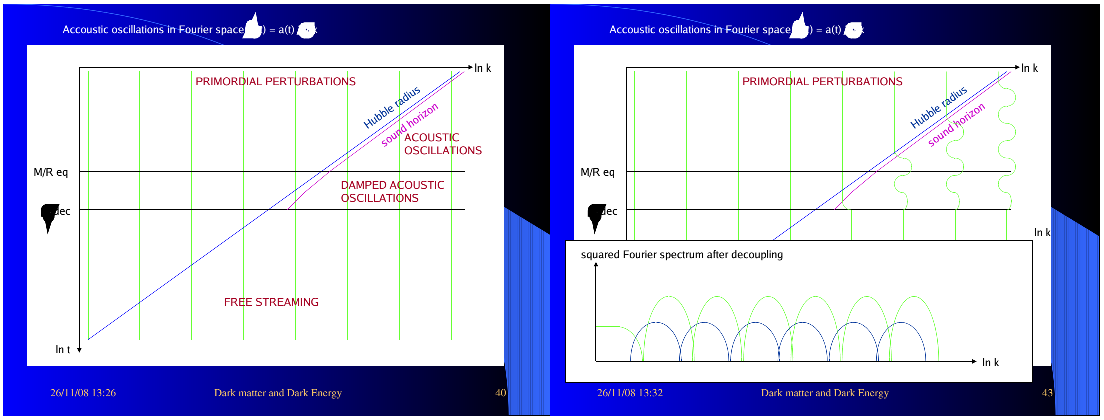

Figure 9: Schematic plots of the different regimes experienced by perturbations of a given comoving wavenumber k (horizontal axis) when time evolves (from top to bottom). The black lines correspond to the time of matter/radiation equality (upper lines) and photon decoupling (lower lines). Wavelengths are smaller than the Hubble radius on the right of the blue lines, and smaller the sound horizon on the right of the magenta line. *(Left)* The photon density/temperature perturbations are frozen above the sound horizon scale. Below this scale, they experience the following regimes: acoustic oscillations (before equality); damped oscillations (between equality and decoupling); and free streaming on all scales after decoupling. *(Right)* Schematic view of the oscillations before decoupling: modes of a given wavenumber oscillate in phase, starting from the time at which the wavenumber is equal to the sound horizon; hence, at decoupling, modes are frozen with an oscillatory structure. *(Bottom right)* The two point correlation function observable today is related to the square of the Fourier spectrum at decoupling (green part) plus the out-of-phase contribution of the Doppler effect (blue curve).

This very qualitative description is a starting point, but doesn't help to reach useful conclusions. Let's switch now to comoving Fourier space. In figure 9, we give a summary of what happens, and of the different regimes experienced by each perturbation of wavenumber k. One after each other, the modes become smaller than the sound horizon, starting from the smallest ones. Before matter/radiation equality, they experience acoustic oscillations inside the sound horizon (this is the equivalent in Fourier space of the mechanism of diffusion of overdensities mentioned in the previous paragraph). Something interesting takes place between equality and decoupling: due to the fact that the gravitational potential is less and less influenced by the photon-electron-baryon fluid (which has pressure), and more and more by dark matter (which has no pressure), the balance between gravity and pressure breaks down and the oscillations are damped. At the time of decoupling, all perturbations such that $k > d_{\rm sound}^{\rm comoving}(t_{dec})$ have experienced some oscillations (the smallest wavelenghts with the largest k experienced more periods of oscillation than the small k ones). For $k > d_{\rm sound}^{\rm comoving}(t_{dec})$, no oscillations ever occurred: these modes correspond to wavelenghts still outside the sound horizon at decoupling.

Since photons free-stream after decoupling, the structure that we see today in the CMB temperature map has a two-point correlation function (called the CMB power spectrum) corresponding to the squared Fourier spectrum of fluctuations at decoupling. On large scales, no oscillations occured. So, in this region, the CMB spectrum only reflects the spectrum of primordial fluctuations, which is smooth and nearly scale-independent. Hence, the observed spectrum should be nearly flat in this range. Beyond this plateau region, the CMB power spectrum should have a series of peaks (corresponding to modes which oscillated for a given number of half-periods since they entered inside the sound horizon). This squared

Fourier spectrum should in principle reach zero between each maximum.

However, the temperature anisotropies that we see today do not only reflect the value of the plasma overdensity in each point of the last scattering surface (LSS). This first source of anisotropy, called the Sachs-Wolfe term, is the dominant one, but there are other terms. the second most important term is the Doppler one: we see photons emitted from a region of the LSS where the plasma had a bulk velocity, leading to a Doppler shift of the photon frequency. This Doppler term has the same oscillatory pattern as the Sachs-Wolfe term, but is out of phase with it (like for an ordinary harmonic oscillator). The sum of the Sachs-Wolfe and Doppler terms leads to a total Fourier spectrum with maxima and minima, but no points where the spectrum reaches zero.

The third important effect is the so-called integrated Sachs-Wolfe (ISW) effect, corresponding to the fact that between the last scattering surface and today, the photons cross regions where metric fluctuations (associated to matter density fluctuations) are not constant in time. Hence, the redshift and blueshift experienced by a photon crossing such regions do not compensate each other, and some extra anisotropies are generated along each photon line-of-sight, in addition to primary anisotropies acquired on the last scattering surface. This effect is particularly important during a possible Λ (or dark energy) dominated epoch: then, the gravitational potential fluctuations decay, inducing some temperature shift of the photons; this effect, know as the late ISW effect, contributes to the CMB spectrum on the largest wavelengths (smallest k), and gives a slope to the previously mentioned plateau.

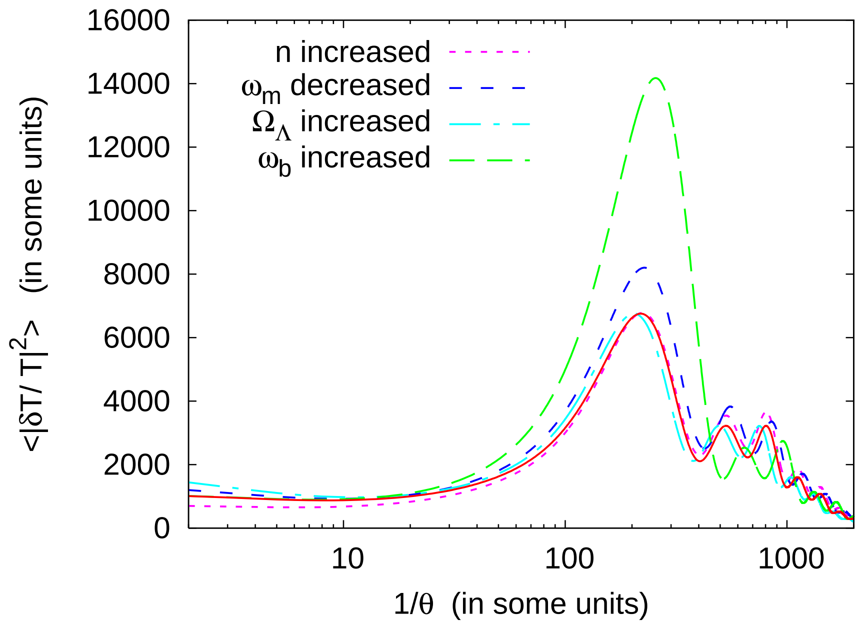

Figure 10: The red solid line shows the a reference CMB temperature spectrum, computed precisely with a numerical codes for standard values of the cosmological parameters of the ΛCDM model (these are Ω_Λ, ω_m, ω_b, plus two parameters describing the primordial spectrum: and amplitude and a tilt n, and one parameter describing an astrophysical process, which we do not discuss in this course: reionization). The other lines show the effect of varying one of the following quantities: n, ω_m, ω_Λ and finally ω_b. The corresponding effects are described in the text.

In summary, and simplifying a lot, the CMB spectrum is expected to consist in a smooth plateau with some slope, and then a series of local maxima and minima. This spectrum can be predicted very accurately, using numerical codes which integrate over the full system of coupled linear differential equation describing precisely the evolution of cosmological perturbations for each species. Qualitatively, the dependence of this spectrum on the main cosmological parameters is the following (all these effects are shown in figure 10, which is based on a precise numerical calculation of the spectrum):

- *dependence on the matter density* ω_m. The radiation density today is fixed by the CMB temperature $T = 2.726$ K, while ω_m is a free parameter that we try to measure. When the matter density decrease, equality between matter and radiation takes place later. Hence, there is less time between equality and decoupling (the time of decoupling is fixed by thermodynamics). So, there is less damping of the fluctuations in this regime, and the peaks corresponding to the acoustic oscillations are higher.

- *dependence on the cosmological constant* Ω_Λ. As already mentioned, during Λ domination, gravitational potential wells tend to decay, which generates a late ISW effect. Hence, when Λ increases, the plateau corresponding to large wavelengths is more tilted (more precisely, the smallest wavelengths are boosted).

- *dependence on the baryon density* ω_b. The baryon density mainly influences the complicated evolution of acoustic oscillations between equality and decoupling. When the baryon density is increased, the oscillations in this region are more affected by gravitational compression, and less by photon pressure. This leads to an increase in odd peaks (the first, the third, etc.) and a decrease in even peaks (the second, the fourth, etc.)

So, if the CMB spectrum can be measured accurately, its shape will give indications on the value of each of the above parameters. In addition, the position of the peak will contain some extra information, as we will now explain.

The first peak corresponds to modes which just entered inside the sound horizon at the moment of photon decoupling. Hence, its physical size depends on the sound horizon at decoupling, $d_{\mathrm{sound}}(t_{\mathrm{dec}})$. Because the sound speed is not exactly equal to $c/\sqrt{3}$ but gets corrections from the baryon density and the time of equality, the sound horizon at decoupling depends slightly on ω_b and ω_m.

Moreover, when we observe the CMB anisotropies, we do not probe the three-dimensional structure of the universe at $z \sim z_{dec}$, but we only see fluctuations of a two-dimensional sphere. The angle under which we see a given scale (e.g. the scale corresponding to $d_{\mathrm{sound}}(t_{\mathrm{dec}})$) is given by this scale divided by the angular diameter distance at the redshift of decoupling, $d_A(z_{dec})$. We have seen already that $d_A(z_{dec})$ depends on the parameters $(H_0, \Omega_k, \Omega_m)$.

Hence, the position of the first peak depends on most cosmological parameters. It turns out that the measurement of the peak position in angular space is mainly useful for the determination of Ω_k, since the curvature affects crucially the angular diameter distance. In fact, the sound horizon at decoupling can be seen as a *standard ruler*: this scale can be computed accurately for any given cosmological model, and the measurement of the corresponding angular diameter gives the quantity $d_A(z_{dec})$. Note that this *standard ruler* does not account for the size of a physical object, but for a characteristic wavelength in CMB maps; but this is equally useful.

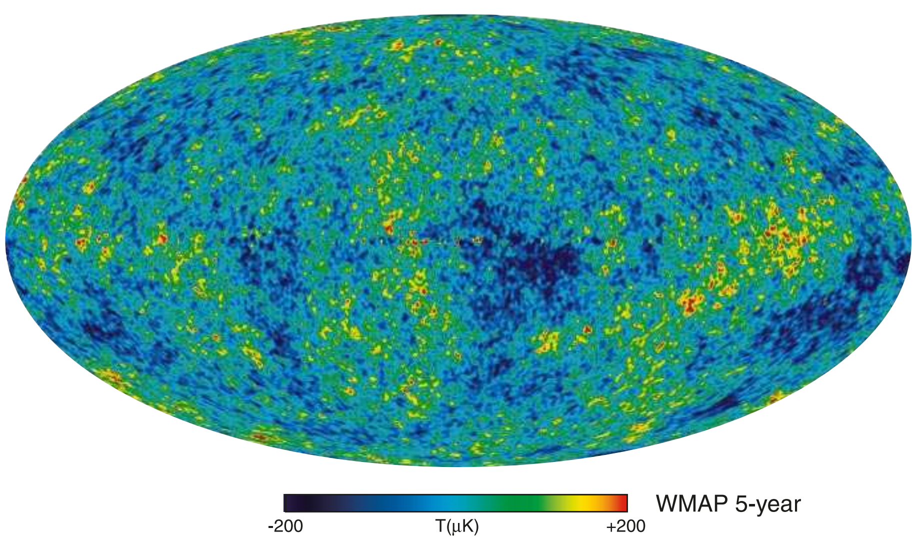

Figure 11: Map of temperature anisotropies obtained by the satellite WMAP (based on five years of data).

The best measurement of CMB anisotropies has been performed so far by the WMAP satellite (see figure 11), which is still acquiring data. The last release (WMAP5), based on five years of observations, constrains accurately the CMB power spectrum for scales seen under an angle $\theta > \pi/1000$ (see figure 12). These measurements are completed by other ground-based experiments, more sensitive to small scales seen under an angle $(\pi/2000) < \theta < (\pi/1000)$. Altogether, the power spectrum obtained from these measurements can be accurately fitted by the theoretical prediction of the ΛCDM model, for some values

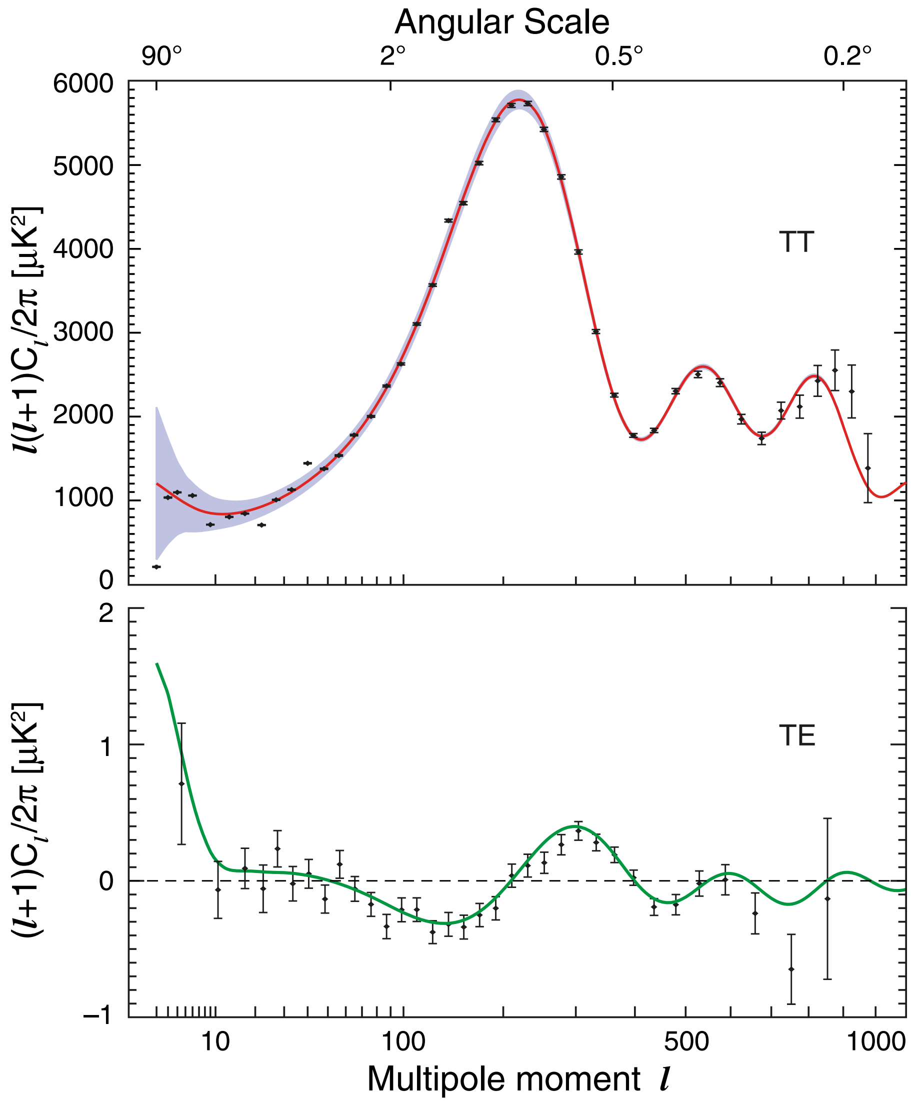

Figure 12: *(Top)* CMB power spectrum, i.e. two-point correlation function of the CMB remperature map, as measured by WMAP (five years of data) for scales seen under an angle $\theta > \pi/1000$ (the x-axis corresponds to a multipole expansion, i.e. the number l is roughly corresponding to an angle $\theta = \pi/l$ and to a Fourier mode on the last scattering surface $k = (l/6000)$ h/Mpc. The red curve shows the theoretical prediction for the best-fitting ΛCDM model.*(Bottom)* Measurement related to the polarization of CMB photons: we will not mention this aspect in the present course for simplicity.

of its six free parameters. This represents the greatest success of modern cosmology. Most cosmological parameters can be measured independently of each other with this technique. For instance, the baryon density is found to be $\omega_b = 0.0233 \pm 0.0006$ (95%CL), in very good agreement with results deduced from light element abundances; it is remarkable that two independent techniques –based on such different physical models as nucleosynthesis and the evolution of perturbations in the FLRW universe– provide consistent answers. Also, CMB data combined with other datasets (see below) show that our universe is nearly or exactly flat: the value $\Omega_{\rm tot} = 1$ is favored modulo a few per cent. There are theoretical reasons to expect that $\Omega_k = 0$, while a small $\Omega_k \ll 1$ would require a lot of fine-tuning: hence, many people assume that Ω_k is exactly zero for simplicity. With the assumption that $\Omega_k = 0$, WMAP alone gives the constraints $\omega_m = 0.132 \pm 0.006$ (95%CL) and $\Omega_\Lambda = 0.74 \pm 0.03$ (95%CL).

1.4.7 Structure formation

So far, we discussed mainly the evolution of temperature fluctuations before photon decoupling. Let us now focus on the evolution of density perturbations for non-relativistic matter: namely, baryons and dark

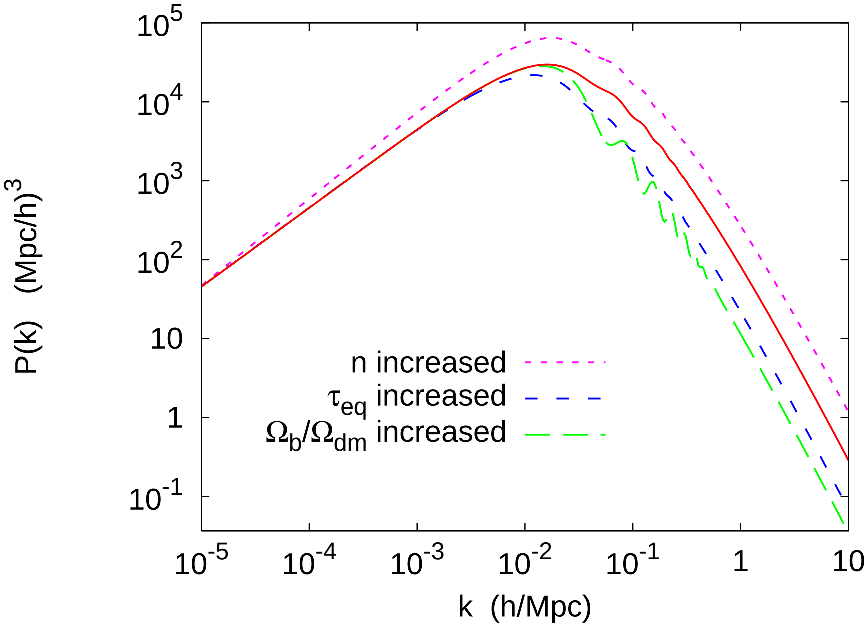

Figure 13: The red solid line shows a reference matter power spectrum $P(k)$ (the square of the Fourier spectrum of matter inhomogeneities in the universe, estimated today, at redshift $z = 0$). This spectrum is computed precisely, using a numerical code for standard values of the cosmological parameters of the ΛCDM model (these are Ω_Λ, ω_m, ω_b, plus two parameters describing the primordial spectrum: and amplitude and a tilt n). This spectrum has a turn-over around the scale $k \sim 10^{-2}$h/Mpc, which marks the limit between wavelengths becoming smaller than the Hubble radius before or after the time of matter/radiation equality. The other lines show the effect of varying one of the following quantities: n, the time of equality $\tau_{\rm eq}$ (increasing $\tau_{\rm eq}$ is equivalent to decreasing ω_m), and finally the ratio of baryons to dark matter, $\Omega_b/\Omega_{dm} = \omega_b/(\omega_m - \omega_b)$. The corresponding effects are described in the text. In summary: varying the tilt changes the slope of the initial power spectrum, and hence also the slope of $P(k)$ today. Postponing the time of equality (by decreasing ω_m) implies less growth of fluctuations during matter domination on small scales, and hence less power for large k. Increasing the baryon density relatively to that of dark matter implies less power and more oscillatory patterns for large k.

matter (DM).

DM before equality: Dark matter overdensities $\delta_{DM} = \delta\rho_{DM}/\rho_{DM}$ are frozen on wavelengths larger than the sound horizon. Their spectrum is just dictated by the primordial power spectrum inherited from the very early universe (namely, from inflation). For wavelengths becoming smaller than the sound horizon, DM particles behave like test particles evolving within the gravitational potential generated by the photons. DM has no pressure, and no reason to resist to compression. Hence, DM particles slowly accumulate inside gravitational potential wells, and δ_{DM} tends to grow with time inside the sound horizon. But the fluctuations of the gravitational potential itself do not grow: the gravitational potential oscillates, following the photons.

DM after equality: δ_{DM} remains frozen on wavelengths larger than the Hubble radius, which plays the role of a causal horizon. For wavelengths becoming smaller than the Hubble radius, DM overdensities grow very quickly, because the more DM falls inside gravitational potential wells, the more these wells become deep, and so on. In two words, this corresponds to gravitational clustering. Before equality, no efficient gravitational clustering of DM could occur, because the gravitational potential oscillated with the photon+baryons; after decoupling, the gravitational potential reacts to the clustering of DM.

Baryons before photon decoupling: baryon overdensities $\delta_b = \delta\rho_b/\rho_b$ are frozen on wavelengths larger than the sound horizon, and equal to DM overdensities in any point, $\delta_b = \delta_{DM}$. For wavelengths becoming smaller than the sound horizon, the evolution of DM and baryon overdensities is radically different. The baryons just track the photons, due to tight-coupling. Hence, they also experience acoustic oscillations, which are damped between equality and decoupling. They do not accumulate in potential wells like DM.

Baryons after photon decoupling: baryons experience gravitational clustering inside the Hubble radius, just like DM, but starting from different initial conditions, since earlier they experienced damped oscillations instead of growing slowly.

Conclusion: The shape of the Fourier power spectrum of matter density today, $P(k) \equiv \langle (\delta\rho_m/\rho_m)_k^2 \rangle$ (with $\delta_m = \delta_b + \delta_{DM}$), is easy to understand. We cannot observe modes which are outside the Hubble radius today, so we disregard this branch of the power spectrum. The scales that we observe fall in two categories: those which entered inside the sound horizon during matter domination, and experienced fast growth; of course those which entered first (the largest k's) grew more; and those which entered during radiation domination, which experienced slow growth due to the behavior of δ_{DM} during that stage, and then a common amplification during matter domination. With such a scheme, it is not difficult to understand that the slope of $P(k)$ changes radically around the scale k_{eq} corresponding to the Hubble radius at the time of equality. Indeed, a detailed calculation shows that $P(k)$ increases with k for $k < k_{eq}$; then there is a turn-over; finally $P(k)$ decreases with k for $k > k_{eq}$ (see figure 13). The shape and slope of this power spectrum can be accurately predicted with the same type of numerical calculation as the CMB spectrum (at least for linear scales, i.e. scales such that $\delta\rho_m/\rho_m \ll 1$). The dependence of $P(k)$ on the main cosmological parameters can be understood in that way:

- *dependence on the matter density* ω_m. We have seen already that when the matter density decreases, equality between matter and radiation takes place later. This means that there is less time for δ_{DM} to grow efficiently during matter domination. Large scales should be affected, but the turn-over is shifted to smaller k's, and $P(k)$ is suppressed at higher k. This can be checked in figure 13 (the dashed blue curve corresponds to a larger time of equality $\tau_{\rm eq}$, i.e. to a lower matter density ω_m than for the red curve).

- *dependence on the baryon density* ω_b. The baryon density mainly influences what happens around decoupling. If there is much more DM than baryons, then baryons behave like test particles at decoupling: they fall inside the gravitational potential wells created by DM, which reflect the evolution of DM before decoupling, i.e.: small growth during radiation domination and fast growth at the beginning of matter domination. If instead, there is much less DM than baryons, the DM will behave like test particles at decoupling: they fall inside the gravitational potential wells created by baryons, which reflect the evolution of baryons before decoupling, i.e.: constant oscillations during radiation domination, and damped oscillations at the beginning of matter domination. In a realistic situation, a kind of equilibrium is found between these two limits: δ_b and δ_{cdm} become quickly equal to each other, because the particles fall inside the same potential wells; for small ω_b, the power spectrum $P(k)$ is large and smooth on small scales, while for large ω_b, $P(k)$ is suppressed and oscillating on small scales. This can be checked in figure 13 (the dashed green curve corresponds to a larger baryon-to-dark-matter ratio $\Omega_b/\Omega_{dm} = \Omega_b/(\Omega_m - \Omega_b) = \omega_b/(\omega_m - \omega_b)$ than the red curve). The oscillations imprinted in $P(k)$ when ω_b is large enough are called Baryon Acoustic Oscillations (BAO); they are the remnants of the same acoustic oscillations that can be observed in the CMB spectrum.

- *dependence on the cosmological constant* Ω_Λ. As already mentioned, during Λ domination, gravitational potential wells tend to decay. This effect does not depend on the scale considered. Hence the overall normalization of $P(k)$ goes down when Λ increases.

If the baryon density is not to small and BAO are visible, it is possible to measure the angle under which we see them. For the CMB, the angular scale of the peak is inferred from the angular correlation function of CMB anisotropy maps; similarly, for the matter distribution, the angular scale of BAO can be obtained from the angular correlation function of observed density fluctuations, for objects located at various redshift. This gives an estimate of the angular diameter distance – redshift relation, this time not at the redshift $z \sim 1100$, but at smaller redshift, as we shall see later.

1.4.8 Difference between CDM, HDM and WDM

Another effect could play a very important role; namely, the free-streaming effect of DM particles. In the above qualitative description, we said that for wavelengths smaller than the Hubble radius, dark matter experiences gravitational clustering and δ_{dm} increases quickly. In this statement, we assumed implicitly that the velocity dispersion of dark matter particles is negligible, so that the DM horizon (defined in the same way as the sound horizon, but using the average DM particle velocity in place of the sound speed) is negligible. This is perfectly valid in many DM scenarios, for which DM particles are heavy, decouple in the early universe when they are non-relativistic, and have an average velocity dispersion which is negligible with respect to the speed of light.

This would not be true anymore for very light DM candidates such as neutrinos, which decouple in the early universe when they are still relativistic, and become non-relativistic only in the recent universe:

typically, during radiation or Λ domination for neutrinos with realistic masses of the order of 10^{-3} to 10^{-1} eV. In this case, the velocity of neutrinos is as large as the speed of light as long as they are relativistic (i.e. until the time at which $T = m$). After that time, their velocity dispersion decays as $\langle v \rangle \sim \langle p \rangle / m \propto a^{-1}$ (since the momentum redshifts like the inverse of a wavelength). Today, $\langle v \rangle$ is smaller than c by one or two orders of magnitude only. Hence, the horizon of these particles (i.e. the typical distance travelled by a neutrino between the early universe and now) is very large; in fact, it is only slightly smaller than the Hubble radius today.

However, particles with a large velocity dispersion cannot cluster for wavelengths smaller than their own horizon: on small scales, their velocity prevent them from falling and getting trapped inside gravitational potential wells. Hence, neutrinos cannot cluster on small scales. This implies that if dark matter consists entirely in neutrinos, the power spectrum will be considerably reduced on small scales with respect to what we discussed in the previous section.

DM particles with a negligible velocity dispersion are called by definition "Cold Dark matter" (CDM). Examples of power spectra for the cosmological model containing baryons, CDM and a cosmological constant (called the ΛCDM model) are shown in figure 13. If DM particles are very light and become non-relativistic after the time of equality or later, they are called "Hot Dark Matter" (HDM). Since δ_{HDM} cannot grow during matter domination on small scales, the power spectrum of any ΛHDM model is considerably suppressed on small scales with respect to the ΛCDM case. Finally, there exists an intermediate case: that of DM particles with a mass of the order of 1000 eV, becoming non-relativistic during radiation domination, with an horizon corresponding to the typical distance between galaxies today (of the order of the mega-parsec). This case is called Warm Dark Matter (WDM). The difference between the matter power spectrum $P(k)$ in ΛCDM and ΛWDM models is the same as between ΛHDM and ΛCDM: a supression on small scales; however, for HDM, the suppression appears for wavelengths of the order of cluster scales (typically, 10 Mpc); while for WDM, it appears for wavelengths of the order of galaxy scales (typically, 1 Mpc).

1.4.9 Galaxy correlation function and Lyman-α forests

The matter power spectrum can be probed by the measurement of a two-dimensional or three-dimensional map of galaxy positions; after a smoothing process, this distribution can be Fourier expanded; as a result, astronomers obtain an estimate of the matter power spectrum $P(k)$. There are two caveats in this technique.

First, the distribution of visible galaxies does not necessarily reflects the density field of total matter, but only that of a particular fraction of visible baryons; hence, this technique does not measure the total matter power spectrum, but the power spectrum of a particular category of baryonic matter. However, both theoretical arguments and numerical simulations indicate that at least on the largest scales, the galaxy overdensity $\delta_{\rm gal}$ is proportional to the total overdensity δ_m. In other words, the two quantities are related by $\delta_{\rm gal} = b\, \delta_m$, where the proportionality factor b (which does not depend on the scale) is called the light-to-mass bias. As a result, the galaxy and matter power spectra are related by $P_{\rm gal}(k) = b^2 P(k)$, and by measuring $P_{\rm gal}(k)$, we measure the *shape* of the matter power spectrum, but not its overall amplitude.

The second caveat is that on small scales, the distribution of galaxies reflects the non-linear evolution of matter perturbations, i.e. the behavior of δ_m after the time at which $\delta_m \sim 1$. Indeed, we have seen that δ_m grows quickly during matter domination; during Λ domination, it growths more slowly, but it still increases. Hence, for each scale, there is a time at which $\delta_m \sim 1$ (this regime is reached earlier for the smallest scales). After that time, the perturbation evolution cannot be studied with *linearised* Einstein equations. The evolution of each Fourier mode is very hard to follow analytically or even numerically, due to mode-mode coupling. It is necessary to perform time-consuming simulations in real space, using the largest available supercomputers. In this regime, we don't have yet robust theoretical predictions. Today, the scale below which non-linear corrections are important is roughly $\sim$ 30Mpc. This scale of non-linearity coincides with the wavelength below which the light-to-mass bias is expected to become scale-dependent. In conclusion, galaxy redshift survey can be used for constraining cosmology only on large scales (above $\sim$ 30Mp), for which the bias is just an unknown normalization factor, and the fluctuations are linear. On those scales, the shape of the observed matter power spectrum can be compared with theoretical predictions.

The largest galaxy redshift surveys to date are the two degree field survey (2dF) and the Sloan Digital Sky Survey (SDSS, see figure 14). The power spectrum estimated from these catalogues (see figure 15) provides a measurement of (ω_m, Ω_Λ, ω_b, etc.), found to be in very good agreement with measurements from the CMB, although this technique is not as precise and leads to larger errorbars. More importantly, the oscillations due to the baryon acoustic oscillations (BAOs) have been clearly detected (see figures

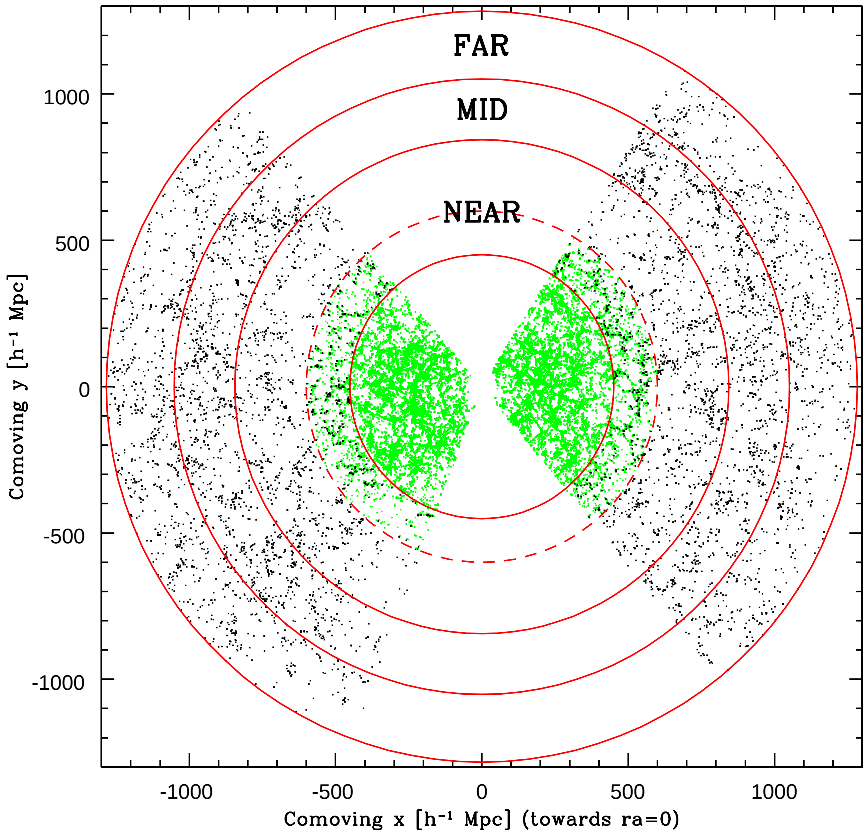

Figure 14: The distribution of galaxies in a thin slice of the neighboring universe centered on us, obtained by the Sloan Digital Sky Survey (SDSS). The radial coordinate is the comoving distance in units of h^{-1}Mpc. The four solid red circles correspond to the redshifts $z = 0.155, 0.3, 0.38, 0.474$. Each point represents a galaxy belonging to one of two different samples: the sample called "main galaxies" by the SDSS group (green points) and that called "Luminous Red Galaxies" (LRG, black dots), which extends further since it represents a selection of very bright galaxies only. *Taken from Phys.Rev.D74:123507,2006 [astro-ph/0608632] by M. Tegmark et al.*

16 and 17). By studying the angular correlation function of galaxies, astronomers have measured the angle under which the correlations associated with BAOs are seen in the sky. This provides an accurate estimate of the angular diameter distance – redshift relation at small redshifts (smaller than one), and brings complementary information on Ω_k and Ω_Λ. We will come back to the corresponding results in the next sections.

Another crucial result is that the slope of the matter power spectrum $P(k)$ measured by galaxy redshift surveys is perfectly compatible with CDM models, and in strong disagreement with HDM models. Hence, light neutrinos cannot be the main component of dark matter. Light massive neutrinos could play the role of a subdominant component, but most dark matter should be either cold or warm.

With galaxy redhsift surveys, it is not possible to distinguish between CDM and WDM models, because they differ only on very small scales corresponding to the non-linear regime. In order to discriminate between CDM and WDM, one should find a way to measure the matter power spectrum on smaller scales and at high redshift, so that the perturbations are caught in our past, at a time when the scale of non-linearity was smaller than today. Such a technique exists, but we don't have time to describe it here. In few words, in the spectrum of distant quasars, we can see absorption lines, called the Lyman-α forest, which provide a measurement of the density fluctuations along the line of sight, mainly at redshifts $2 < z < 4$. These observations allow astronomers to reconstruct the matter power spectrum far in the past and on small scales. So far, Lyman-α observations are consistent with CDM, but not with WDM (unless WDM is a sub-dominant component, or unless the WDM mass is so large that the two are impossible to distinguish with cosmological observations).

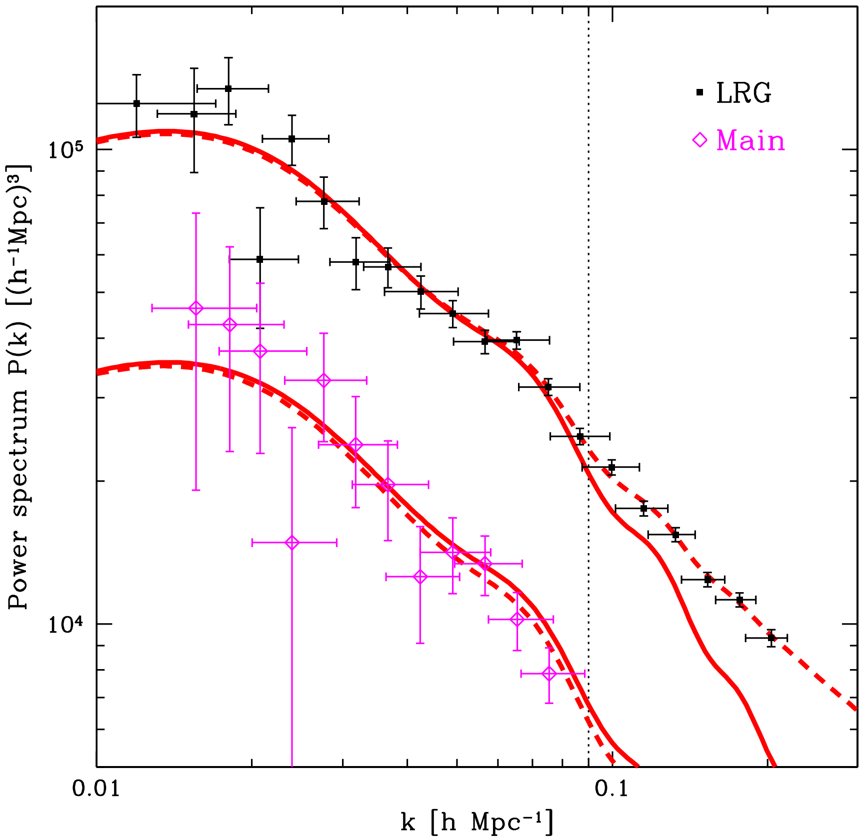

Figure 15: Measured power spectra for the galaxies of figure 14. The upper points are for luminous red galaxies, the lower one for main galaxies. The two samples don't have necessarily the same light-to-mass bias: this is why the data points indicate two different normalisations of the luminous power spectrum $P_{\rm luminous}(k)$. The solid curves correspond to the theoretical prediction for the ΛCDM model best-fitting WMAP3 data, normalized to a light-to-mass bias $b = 1.9$ (top) and $b = 1.1$ (bottom) relative to the $z = 0$ matter power $P(k)$. The dashed curves show an estimate of the nonlinear corrections on small scales, but this aspect is beyond the scope of this course. Note however that the onset of nonlinear corrections is clearly visible for $k \geq 0.09h$/Mpc (vertical line). *Taken from Phys.Rev.D74:123507,2006 [astro-ph/0608632] by M. Tegmark et al.*

In conclusion, Large Scale Structure (LSS) observations bring evidence in favor of the ΛCDM model, and provide complementary information on the cosmological parameters with respect to CMB observations.

1.4.10 Combining observations: results for dark matter

The combination of cosmological data (Nucleosynthesis, age of the universe, SNIa, CMB, LSS) and astrophysical data brings clear evidence for dark matter (or otherwise, for something that would accurately mimic the properties of dark matter, like eventually a very subtle modification of gravity). Observational constrains can be summarized as follows:

- from direct observations of visible matter, we estimate that only 1% of the critical density is luminous; with Nucleosynthesis, we know that $\omega_b \sim 0.022$. Using $h \sim 0.7$, this gives $\Omega_B \sim 0.045$: approximately 4.5% of the critical density is in the form of baryonic matter. In addition, CMB and LSS provide measurements of the total matter density (which affects the time of equality and hence the shape of the CMB and matter spectra), yielding $\omega_m \sim 0.12$: this suggest that we need a dark component with $\omega_{dm} \sim (0.14 - 0.02) \sim 0.12$, i.e. $\Omega_{dm} \sim 0.25$. On top of that, the CMB and LSS spectra are also sensitive to the ratio Ω_b/Ω_{dm}, and their shape is compatible with the above numbers. Hence, cosmological observations of CMB anisotropies, LSS and light element abundances

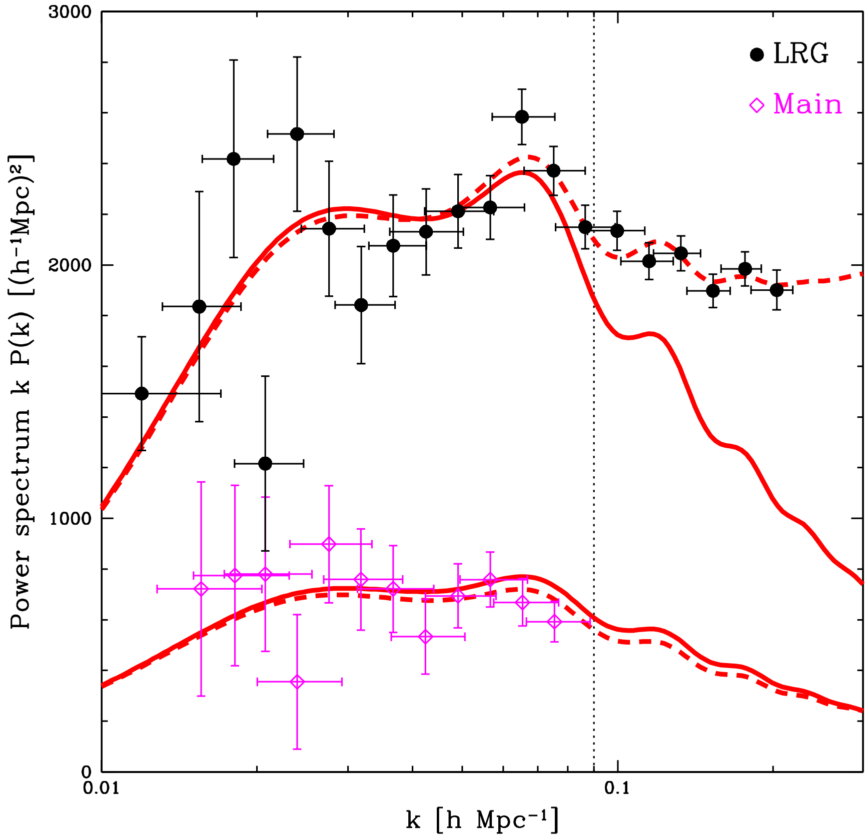

Figure 16: Same as 15, but multiplied by k and plotted with a linear vertical axis to more clearly illustrate the observation of at least the first baryon acoustic oscillation. *Taken from Phys.Rev.D74:123507,2006 [astro-ph/0608632] by M. Tegmark et al.*

all contribute to establish that 25% of the universe energy is in the form of pressureless matter, which is completely decoupled from photons and baryons during the stage of acoustic oscillations.

- astrophysical arguments show that the dynamics of structures (like most galaxies and clusters of galaxies) is dominated by the gravity of a dark component, which is not formed of compact object (MACHOs) and does not interact with the rest of matter (as shown by the bullet cluster).
- the shape of the matter spectrum (probed by galaxy redshift surveys and Lyman-α forests in quasar spectra) proves that dark matter is cold (or at least, most of it), with a velocity dispersion negligible with respect to the speed of light.

In conclusion, observations tell us that our universe contains 25% of pressureless, non-interacting, cold dark matter (or something indistinguishable from cold dark matter). Finding a dark matter candidate fulfilling all these constraints will be the topic of section 2.

1.4.11 Combining observations: results for dark energy

Evidence for dark energy comes from the following observations:

- remote supernovae at a given redshift are fainter than they should be in a universe without a cosmological constant. The luminosity distance – redshift relation $d_L(z)$ of supernovae with redshifts in the range $0.4 \leq z \leq 1.6$ can only be explained within an accelerating Universe. Constraints from SNIa in the plane $(\Omega_m, \Omega_\Lambda)$ are shown in figure 8 and 18 (the latter corresponds to slighly more recent data). It is clear from these figures that this type of observation constrains mainly the difference $(\Omega_m - \Omega_\Lambda)$: the great axis of the SNIa ellipses is almost orthogonal to the line along which $\Omega_m + \Omega_\Lambda = 1$. This property comes from the expression of $d_L(z)$ in a ΛCDM universe for

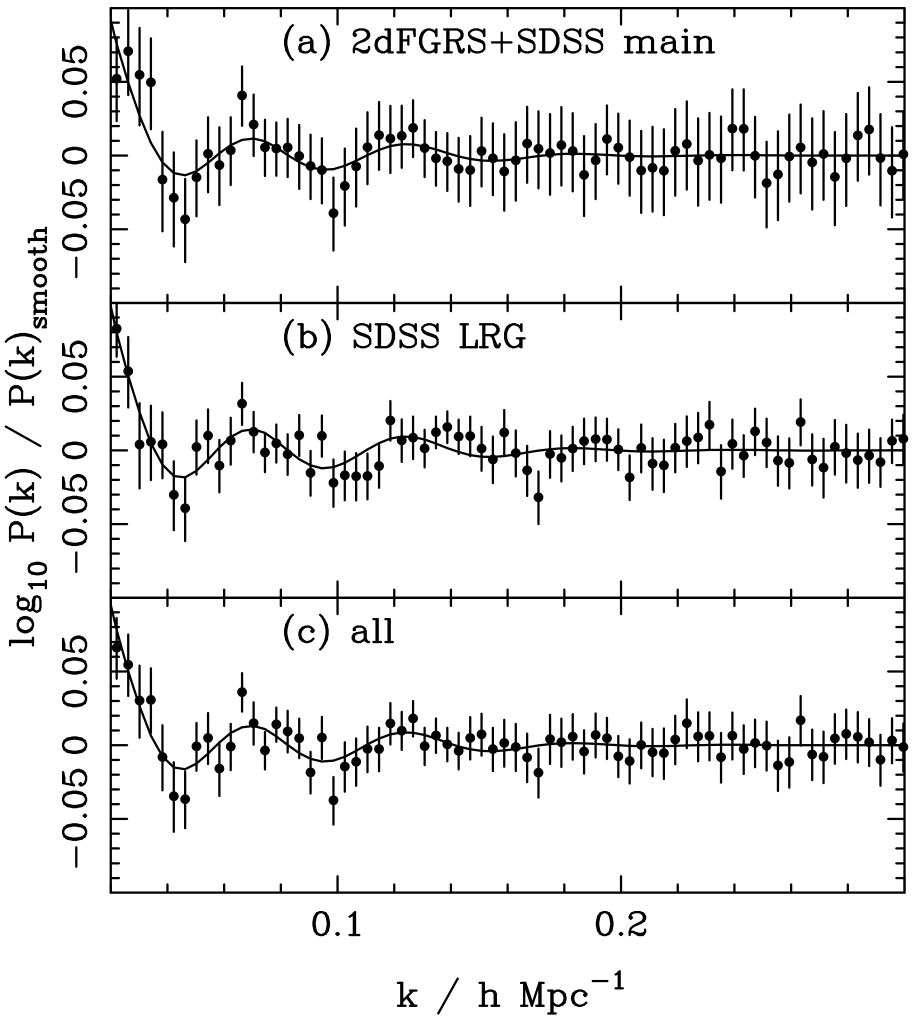

Figure 17: Same as 16, but with a different way of showing the oscillation: instead of multiplying $P(k)$ by k, the measured $P(k)$ has been divided by a smooth spectrum, in such way that in absence of observable oscillations one would obtain a straight line. This data is the most recent one on BAOs. *Taken from Mon.Not.Roy.Astron.Soc.381:1053, 2007, arXiv:0705.3323v2 [astro-ph] by W. Percival et al.*

$0.4 \leq z \leq 1.6$. Indeed, it is be possible to do the following exercise: picking up some redshift $z \sim 1$, one can compute numerically $d_L(z)$ as a function of $(\Omega_m,\, \Omega_\Lambda)$, using equation (57). The resuts show that $d_L(z)$ varies more quickly in the direction $(\Omega_m - \Omega_\Lambda)$ than in the direction $\Omega_m + \Omega_\Lambda = 1$. This means that the luminosity distance is mildly affected by the spatial curvature of the universe, and strongly affected by variations in the Hubble rate. Indeed, when computing the universe acceleration today (by taking the derivative of the Hubble rate), one finds that the acceleration depends roughly on the difference between Ω_m and Ω_Λ, while the curvature depends on the sum of the same parameters.

- the observed angular scale of CMB peaks tells us that the Universe is nearly flat: $\Omega_m + \Omega_\Lambda \simeq 1$. Actually, we should recall that this constraint comes from an estimate of the sound horizon at decoupling, divided by the angular diameter distance $d_A(z \sim 1100)$. The angular diameter distance at this redshit is very sensitive to the spatial curvature, but also slightly sensitive to the splitting between matter and Λ (which affects the expansion history at small redshift). Hence, the constraint coming from the CMB peak position is not exactly a constraint on $\Omega_m + \Omega_\Lambda$, but on a slightly different direction (see figure 18). The same figure shows that the combination of SNIa data with information on the CMB peak position indicates that $(\Omega_m, \Omega_\Lambda) \simeq (0.3, 0.7)$.

- the observed angular scale of BAOs provides another independent constraint. Note that the CMB map is a two-dimensional representation of the sky at a given redhsift. If BAOs were observed by taking the angular correlation function of two-dimensional galaxy maps, corresponding to the

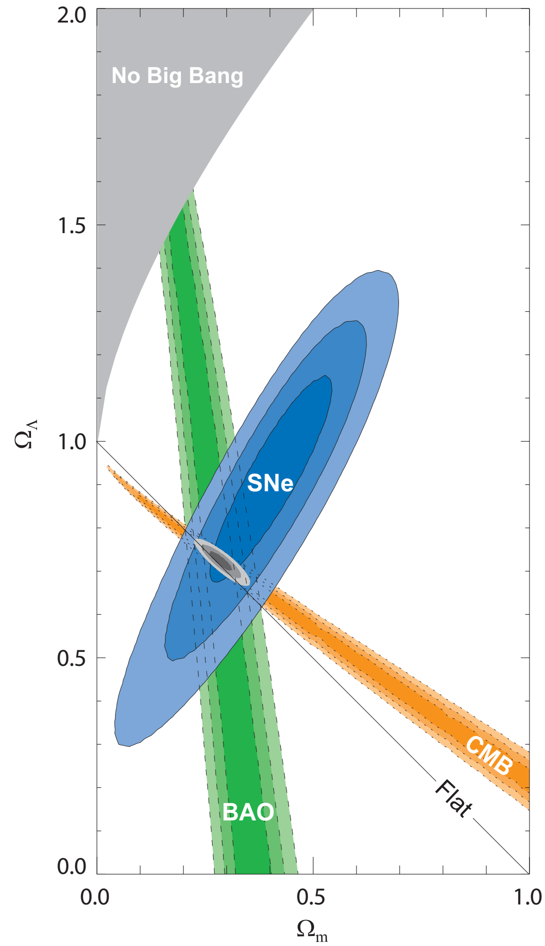

Figure 18: Contours at 68.3%, 95.5% and 99.7% confidence levels in the (Ω_m, Ω_Λ) plane from recent supernovae data (blue solid lines), baryon acoustic oscillations (green dashed), and CMB peak positions (orange dotted). These plots are all assuming a ΛCDM cosmological model. *Plot taken from arXiv:0804.4142 [astro-ph] by M. Kowalski et al.*

catalogue of all visible galaxies at a given redhsift, then the measurement of the angular scale of BAOs would be equivalent to that of CMB peaks: it would provide an estimate of the ratio between the sound horizon at decoupling and the angular diameter distance $d_A(z)$, where z is the redshift of these galaxies. However, things are a bit more complicated because the galaxy redshift surveys are three-dimensional (for each galaxy, we measure (z, θ, ϕ)), and the BAO correlation length is reconstructed by Fourier expanding the three-dimensional catalogue. The third coordinate is z, and the redshift difference Δz must be translated in terms of a physical distance d; this is not trivial; as a result, the constraint provided by BAOs is not aligned with that from supernovae, as would be the case if BAOs where just measuring $d_A(z)$; instead, it probes a different direction in the (Ω_m, Ω_Λ) space, as can be checked from figure 18. It is very nice to see that SNIa, CMB and BAO measurements provide constraints in three different directions, and intersect each other around (Ω_m, Ω_Λ) = (0.3,0.7).

- the shape of the CMB spectrum could constrain Ω_Λ through the late ISW effect discussed previously. We don't have time to give details on this subject; let us just mention briefly that this effect is difficult to see, and not very constraining at the moment[1].

- we have seen that the CMB and LSS spectra are sensitive to the time of equality, and therefore to ω_m; knowing the value of h from Hubble diagrams, one can infer some constraints on Ω_m; this allows to restrict the region allowed by CMB experiments in the (Ω_m, Ω_Λ) space (the orange region in figure 18 is based on the measurement of the CMB peaks position, not on the shape of the

[1]but in the future, the correlation between CMB maps and LSS maps could provide accurate measurements of the late ISW effect and of the cosmological contant value.

CMB spectrum). This way of using the data shows again that Ω_Λ should be close to 0.7, but this technique leads to a larger error bar on Ω_Λ than the combination of SNIa, CMB peak scale and BAO measurements.

So, in summary, the best measurements that we have today concerning the value of the cosmological constant come from the relation between luminosity distance or angular distance and redhsift: at $z \sim 1100$ for the CMB peaks, at $z \sim 1$ for supernovae luminosity, and at $z \sim 0.2$ from BAOs. Becasue of the different redhsifts, and also because of different experimental techniques corresponding to different relations between observed quantities and physical distances, these techniques probe different direction in the space $(\Omega_m, \Omega_\Lambda)$, as can be seen in figure 18; their intersection near the point $(\Omega_m, \Omega_\Lambda) = (0.3{,}0.7)$ provides convincing evidence in favor of a cosmological constant, or for something with a similar effect (in particular, this something must be responsible for an acceleration of the universe expansion today). The generic name for such a component is Dark Energy (DE): the cosmological constant is a particular case of DE, with a density which is exactly constant in time. We will come back to different possible explanations of this Dark Energy in section 3. At the end of that section, we will also come back to observations, and see how they can help us to discriminate between different DE models.

2 Dark matter
(Céline Boehm)

2.1 Evidence for dark matter

Although the presence of invisible matter in the universe now seems a well established concept, it took about 40 years of research to admit/convince the community that this hypothesis was actually interesting and perhaps, even, the correct answer to several puzzling observations.

It all started in 1933 when F. Zwicky noticed that the velocity in the COMA cluster was too large to maintain its cohesion [1, 2]. This puzzling observation lead him to postulate the existence of a new invisible substance in the Universe, a reasonable hypothesis if one remembers that both the neutron and neutrino were discovered in the 1930s (1932 and 1930-1933 respectively).

Although Zwicky's idea did not appeal to many of his colleagues, evidence in the same direction continued to be accumulated: S. Smith thus obtained a similar conclusion as Zwicky in 1936 by studying the Virgo cluster [3] while, in 1939, both Babcock and J. Oort noticed a too large rotation curve in the Andromeda and NGC 3115 galaxies respectively which was the sign that there was also a missing piece in the understanding of galaxy dynamics [4, 5]. However, despite the many efforts to measure the rotation velocity of several spiral galaxies using optical and radio observations [6, 7, 8, 9, 10, 11, 12, 13], it is only in 1978, with better optical measurements and radio observations of the neutral hydrogen gaz at large distance from the galactic centre – that the evidence for flat rotation curves of galaxies could be firmly established [14, 15, 16], thus confirming Zwicky's hypothesis.

During all this time (from 1933 to 1978), indications of the existence of a dark substance continued to be accumulated in cosmology. For example, the authors of Ref. [17] noticed that the early mass measurements of the M31,81,101 galaxies could be translated into a total energy density which largely exceeds the baryonic energy density which was estimated from primordial big bang nucleosynthesis observations (see [18]). Also, J. Silk demonstrated that a baryonic Universe could not give rise to "small" galaxies [19]. Since those exist (and have been accurately counted since), J. Silk's argument can be interpreted as the first theoretical argument in favour of the presence of dark matter in our Universe.

Nowadays, the following points:

- the anomalous behaviour of the rotation curves of galaxies
- strong gravitational lensing effects
- primordial Big Bang Nucleosynthesis
- Silk damping and CMB measurements of the cosmological parameters.

are (or remain), in my opinion, the most serious pieces of evidence in favour of dark matter. I will give more detail in the next subsections.

2.1.1 Rotation curves of galaxies and density profile

As previously mentioned, flat rotation curves of spiral galaxies are often presented as the most serious evidence of the presence of dark matter. Indeed, according to the Kepler law, rotation curves of galaxies should decrease with the distance r to the centre of the galaxy, as

$$v^2 \propto \frac{G\,M}{r},$$

while observation indicate that they remain constant far from the galactic centre.

To solve the apparent discrepancy between theoretical expectations and observation, one has to assume that either the Kepler law or our estimate of the galactic mass is incorrect. If one refuses to modify gravity (i.e. Newtonian dynamics) directly, then one has to admit that the mass of each spiral galaxy has been underestimated. Since rotation curves of galaxies are obtained using e.g. luminous matter (stars) or radio observations of neutral hydrogen gaz, one has to postulate that the mass can be decomposed as follows:

$$M(r) = M_{luminous\ matter} + M_{neutral\ gaz} + M_{dark}(r)$$

where $M_{dark}(r)$ is supposed to be the additional (yet invisible) mass which is responsible for the anomalous behaviour of rotation curves of spiral galaxies. This, in fact, requires that $M_{dark}(r)$ increases with the distance r from the centre of the galaxy.

Hence, such an hypothesis suggests that there exists, in spiral galaxies, an extra component which – unlike (luminous or dark) ordinary matter–, does not obey the Kepler law. Although this may appear rather disturbing, one can explain why "dark matter" does not obey the same physical laws as ordinary matter in galaxies by assuming that it does not undergo the same type of interactions as ordinary matter. This very property is actually confirmed by Large-Scale structure theory and observations, although dark matter seems to obey Newtonian dynamics on very large-scale (at least down to 100 kpc).

Once one has accepted to introduce a new kind of matter to avoid changing the Kepler law for ordinary matter, all our ignorance about galaxy dynamics is transferred onto a dark sector that remains to be characterized.

2.1.2 Gravitational Lensing

Strong gravitational lensing magnifies and distorts light from a source, generating – depending on the case – Einstein rings, luminous arcs or even multiple images. This effect is used to estimate the dark matter distribution in cluster of galaxies. Although this definitely indicates that there is more matter than luminous matter in clusters, this method does not give a precise information on the nature of dark matter.

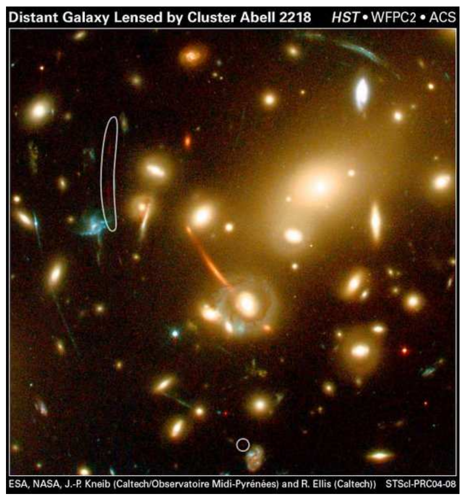

Weak gravitational lensing effects are also used to trace the distribution of dark matter in the Universe [20]. These methods apply when the distortion is too weak to induce Einstein rings or giant arcs but is large enough to distort the images of the background galaxies. Perhaps the most beautiful application of weak lensing is the 3-d map of the dark matter distribution in large-scale structures of the Universe. Not only does this show that using weak lensing techniques to get information of dark matter is feasible (albeit very hard) but also this demonstrates the importance of dark matter with redshift, thereby confirming that dark matter is part of the key elements to form large-scale structures.

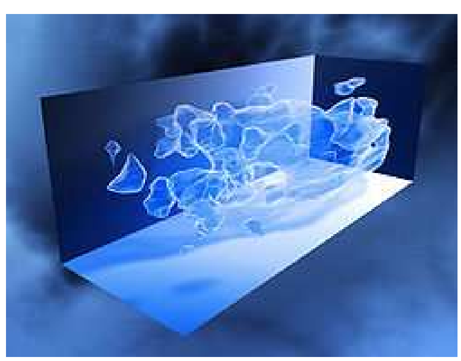

Although gravitational lensing observations suggest the presence of non-luminous matter in clusters of galaxies and, more generally, in the Universe at different redshift, it is hard to exclude other possibilities (which would mimic the presence of dark matter), such as a modification of gravity and/or the presence of dark baryons. More evidence are required but, from gravitational lensing, we definitely learn that most of the matter in the Universe is indeed invisible.

2.1.3 primordial Big Bang Nucleosynthesis

Perhaps a less controversial evidence in favour of non baryonic dark matter in the Universe is the quantity of baryons in astronomical objects in which very little stellar nucleosynthesis has taken place or in the past universe.

At high temperature, neutrons scatter with proton, electron and neutrino, thus being maintained in thermal and chemical equilibrium. Free (interacting) neutrons nevertheless decay into proton, neutrino and electron as soon as their mean temperature is lower than their mass. Below $T \sim 1GeV$, the neutron to proton ratio is given by $\frac{n_n}{n_p} \propto e^{(-\frac{(m_n - m_p)}{T})} \sim 1$.

This ratio remains of order unity until the temperature of the Universe drops below $\Delta T = m_n - m_p =$ 1.293 MeV. Below 1.3 MeV, interesting physics start to kick in. In particular the neutron to proton ratio decreases and the electroweak interactions, which are meant to maintain the thermal and chemical equilibrium, freeze-out[2] at a temperature of about 0.7 MeV.

At this moment, there is only one neutron left per six protons. But, since the reaction $n + p \to D + \gamma$ – which is faster than the electroweak interactions– remains slightly more efficient than the expansion rate of the Universe, Deuterium start to be formed. However the back reaction $D + \gamma \to n + p$, namely the photodissociation of the Deuterium, remains significant and destroys all the Deuterium which has been formed. When the Universe finally cools down to a (photon) temperature of about 0.1 MeV, the Deuterium photodissociation freezes out while the formation of Deuterium still continues. During this time, Deuterium can be produced, leading to the formation of ^3H_e, ^3H which will produce ^4H_e and which, in turn, will produce ^7Li.

One can therefore predict the yield of each element, based on simple thermodynamics and nuclear physics and compare these estimates with the fraction of Lithium, Beryllium, Helium-3 and -4, tritium, deuterium which are found in the Universe [21]. The comparison between predictions and observations is not completely trivial as nucleosynthesis in stars tend to increase the fraction of Helium and destroy that of Deuterium. Nonetheless, Helium and Deuterium measurements seem to converge towards less than 5% of ordinary matter in the Universe.

This suggests that in a flat Universe, 95% of the energetic content of the Universe – at least– are basically missing [22]. This has been confirmed by CMB measurements.

The physics of BBN was worked out in the late 1940s by Gamow, Herman and Alpher but Peebles [23] performed the first code to estimate the yield of each element in 1967, soon after the discovery of the cosmological microwave background.

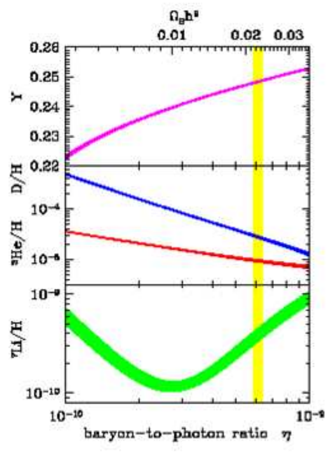

Figure 1: Abundance predictions for standard BBN [12]; the width of the curves give the $1-\sigma$ error range. The WMAP η range (eq. 1) is shown in the vertical (yellow) band.

2.1.4 Silk damping and CMB observations

Another element in favour of the presence of non-baryonic matter is the question of survival of primordial matter fluctuations in the early Universe. This question was first addressed by Misner in 1967 [24] who wondered whether or not the neutrino-electron interactions could damp the small matter fluctuations introduced by Peebles in 1965[25] to explain the formation of large-scale structures.

[2] Their interaction rate becomes comparable with the Hubble rate, which describes the expansion of the Universe.

Indeed, if one assumes that galaxies and clusters of galaxies originate from dense and under dense regions in the primordial Universe which grows with gravity (the dense regions become even more dense while the under dense regions tend to form void), then the size of this regions must be related to the size of the structures which are meant to form. For example, a galaxy of $10^{12} M_{\odot}$ as the Milky Way corresponds to fluctuations with a size of about 1 Mpc. Particles in matter fluctuations of 1 Mpc should therefore remain in these fluctuations; otherwise no Milky-Way size galaxies could form (which would lead to a conflict with observations since we live in a galaxy of $10^{12} M_{\odot}$). Combining observations and theoretical predictions, we now know that the smallest size of matter fluctuations which should have survived all damping processes is about 100 kpc. Objects of $10^{6} M_{\odot}$ have been discovered but their number is not certain enough yet to determine whether the corresponding fluctutations have been damped or not.

Unlike Misner, who found that the damping scale – due to neutrino-electron interactions– was about 1 $M_{\odot}$, J. Silk noticed in 1967 and 1968 [19] that electromagnetic interactions could damp the baryonic fluctuations up to 1 Mpc. This basically means that no (or too few) Milky Way size galaxy could have formed. Hence the Silk damping forbids the hypothesis of a baryonic matter dominated Universe and, in fact, can be seen as the first theoretical evidence in favour of non baryonic dark matter.

The electron interaction rate with photons is the product of the Compton or Thomson cross section (depending on their temperature) times the number density with photons. The number of photons in the Universe evolves as T^3. Below 1 MeV, the electron interaction rate is therefore roughly given by $\Gamma_e = \sigma_T n_\gamma \sim 10^{-15}\mathrm{cm}^3/\mathrm{s} \times \mathrm{T}^3/(10^{-4}\mathrm{eV})^3 \sim 10^{-3}(\mathrm{T/eV})^3\mathrm{cm.eV}^3$. Indeed, since the temperature nowaways is about $T_0 = 10^{-4}$ eV there is about 400 photons per cm^3, there must have been $\sim T^3/(10^{-4}\mathrm{eV})^3$ more photons at a temperature $T > T_0$. The electron thermally decouple from the plasma when this interaction rate becomes comparable to the expansion rate, that is when $\Gamma_e \simeq H$. This occurs at a temperature $T_{dec(e)}$.

However, at a temperature $T_{dec(\gamma)} > T_{dec(e)}$, the photons already becomes free (they do not "feel" the interactions with electrons, i.e. these interactions do not change the property of the photon fluid) and freely-propagate. Indeed, their interaction rate $\Gamma_\gamma \simeq \sigma_T n_e$, involves the electron number density which is, for $T < 511 keV$, much smaller than the photon number density due to the electron-positron annihilations into photons. Hence, after $T_{dec(\gamma)}$, the photons freely propagate out the fluctuations while the electrons remain coupled to the photons.

During the period $[T_{dec(\gamma)}, T_{dec(e)}]$, the photons drag the electrons out of the fluctuations due to the electron-photon coupling and the photon free-streaming, and therefore damp the primordial matter fluctuations. In a sense, one could say that the photon transmit their free-streaming to the collisional fluid of electrons.

A solution, to avoid the so-called Silk damping (which has actually been observed, see WMAP angular power spectrum, [**?**]), is to postulate that the Universe is not dominated by charged particles but rather by neutral particles. This has lead to the introduction of Neutral, Weakly-Interacting Massive particles (namely WIMPS), i.e. particles which do not have electromagnetic interactions and which, therefore, do not undergo the Silk damping. However, I would like to insist that dark matter may have interactions of stronger strength than the Standard Model weak interactions.

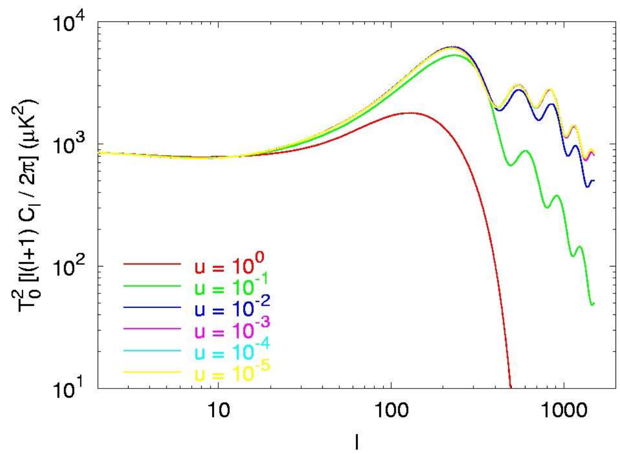

Indeed as can be seen in Fig. 2.1.4, the dark matter-photon cross section can take very large values (up to 10^{-6} times the Thomson cross section) and, yet, be compatible with CMB and large-scale-structure observations [26].

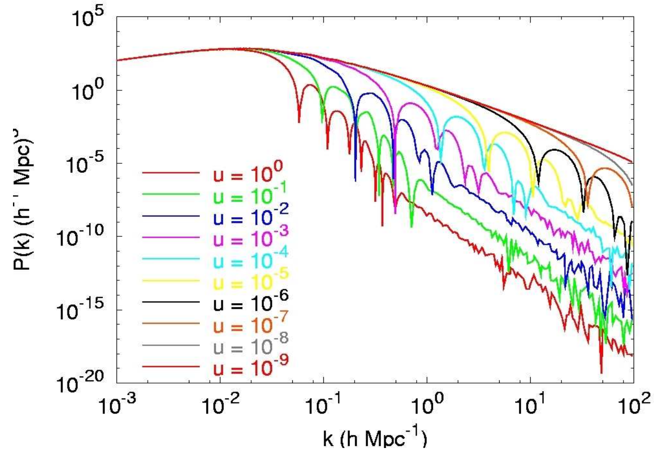

2.2 Dark Matter candidates

Let us now discuss the type of solutions which have been proposed to explain the presence of dark matter.

2.2.1 MACHOs and dark astrophysical objects

The first hypothesis that can be made concerning the nature of dark matter (although this would still conflict with J. Silk's argument) is that it is purely baryonic but bounded. Such an hypothesis implies that there should be dark baryons in our galaxy. Those objects with be under the form of Massive Astrophysical Compact Halo objects (MACHO) and may induce a microlensing effect when passing in front a light source. The idea is therefore to detect a variation of the luminosity of this source, providing that this variation (or amplification) is large enough to be detected, i.e. that there is enough lenses per unit of volume and that the magnificaztion is significant.

When the observer, the lens and the source are aligned, the radius of the Einstein ring is proportional to the distances from the observer to the source (d_{os}), from the observer to the lens (d_{ol}) and from the lens to the source (d_{ls}):

$$\theta_E = \sqrt{\frac{4GM}{c^2}\frac{d_{ls}}{d_{os}\ d_{ol}}}.$$

The optical depth is then the product of the geometrical cross section (that the surface of the Einstein ring, $\sigma = \pi\theta_E^2$) times the density distribution of MACHOs integrated over the volume and a solid angle $d\Omega$:

$$\begin{aligned}
\tau &= \int d\Omega \int d^3V\ f_{MACHOs}\ \sigma \\
&= \int d\Omega \int d^3V\ f_{MACHOs}\ \pi\theta_E^2 \\
&= \frac{4\ \pi\ G\ M}{c^2}\int d\Omega\ dd_{ol}\ d_{ol}^2\ f_{MACHOs}\ \frac{d_{ls}}{d_{os}\ d_{ol}}. \\
&= \frac{4\ \pi\ G\ M}{c^2}\int d\Omega\ dd_{ol}\ f_{MACHOs}\ \frac{d_{ls}\ d_{ol}}{d_{os}}.
\end{aligned} \tag{62}$$

Two experiments have searched for MACHOs, namely EROS and MACHO experiments, by looking at microlensing effects on the stars of the Large Magellan Cloud. The only candidate which has been found has a mass of about $1M_\odot$ and would represent about 20% of the mass of our halo.

2.2.2 Modifying gravity

It was indeed suggested that one could change the acceleration parameter so as to account for the rotation curves of galaxies. This is the idea which was explored in the MOdified Newtonian Dynamics (MOND) programm (introduced by Milgrom [27]). Indeed, if one modifies the force $\vec{F} = m\vec{a}$ as $F = m\,\mu(\frac{|\vec{a}|}{a_0})\,\vec{a}$ so that when $|\vec{a}| > a_0$, $\mu = 1$ and when $|\vec{a}| < a_0$, $\mu = |\vec{a}|/a_0$, the force reads (for small acceleration) as:

$|\vec{F}| = m \times |\vec{a}|^2/a_0$. Since $|\vec{a}| = v^2/r$, we obtain $|\vec{F}| = m \times v^4/(r^2 \times a_0)$. Equalizing this expression with the gravitational force, that is $F_g = GmM/r^2$, one immediately obtains:

$$v^4 = \ G \times M \times a_0$$

which translates the fact that the fourth of the rotation velocity of a galaxy is proportional to the baryonic mass of a galaxy. This is the so-called Tully-Fisher relation (a little bit modified by Sanders who replace the Luminosity by the mass [28]) which is obtained from galaxy observation.

Modifying gravity in order to explain the rotation curves of galaxies is however unsatisfactory. Indeed, MOND assumes a baryonic matter Universe which, as previously explained, necessarily leads to a prohibitve Silk damping effect. However, the idea of modifying gravity (that is an extension of the MOND programm) became very popular during the last decade due to the possible link with dark energy and new theories (notably a general relavistic version of MOND, based on scalar-vector-tensor field) which could circumvent the Silk damping despite many other defects. Such a theory of Tensor-Vector-Scalar (TeVeS) was proposed by Bekenstein [29] and is briefly summarized in the following.

In Einstein's general relativity (GR), the action is basically the sum of two quantities. One is the Einstein-Hilbert action and can be written as:

$$S_{EH} = \frac{1}{2\kappa} \int \frac{d^4x}{c} \ \sqrt{-g_\star} \ R_\star \tag{63}$$

(where $\sqrt{-g_\star}$ is the determinant of the metric, R is the scalar curvature and $\kappa = \frac{8\ \pi\ G}{c^4}$) and the other one is the action associated with matter $S_m = S_m[\psi, \tilde{g}_{\mu\nu}]$.

The Einstein-Hilbert action decribes the dynamics of a spin-2 field, also called the "Einstein" metric while S_m describes the action associated with all matter fields (here referred to as ψ) minimally coupled to a "physical" metric $\tilde{g}_{\mu\nu}$ that is also referred to as the Jordan metric.

The action S_{EH} can be rewritten using the Lagrangian parameter Φ, which after using the field equations, leads to a Scalar-Tensor action:

$$\begin{aligned} S_{S-T} \ &= \ \frac{1}{4\ \pi\ G} \int \frac{d^4x}{c} \ \sqrt{-g_\star} \ \left(\frac{R_\star}{4} - \frac{1}{2} g_\star^{\mu\nu} \partial_\mu \phi \partial_\nu \phi - V(\phi) \right) \\ &+ S_m[\psi, \tilde{g}_{\mu\nu} = A^2(\phi) g^\star_{\mu\nu}]. \end{aligned}$$

In this expression the term $A^2(\phi)$ represents a matter-scalar coupling and is equal to $e^{2/3\phi}$. These scalar-tensor theories are referred to as Brans-Dicke theories and are well-defined but they do not explain the rotation curves of galaxies.

So another modification that can be done is to introduce a disformal coupling in the metric. Indeed, instead of writing $\tilde{g}_{\mu\nu} = A^2(\phi) g^\star_{\mu\nu}$, Bekenstein proposed the following Jordan metric:

$$\tilde{g}_{\mu\nu} = e^{-2\,\alpha\,\phi}(g^\star_{\mu\nu} + U_\mu U_\nu) - e^{2\,\alpha\,\phi} U_\mu U_\nu$$

where $g^\star_{\mu\nu}$ is the Einstein metric. In the preferred frame where $U_\mu = (1, 0, 0, 0)$ and assuming that $g^\star_{\mu\nu} = (-1, 1, 1, 1)$, it is easy to see that $-U_\mu U_\nu$ behaves like $\simeq g^\star_{00}$ while $g^\star_{\mu\nu} + U_\mu U_\nu$ behaves like $g^\star_{ij}$. Therefore, one obtains that the components of the physical metric are related to the Einstein's metric component as follows:

$$\tilde{g}_{00} = e^{2\,\alpha\,\phi} g^\star_{00}$$

and

$$\tilde{g}_{ij} = e^{-2\,\alpha\,\phi} g^\star_{ij}$$

Bekenstein proposed the actions for the scalar, vector and matter fields. In particular, it is interesting to note that the action for the scalar field is given by:

$$S_\phi = -\frac{1}{16\ \pi\ G} \int d^4x \ \sqrt{-g^\star} \ \left(\mu(g^{\star\mu\nu} - U^\mu U^\nu)\partial_\mu\phi\partial_\nu\phi + V(\mu)\right)$$

where the parameter μ of MOND appears both in the function V (the equivalent of scalar potential, although not exactly the potential) and in front of the kinetic term.

The important point is that this TeVeS theory does reproduce the CMB observations up to the 2nd peak (especially if one takes into account the fact that ordinary neutrinos have a non-negligible mass which can be as large as 2 eV for the electron neutrino, since it is not yet experimentally excluded) [30].

On the other hand, problems start for the 3rd peak where the absence of dark matter (and therefore the presence of Silk damping) is difficult to avoid. Interestingly enough, the matter power spectrum is also in agreement with observations. This therefore suggests that such a theory –although it is far from being perfect– can mimic (at least to some extent) the presence of dark matter. Disregarding such scenarios may therefore be dangerous till no dark matter particle has been found in a laboratory experiment.

2.2.3 New type(s) of particles

Another suggestion is the existence of neutral particle as we have already explained. Although it seemed in the early 1980s that neutrinos could do the job, it was quickly realized that their free-streaming length was in fact too large to allow for the formation of small galaxies [31, 32, 33, 34]. Since, in addition, dark matter is meant to constitute halos of galaxies, dark matter must be stable or quasi-stable. This property excludes the Higgs particle as a possible candidate, thereby suggesting that – if dark matter is made of particles–, it must originate from a theory beyond the Standard Model.

Dark matter particles could have been produced during the reheating and thermalized with the rest of the particles due to their interactions. Example of " thermal" dark matter are e.g. neutrinos, neutralinos and sneutrinos (originating from supersymmetry), Kaluza-Klein particles, light dark matter. These particles tend to be stable. Their number density today may match the observed dark matter abundance thanks to their ability to annihilate into Standard Model particles, as we will explain in the next section. These particles often belong to the Cold Dark Matter scenario.

Dark matter particles could also originate from the decay of another particle. This type of "non-thermal" particles are generally long-lived but unstable particles and their density today originates from a specific mechanism in the early universe (which generally requires the fine-tuning of the epoch at which the density is achieved). Examples of non-thermal candidates are e.g.: axions, sterile neutrinos, Wimpzillas. They generally have extremely weak (if any) interactions and can be sometimes WDM candidates.

For all the possible candidates, one has to pay attention to possible constraints such as e.g.: the cosmological parameters, the matter and angular specta ($P(k)$ and $C(l)$), annihilations in the Sun, transport of energy inside Supernovae, annihilations in the centre of the galaxy (or in dwarf companions galaxies) and an unwanted production of Gamma or cosmic rays.

2.3 Relic density

One of the most important constraint on particle dark matter candidates is their energy density today. It has to be computed for each individual candidate and compared with observations. Generally there is enough freedom in each model to turn the relic density requirement into a constraint on the model. However, combined with other measurements or constraints, the relic density argument can be powerful enough to exclude particle physics candidates.

To use this argument, one has to define the notion of energy density and number density [35, 36, 37, 38]. The number density being a number per volume, and the volume being related to the inverse of the temperature of the Universe (T) to the cube, one easily understand that this number density will generally be proportional to T^3. However one can compute this quantity easily by summing the energy distribution over the momentum space:

$$n = \int d^3p \; f(p)$$

with

$$f(p) = \frac{1}{e^{\beta E} - 1}.$$

In the same way, one can define the energy density as:

$$\rho = \int d^3p \; E \; f(p). \tag{64}$$

Let us now investigate the evolutions of the energy density associated with a particle of mass m with the temperature. When the particle is relativistic, i.e. $T > m$, Eq. 64 leads to $\rho \propto T^4$. The particle can annihilate with its anti particle (which in some cases can be itself, notably in the case of Majorana particle) and produce relativistic particle a and b. However the energy liberated into a, b is in principle large enough so that, despite the evolution of the Universe (and the decrease of the temperature of the thermal bath), a, b can annihilate and produce the dark matter particle and its anti particle. When the temperature becomes comparable to the mass m, the energy density is given by

$$\rho = n\ m = m \left(\frac{mT}{(2\pi)^3} \right)^{3/2} \ e^{-\beta E}$$

(where we have neglected the chemical potential). This describes the Boltzmann suppression factor associated to the particle annihilation. Indeed, during this phase, the a, b particles created by the dark matter annihilation do not have enough energy to annihilate into the dark matter particle. This results into a net deficit of dark matter particles and therefore a reduction of the dark matter energy density which can bring it to an acceptable value with respect to the precise measurement of the dark matter relic density by the latest CMB experiments [39].

The annihilations actually stop when the annihilation rate becomes comparable to the Huble expansion rate H. This moment is called freeze-out and can be found by solving the Boltzmann equation (that is the evolution of the energy distribution with conformal time due to dark matter interactions):

$$\frac{df}{d\eta} = C[f]$$

where $C[f]$ is the collision term, f is the momentum distribution and η the conformal time, that is $t = a(t)\eta$ with $a(t)$ the scale factor. The distribution function f depends on the coordinates and momentum (x^μ and p^μ). Hence

$$\frac{df}{d\eta} = \left(\frac{\partial f}{\partial x_\mu} p^\mu + \frac{\partial f}{\partial p_\mu} \frac{dp_\mu}{d\lambda} \right) \frac{d\lambda}{d\eta} \tag{65}$$

with $p^\mu = \frac{dx_\mu}{d\lambda}$. To continue this calculation further, one needs to write the geodesic equation:

$$\frac{dp^\mu}{d\lambda} = \Gamma^\mu_{\alpha\beta} p^\alpha p^\beta.$$

To understand where the geodesic equation comes from, it is useful to start with a Lagrangian

$$L = \frac{1}{2} \ \ g_{\alpha\beta}\ \dot{x}^\alpha \ \dot{x}^\beta$$

(where the dot symbolize a derivative with respect to the conformal time η) and write the Lagrange equation (using a Friedman-Robertson-Walker metric):

$$\frac{d}{dt} \frac{\partial L}{\partial \dot{x}^\nu} - \frac{\partial L}{\partial x^\nu} = 0.$$

This yields:

$$\begin{aligned} g_{\nu\beta}\ \ddot{x}^\beta + g_{\nu\beta,\alpha}\ \dot{x}^\alpha \dot{x}^\beta - \frac{1}{2} g_{\alpha\beta}\ \dot{x}^\alpha \dot{x}^\beta &= 0 \\ g_{\nu\beta}\ \ddot{x}^\beta + (g_{\nu\beta,\alpha} \ - \frac{1}{2} g_{\alpha\beta,\nu})\ \dot{x}^\alpha \dot{x}^\beta &= 0 \end{aligned} \tag{66}$$

Since the last two terms are symmetric, they can be written as:

$$g_{\nu\beta}\ \ddot{x}^\beta + \frac{1}{2}\ (g_{\nu\beta,\alpha} \ + g_{\nu\alpha,\beta} - g_{\alpha\beta,\nu})\ \dot{x}^\alpha \dot{x}^\beta = 0 \tag{67}$$

And if we now multiply this equation by $g^{\nu\mu}$, we obtain:

$$\ddot{x}^\mu + \frac{1}{2}\ g^{\mu\nu}\ (g_{\nu\beta,\alpha} \ + g_{\nu\alpha,\beta} - g_{\alpha\beta,\nu})\ \dot{x}^\alpha \dot{x}^\beta = 0 \tag{68}$$

where we use the fact that $g_{\nu\beta}\ g^{\nu\mu} = \delta^\mu_\nu$. We can now define Christoffel symbols:

$$\Gamma^\mu_{\alpha\beta} = \frac{1}{2}\ g^{\mu\nu}\ (g_{\nu\beta,\alpha} \ + g_{\nu\alpha,\beta} - g_{\alpha\beta,\nu})$$

leading to the geodesic equation:

$$\dot{p}^{\mu} + \Gamma^{\mu}_{\alpha\beta}\ \dot{x}^{\alpha}\dot{x}^{\beta} = 0 \tag{69}$$

Taking $\lambda = \eta$, we obtain:

$$\frac{df}{d\eta} = \left(p^{\mu}\ \frac{\partial f}{\partial x_{\mu}} - \Gamma^{\mu}_{\alpha\beta}\ p^{\alpha}\ p^{\beta}\ \frac{\partial f}{\partial p_{\mu}} \right) \tag{70}$$

which gives:

$$E\frac{\partial f}{\partial t} + \vec{p}\ \frac{\partial f}{\partial \vec{x}} - H\ p^2\ \frac{\partial f}{\partial E} = \mathcal{C}[f]$$

using $\Gamma^0_{\alpha\beta} \equiv \Gamma^0_{ij} = \frac{1}{2\ a^2}\ \frac{da^2}{dt} = H$. If we also assume isotropy (no dependence in $\vec{p}$), the Boltzmann equation reads:

$$E\frac{\partial f}{\partial t} - H\ p^2\ \frac{\partial f}{\partial E} = \mathcal{C}[f]$$

We can now integrate over the volume: $\int d^3p$, we obtain:

$$\int d^3p\frac{\partial f}{\partial t} - H\frac{p^2}{E}\frac{\partial f}{\partial E} = \int d^3p\ \mathcal{C}[f]$$

which gives:

$$\begin{aligned}
&\frac{dn}{dt} - \int d^3p\ H\frac{p^2}{E}\frac{\partial f}{\partial E} = \int d^3p\ \frac{\mathcal{C}[f]}{E} \\
&\frac{dn}{dt} - H\int dp\ p^3\frac{\partial f}{\partial p} = \int d^3p\ \frac{\mathcal{C}[f]}{E} \\
&\frac{dn}{dt} - H[p^3\ f] + 3H\int \frac{d^3p}{(2\pi)^3}\ f = \int \frac{d^3p}{(2\pi)^3}\ \frac{\mathcal{C}[f]}{E}
\end{aligned}$$

and which can finally be written as

$$\frac{dn}{dt} + 3H\ n = \int \frac{d^3p}{(2\pi)^3}\ \frac{\mathcal{C}[f]}{E}$$

where the term of collision is given by the sum over all the 2-momenta of the initial and final particles of the squared matrix amplitude:

$$\begin{aligned}
&\int d^3p\frac{\mathcal{C}[f]}{E} = \int \frac{d^3p}{(2\pi)^3E}\ \frac{d^3p_2}{(2\pi^3)2E_2}\ \frac{d^3k_1}{(2\pi^3)2E_{k_1}}\frac{d^3k_2}{(2\pi^3)2E_{k_2}} \\
&\times\ (2\pi)^4\delta^4(p+p_2-k_1-k_2) \\
&\times\Big(|M|^2_{p_1+p_2\to k_1+k_2}\ f(p)\ f(p_2)(1\pm f(k_1))(1\pm f(k_2)) \\
&\qquad -|M|^2_{k_1+k_2\to p_1p_2}\ f(k_1)\ f(k_2)(1\pm f(p_1))(1\pm f(p_2))\Big)
\end{aligned}$$

which can finally be written as

$$\frac{dn}{dt} + 3H\ n = -\langle\sigma v\rangle(n^2 - n^2_{eq}) \tag{71}$$

with $\langle\sigma v\rangle$ the thermal average of the annihilation cross section. Note that I neglected all the internal factors.

To compute the energy density of a candidate at a given time, it is convenient to disentangle the evolution of the number density due to the expansion of the Universe and the annihilations. This can be done by computing the ratio Y of the number density to the entropy

$$s = \frac{2\pi^2}{45}\ g_\star(t)\ T^3,$$

(with $g_\star$ the number of effective degree of freedom). We finally obtain:

$$\frac{dY}{dx} = -x\frac{\langle\sigma v\rangle\ s}{H(m)}(Y^2 - Y_{eq}^2)$$

with

$$Y_{eq} \propto\ x^{3/2}\ e^{-x},$$

$H(m) = x^2 H$ and $x = m/T$. Finally we obtain:

$$\frac{x}{Y_{eq}}\ \frac{dY}{dx} = -\frac{\Gamma_{ann}}{H}\ \left[\left(\frac{Y}{Y_{eq}}\right)^2 - 1\right]$$

with $\Gamma_{ann} = \langle\sigma v\rangle\ Y_{eq}\ s$. The freeze-out occurs when the energy distribution does not follow the equilibrium distribution anymore. I.e. when the ratio $\frac{Y}{Y_{eq}}$ departs from unity. Since the above equation can be written as $\Delta Y/Y = -\frac{\Gamma_{ann}}{H}\ \left[\left(\frac{Y}{Y_{eq}}\right)^2 - 1\right]$, it is easy to see that the equilibrium is maintained when $\Gamma_{ann} > H$ and is lost when $\Gamma_{ann} \leq H$. The exact value of the freeze-out temperature and the dark matter relic density can then be found numerically by solving the above equation.

One can also compute analytically (and very quickly) the relic density of a specific candidate by observing that when the term $3H\ n$ is greater than $-\langle\sigma v\rangle(n^2 - n_{eq}^2)$, the Boltzmann equation reads as $\frac{dn}{dt} \simeq -3H \times n$, which indicates that the number density only changes due to the expansion of the Universe. Hence the annihilations stop changing the dark matter number density when $\Gamma \sim H$, that is when $\sigma v \times n \sim H$. This basically defines the freeze-out, i.e. the moment at which the number of particles (the number density times T^3) remains constant:

$$\langle\sigma v\rangle n_{fo} = H_{fo}. \tag{72}$$

where fo denotes the freeze-out. This property can also be translated into the following equation:

$$n_{fo}\ a_{fo}^3 = n_0\ a_0^3 \tag{73}$$

with a_{fo} the scale factor at freeze-out and $a_0 = 1$, the scale factor nowadays.

The expansion rate is $H = \frac{\dot{a}}{a}$ with $a = (t/t_\alpha)^\alpha = T_0/T$ and $T_0 = 2.73k$ (the present photon temperature). Hence $H = \frac{\alpha}{t}$, that is

$$H = H_\alpha\ a^{-\alpha},$$

where we denote $H_\alpha = \frac{\alpha}{t_\alpha}$. Using Eqs. 73 and 72, we then obtain:

$$\langle\sigma v\rangle\ n_0\ a_{fo}^3\ \ =\ \ H_\alpha\ a_{fo}^{-1/\alpha}.$$

In the radiation area, where $\alpha = 1/2$ (which is relevant for dark matter particles heavier than a few eV), we obtain:

$$n_0 = \frac{H_\alpha}{\langle\sigma v\rangle}\ a_{fo}.$$

Since the dark matter energy density today is given by $\rho_{dm} = m_{dm}\ n_0$, the cosmological parameter associated with dark matter is given by:

$$\Omega_{dm} = \frac{m_{dm}}{\rho_c}\ \frac{H_\alpha}{\langle\sigma v\rangle}\ a_{fo}$$

This can be written more conveniently as:

$$\Omega_{dm} = \frac{T_0}{\rho_c}\ \frac{H_\alpha}{\langle\sigma v\rangle}\ x_{fo} \tag{74}$$

with $x_{fo} = \frac{m_{dm}}{T_{fo}}$, leading to:

$$\Omega_{dm}\ h_{65}^2\ \ =\ \ \frac{2.6\,10^{-27}\mathrm{cm}^3/\mathrm{s}}{\langle\sigma v\rangle}\ \frac{1}{x_{fo}}\ \frac{1}{g_\star(t_{fo})} \tag{75}$$

with $h_{65} = h/0.65$,

One can obtain x_{fo} by plugging the number density at equilibrium ($n_{eq} = cst \times m^3 \times x^{-3/2}\ e^{-x}$) into the Boltzmann equation (see Eq. 71). After simplifications, one obtains:

$$x_{fo}^{-1} \simeq \ln \frac{\langle \sigma\ v \rangle\ T_0^2\ m}{H_\alpha\ (2\pi)^{3/2}\ \sqrt{x_{fo}}}. \tag{76}$$

which indicates that the freeze-out occurs at $T \simeq m/12$ for MeV particles and rather $T \simeq m/23$ for a 100 GeV particle.

The important point is that, whatever the mass of the dark matter particle, the ratio of the freeze-out temperature to the dark matter mass is about the same order of magnitude (in between 10 and 25 for realistic candidates ranging from 1 MeV to 1 TeV).

Reporting this range of values for x_{fo} into Eq. 74, one readily sees that – if the cross section is independent of the dark matter mass (as could be the case for scalars [40]) – then the relic densities obtained for a 1 MeV or a 1 TeV candidates only differ by a factor two. Therefore, when the cross section is independent of the dark matter mass, the relic density mostly constrains the type of interactions that dark matter can have. If the cross section depends on the dark matter mass as m^2/m_X^4 where m_X would be the mass of the exchanged particle (as it is the case for fermions), then the relic density does constrain the dark matter mass. In this case, only candidates with a mass in between 1 GeV to 1 TeV can have the observed relic density (using no other experimental contraint).

2.4 Exceptions to relic density calculations

In the previous section, we have explained how to estimate the relic density of a specific candidate and show that there is a simple relationship between the dark matter pair annihilation cross section and the relic density. We also mentioned that if the dark matter annihilation cross section was proportional to the dark matter mass, it is rather straightfoward to constrain the dark matter mass using the relic density criterion. However there are several exceptions to this method.

The first example is called coannihilation and denotes the situation where the dark matter is almost mass degenerated with another particle (the next to lightest particle of the spectrum). Let us assume that there is indeed new physics beyond the Standard Model of particle physics and that the lightest particle associated with this new spectrum is our dark matter candidate (which will be referred to as d_1 hereafter). Let us call the next to lightest particle of the spectrum by d_2 and the next-to-next d_3 and so on.

If $m_{d_1} \leq m_{d_2} << m_{d_3}$, then d_3 decays long before d_2. The particle d_2 becomes non-relativistic slightly before d_1. Although d_2 can decay into d_1 particles + Standard Model particles, the phase space associated with this 2-body decay is significantly reduced, thus increasing the lifetime of d_2 particles. This means that there are still many d_2 particles when d_1 becomes non-relativistic. Since d_1 and d_2 particles can interact and eventually annihilate together, i.e. *co-annihilate*, one has to solve a system of two coupled equations, namely:

$$\frac{dn_1}{dt} = -3Hn_1 - \langle \sigma v \rangle_{ann} (n_1^2 - n_{1,0}^2) - \langle \sigma v \rangle_{coa} (n_1\, n_2 - n_{1,0}\, n_{2,0})$$
$$\frac{dn_2}{dt} = -3Hn_2 - \langle \sigma v \rangle_{ann} (n_2^2 - n_{2,0}^2) - \langle \sigma v \rangle_{coa} (n_1\, n_2 - n_{1,0}\, n_{2,0})$$

where $n_{i,0}$ denotes the equilibrium distribution of the i particle.

Since d_2 is non-relativistic before d_1, its equilibrium distribution is also Boltzmann suppressed. Hence the efficiency of coannihilations can be estimated by comparing the coannihilation rate with the annihilation rate:

$$\begin{aligned} \frac{\Gamma_{ann}}{\Gamma_{coann}} &= \frac{\langle \sigma v \rangle_{ann}}{\langle \sigma v \rangle_{coa}}\ \frac{n_1}{n_2} \\ &= \frac{\langle \sigma v \rangle_{ann}}{\langle \sigma v \rangle_{coa}}\ \frac{m_{d_1}}{m_{d_2}}\ e^{-\beta(m_{d_2} - m_{d_1})} \end{aligned} \tag{77}$$

indicating that the difference of mass $\Delta m = m_{d_2} - m_{d_1}$ plays a fundamental role. When the difference is too large, there are not enough d_2 to coannihilate with and the annihilations are dominant. However, this strongly depends on the ratio of the annihilation and coannihilation cross sections. Indeed, if d_1

and d_2 interact very strongly and if the lifetime of the d_2 particle is long enough, the prohibitive effect of a large mass difference can be compensated by the strong interactions. By making coannihilations more important than annihilations, one can ensure the correct the relic density while avoiding to directly constrain the dark matter mass. The “nice” effect of coannihilations is therefore to allow for larger values of the dark matter mass, as shown in Fig. 2.4 for coannihilations of stops with neutralinos LSP [41].

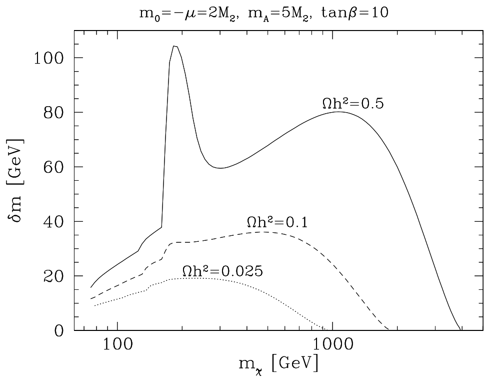

Another effect is associated with the possibility of having resonant s-channel. If the mass of the exchanged particle in the propagator of a s-channel dark matter pair annihialtion diagramm is about half the dark matter mass, the annihilation cross section becomes much larger than previously expected. This is handy as one can then consider smaller dark matter couplings and a larger dark matter mass. Note that one can extend this concept of resonance to composite or excited state particles.

At last, there is another effect called focus point. It is valid in supersymmetry and denote a situation where the neutralino (i.e. in this case the dark matter) and the chargino are mass degenerated [42].

2.5 Direct detection

The rotation curves of galaxies indicate that dark matter particles are distributed in a (almost) spherical halo, surrounding the galactic disk. This characteristic opens up a window on the dark sector since it means that dark matter particles could be detected either directly or indirectly.

Depending on the strength of their interactions, dark matter particles may significantly interact with the protons (and potentially electrons) of a detector and yield a visible signature such as e.g. heat, recoil energy, heat. Such a possibility of direct detection was first proposed by Goodman and Witten in 1985 (based on a work by Druckier and Stodolski) and is still relevant nowadays.

One can give a rough estimate of the number of events dn that could be seen by a detector of a given size, as follows:

$$\boxed{dn = \text{number of interactions} \times \mathrm{dS} \times \mathrm{dt}}$$

where dS is the surface of the detector and dt the time scale of observation. The number of interactions in the detector depends on the interaction cross section between dark matter and the protons or electrons $\sigma_{dm-p,e}$, the number density of dark matter n_{dm} and that of protons or electrons $n_{p,e}$:

$$\text{number of interactions} = \sigma_{\mathrm{dm-p,e}} \times \mathrm{n_{dm}} \times \mathrm{n_{p,e}} \times \text{detector size}.$$

The number density n_p (i.e. the number of protons per unit of volume of the detector) is equal to:

$$n_p = \frac{Z}{A} \frac{\rho_{material}}{m_p}$$

where we have disregarded the interactions with electrons. That is,

$$n_p = \frac{Z}{A} \frac{M_{material}}{\mathrm{Volume} \times \mathrm{m_p}}$$

leading to a number of events:

$$dn = \sigma_{dm-p,e}\ n_{dm}\ \frac{Z}{A}\ \mathcal{N}_a \frac{M_{material}}{\mathrm{Volume} \times \mathrm{m_p}} \times \text{detector size} \times \mathrm{dS} \times \mathrm{dt}$$

which (noticing that $dS \times$ detector size $\simeq$ volume) gives:

$$\boxed{dn = \sigma_{dm-p,e}\ n_{dm}\ \frac{Z}{A}\ \mathcal{N}_a\ \frac{M_{material}}{m_p} \times dt}$$

with $\mathcal{N}_a$ the number of Avogadro. Therefore one readily sees that the number of events that is to be expected in the detector depends strongly on:

1. the ability of dark matter to interact with the protons (or electrons) of the detector,
2. the dark matter number density (that is the dark matter local energy density in the halo and its mass)
3. the mass of material constituting the detector
4. the time scale of observation

There are different possible signatures of dark matter interactions with protons and electrons inside the detector. Dark matter can induce a nucleus recoil, heat, ionization, scintillation and generate photons in crystals. Most of the experiments generally try to detect the nuclei or electron recoil very precisely so this means that they consider each event as determine whether it is due background particles (e.g. neutrons) which have interacted within the detector or not. However, another technique, consists in cumulating statistics (i.e. number of events, whether they are background events or not) and determining if this cumulative signal is oscillating or not. Oscillations could actually be indeed the indication of dark matter for the following reason:

Dark matter particles have a virialized velocity which is basically equal to the sun velocity. However the earth is revolving around the sun with a velocity

$$\boxed{v_{\oplus} = v_{\odot} + v_{orb}\ \cos\gamma\ \cos[w(t-t_0)]}$$

with $\gamma = 60°$ the inclination of the Earth orbital plane with respect with the galactic plane, v_{orb} the Earth orbital velocity, $w = 2\pi/365$rad/day and t_0 corresponding to half a year, that is coinciding with the 2nd of June. Hence, not only should one detect an oscillation but the period of oscillation should also correspond to the 2nd of June. The DAMA/LIBRA [43] (based on a NaI cristal) claims since 1998 that they have detected such a modulation signal. However it remains to be understood whether such a signal is indeed due to dark matter particles or not.

In this respect, the results of other experiments based on different material and not looking for the annual modulation are important. None of the other experiments indeed detected a positive signal. The absence of nuclear recoil or anomalous electron events in e.g. Edelweiss [44], CDMS [45], CRESST [46], COUPP, XENON experiments have enables experimentalists to constrain the dark matter interaction cross sections. However, one can distinguish two kind of dark matter interactions: those sensitive to the spin of the nuclei of the material detector and those which are not. The former involve a γ_5 matrix which is sensitive to the spin of the particles dark matter interact with (and which therefore generates coherent interactions) while the latter are not. Experiments can therefore set constraints on dark matter spin-dependent and spin-independent cross sections. Latest results enable to exclude dark matter spin-independent interactions with protons larger than $\sigma_{SI} \geq 6 \times 10^{-44}$cm^2 for particles of 10-a few 100 GeV and spin-dependent cross sections of $\sigma_{SI} \geq 10^{-36}$cm^2. These limits are displayed in the following figures:

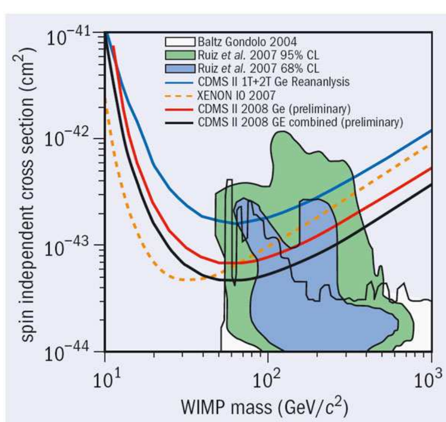

The reason why such detectors are insensitive to masses smaller than a few GeV is that the recoil is too small to be detected. Also limits are not good for very heavy particles (TeV) because the number

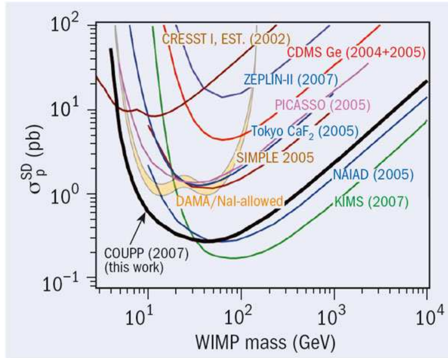

density of dark matter becomes very small and the number of events is suppressed accordingly meaning that the constraint on the cross section scales with the dark matter mass.

2.6 Indirect detection

Another way of detecting dark matter is to focus on its annihilations (or very slow decay) into standard model particles and consider these particles as messengers. For example any dark matter particles heavier than 511 keV could (if it is its own anti particle or if there is no asymmetry between the number densities of dark matter and its anti particle) produce a pair electron-positron. Depending on the dark matter annihilation or decay rate, the electrons and positrons can be significantly produced and detectable nowadays.

To determine, however, whether this is the case or not, one has to compute the flux that can be received on earth.

2.6.1 "Bare" flux calculations

Let consider that dark matter annihilates into X particles directly, namely $dmdm \to X\bar{X}, XX$ and that there is no propagation at all of the X particles nor any other particle produced. Let us also disregard the decaying dark matter scenario but similar calculations can be done. The flux of X particles that we can detect on earth is then basically given by the integral over the line of sight (passing through the region of emission of the X particles) of the number of X particles which have been produced by the dark matter, namely:

$$\phi_X = \int dl.o.s \, \frac{dn_X}{dt}.$$

The number of X particles produced by dark matter particles per unit of time is given by the Boltzmann equation, namely:

$$\frac{dn_X}{dt} = -g \, \frac{dn_{dm}}{dt} = g \, \sigma v \, n_{dm}^2.$$

in which we have neglected the effect of expansion (since it is negligible in a galaxy or in a cluster of galaxies) and the equilibrium distribution since dark matter left chemical equilibrium at freeze-out, implying that the dark matter number density is greater than what it should be according to the equilibrium density. The factor g accounts for the number of X produced by the dark matter. Therefore we obtain that the flux is proportional to:

$$\phi_X = g \int dl.o.s \, \sigma v \, n_{dm}^2. \tag{78}$$

Calling $dl = dl.o.s$ and using the definition of the dark matter number density: $\rho_{dm} = n_{dm} \times m_{dm}$, we have:

$$\phi_x = g \int dl \, \sigma v \, \left(\frac{\rho_{dm}}{m_{dm}}\right)^2.$$

We can now use the parametrization of the dark matter halo profile that is obtained from the rotation curves of galaxies [47]:

$$\boxed{\rho_{dm} = \frac{\rho_0}{\left(\frac{r}{r_s}\right)^{\gamma}\ \left(1+\left(\frac{r}{r_s}\right)^{\alpha}\right)^{\frac{(\beta-\gamma)}{\alpha}}}}$$

Note that at large radius from the galactic centre ($r > r_s$), the profile behaves as $\rho_{dm} = \rho_0 \left(\frac{r_s}{r}\right)^{\beta}$ while at small distance it is proportional to $\rho_{dm} = \rho_0 \left(\frac{r_s}{r}\right)^{\gamma}$. Numerical simulations agree well on the shape of the outer profile. Indeed, they all agree that β 3. However, the shape of the inner profile is much more discussed since finding the slope of the profile close to the centre requires a very high resolution.

To understand the origin of this radial dependence, it is illuminating to compute the relation between the dark matter halo profile and the dark matter rotation velocity:

$$v^2(r) = \frac{2\ G\ M(r)}{r}$$

The energy density (mass per volume) is given by:

$$M(r) = 4\ \pi \int^{r} dx\ x^2\ \rho_{dm}(x).$$

Therefore, we have (assuming a spherical halo)

$$v^2(r) = \frac{8\ \pi\ G\ \int^{r} dx\ x^2\ \rho_{dm}(x)}{r}$$

One readily sees that when $\rho_{dm}(x) \sim 1/x^3$ (corresponding to the outer region, $r > r_s$, where the dark matter halo is about to decline), the rotation velocity is almost constant. In the intermediate region (where the presence of baryonic matter is not enough to explain the rotation curve), the velocity rotation is flat, yielding $\rho_{dm}(x) \propto 1/x^2$ and, in the inner region, $\rho_{dm}(x) \sim 1/x$. However, numerically, inner profiles can be as steep as $\rho_{dm}(x) \sim 1/x^2$. The most common profile in the literature is the NFW profile ($\rho_{dm}(x) \sim 1/x$ in the inner part but there is also the Moore profile $\rho_{dm}(x) \sim 1/x^{1.5}$ or adiabatic contraction profiles $\rho_{dm}(x) \sim 1/x^2$).

We finally obtain for the flux of X particles obtained from a dark matter halo parameterized with this universal function:

$$\phi_X = g_X \int dl\ \sigma v\ \left(\frac{\rho_0}{m_{dm}}\right)^2 \left(\frac{r}{r_s}\right)^{-2\gamma} \left(1+\left(\frac{r}{r_s}\right)^{\alpha}\right)^{-2\frac{(\beta-\gamma)}{\alpha}} \tag{79}$$

which is well approximated by:

$$\phi_X = g_X \int dl\ \sigma v\ \left(\frac{\rho_0}{m_{dm}}\right)^2 \left(\frac{r}{r_s}\right)^{-2\gamma}$$

since most of the annihilations will take place in the inner part of the galaxy, where the dark matter number density is the largest (that is where dark matter is most concentrated).

It is very easy to perform the integration in Eq. 79, either numerically by replacing the radial dependence of the profile by using

$$r = \sqrt{l^2 + d^2 - 2\,d\,l\,\cos\psi},$$

or analytically, by using the relation:

$$l_{\pm} = d\,\cos\psi \pm \sqrt{r^2 - d^2\,\sin^2\psi}$$

where $a = \sqrt{r^2 - d^2\,\sin^2\psi}$ and where $l_+ = l_-\ + 2a$

$$\int\ dl\ \left[\frac{\rho_{dm}}{\rho_0}\right]^2\ =\ \int_b^{r_m}\ dr \frac{1}{r^{2\gamma-1}\ \sqrt{r^2-b^2}} \tag{80}$$

where $r_m < r_s$ and $b = d\,\sin\psi$. Using now $v^2 = (r^2 - b^2)/b^2$ we find that

$$\int dl \left[\frac{\rho_{dm}}{\rho_0}\right]^2 = \left(\frac{r_s}{b}\right)^{2\gamma} b \int_0^{\frac{\sqrt{(r_m^2-b^2)}}{b}} \frac{dv}{(1+v^2)^{2\,\gamma/2}}$$
$$= \left(\frac{r_m}{b}\right)^{2\gamma} b \left[I_\gamma(v)\right]_0^{\frac{\sqrt{(r_m^2-b^2)}}{b}}$$

For $\gamma = 1$ (NFW profile), we obtain that:

$$[I_1]_0^{\frac{\sqrt{(r_s^2-b^2)}}{b}} = \arctan\left(\frac{\sqrt{r_m^2-b^2}}{b}\right),$$

that is

$$I_1 \simeq \arctan\left(\frac{\sqrt{r_s^2-b^2}}{b}\right)$$

(setting $r_m \sim r_s$). Therefore the flux is given by:

$$\phi_X = g_X\,\sigma v \left(\frac{\rho_0}{m_{dm}}\right)^2 \left(\frac{r_s}{d}\right)^2 \left(\frac{d}{\sin\psi}\right)$$
$$\arctan\left(\frac{\sqrt{r_s^2-(d\sin\psi)^2}}{(d\sin\psi)}\right).$$

Since a realistic experiment has a given resolution δ, one has to average the inverse of $\sin\psi$ (when one takes into account the experimental resolution, the relevant quantity is $\sin\psi \to \sin(\psi+\zeta)$) over $\zeta = \pm\delta$. Assuming that the line of sight passes through the cluster we find that the expected flux is about:

$$\begin{aligned}
\phi_X &= g_X\;\sigma v \left(\frac{\rho_0}{m_{dm}}\right)^2 \left(\frac{r_s}{d}\right)^2 \\
&\quad \int_{-\delta}^{\delta} d\zeta \left(\frac{d}{\sin\zeta}\right) \arctan\left(\frac{\sqrt{r_s^2-(d\sin\zeta)^2}}{(d\sin\zeta)}\right), \\
&\overset{\zeta\to 0}{=} g\;\sigma v \left(\frac{\rho_0}{m_{dm}}\right)^2 \left(\frac{r_s}{d}\right)^2 \\
&\quad \int_{-\delta}^{\delta} d\zeta \left(\frac{d}{\zeta}\right) \arctan\left(\frac{\sqrt{r_s^2-d^2\zeta^2}}{(d\;\zeta)}\right), \\
&\overset{\zeta\to 0}{=} g\;\sigma v \left(\frac{\rho_0}{m_{dm}}\right)^2 \left(\frac{r_s}{d}\right)^2 \\
&\quad \left[d\;\zeta\;\arctan\left(\frac{\sqrt{r_s^2-d^2\zeta^2}}{d\;\zeta}\right) - \sqrt{r_s^2-d^2\;\zeta^2}\right]_{-\delta}^{+\delta}
\end{aligned}$$

Hence, after calculations, one obtains that the flux of X particles:

$$\boxed{\phi_X \simeq g_X\;\sigma v\;\left(\frac{\rho_0}{m_{dm}}\right)^2 \left(\frac{r_s}{d}\right)^2 \left[d\;\zeta\;\arctan\left(\frac{\sqrt{r_s^2-d^2\zeta^2}}{d\;\zeta}\right)\right]_{-\delta}^{+\delta}}$$

For example, if X is produced in the galactic centre (which is located at a distance $d \simeq 8.5$ kpc from the Earth), one has:

$$\begin{aligned}
\phi_X &\simeq 6\times 10^{-5}/\mathrm{cm}^2/\mathrm{s}\left(\frac{\sigma \mathrm{v}}{10^{-26}\mathrm{cm}^3/\mathrm{s}}\right)\left(\frac{\rho_0}{0.3\mathrm{GeV/cm}^3}\right)^2 \\
&\quad \times \frac{g_X}{2} \times \left(\frac{m_{dm}}{\mathrm{GeV}}\right)^{-2} \times \left(\frac{r_s}{8.5\mathrm{kpc}}\right)^2 \times \left(\frac{d}{8.5\mathrm{kpc}}\right)^{-1}
\end{aligned}$$

$$\times \left[\zeta \ \arctan\left(\frac{\sqrt{r_s^2 - d^2\zeta^2}}{d\ \zeta}\right)\right]_{-\delta}^{+\delta} \tag{81}$$

$$\tag{82}$$

2.6.2 Bare neutrino flux calculations

Let us now consider the case of neutrinos produced by dark matter annihilations. The neutrino losses are negligible. Hence neutrinos can freely propagate from the source to the Earth. However, to claim detection of a neutrino flux, one has to look for charged particles. In particular, one expects neutrino to convert into muons inside the Earth (so neutral invisible particles, the neutrinos, turn into charged visible particles,the muons, making detection possible).

This conversion mechanism is sensitive to the inelastic scattering cross section $\nu N \to \mu X$ and the number density of nuclei. Besides one has to take into account the losses of the muons inside the Earth. Indeed, a muon which has been created by the reaction $\nu N \to \mu X$ can only be detected if the distance between the place of creation and the detector is small compared to the mean distance that a muon can travel despite its energy losses. This conversion process and the losses thus imply that the flux of converted muons (i.e. the flux of neutrinos which have been transformed into muons) is about

$$\boxed{\phi_\nu \simeq \mathcal{R} \ \times \ \phi_X}$$

with the conversion factor $\mathcal{R}$ of about $\mathcal{R} \ \approx \ 10^{-9}$.

2.6.3 Simplified cosmic ray flux calculations

To compute the flux of positrons, electrons, proton, anti proton generated by dark matter annihilation or decay, we now have to account for the energy losses of the primary cosmic rays produced by dark matter.

$$\boxed{\tfrac{d}{dE}\phi(E)_{cr} = \int dl \ \sigma v \ n_{dm}^2 \times boost \times BR(cr) \times B(E),}$$

where the word boost reflects the possibility that inhomogeneities (namely dark matter clumps) exist in the dark matter halo and $BR(cr)$ is the Branching ratio $\sigma v(cr)/\sigma v_{tot}$ and $B(E)$ is a function of the energy that we shall define. This formula is very similar to the expression Eq. 78 for the flux of photons. However the term $B(E)$ is of crucial importance since it reveals how the flux depends on energy.

To understand the origin of this term, one has to understand that the dark matter annihilates and produces particles with an initial energy $E = m_{dm}$ (assuming that the two particles in the final state are anti particles). These particles eventually lose their energy while propagating in the medium. This is described by the transport (or propagation) equation:

$$\partial_t N(E,r) = K(E)\nabla^2 N(E,r) + \partial_E \left(b(E)N(E,r)\right) + \mathcal{Q}(E,r). \tag{83}$$

Neglecting the spatial propagation and assuming a stationary regime, this equation simplifies and reads:

$$\frac{\partial}{\partial E}[\ b(E)\ N(E,r)] = Q(E,r),$$

with $Q(E,r) = \sigma v \ n_{\rm dm}(r)^2 \ \mathcal{X}(E)$ and $\mathcal{X}(E)$ a function that can be defined as:

$$\mathcal{X}^p(E) = \delta(E - m_{\rm dm})$$

if the cosmic rays are produced directly by dark matter annihilations and

$$\mathcal{X}^s(E) = \left(\frac{E}{E_0}\right)^{-m} \quad \Theta(m_{\rm dm} - E)$$

or

$$\mathcal{X}^s(E) = \left(\frac{E}{E_0}\right)^{-m} \quad e^{-aE}$$

We thus have:

$$N(E,r) = \frac{1}{b(E)} \int^E dx\ Q(x,r)$$

or, replacing $Q(E,r)$ by its expression,

$$N(E,r) = \frac{\sigma v\ n_{\rm dm}(r)^2}{b(E)} \int^E dE'\ \mathcal{X}^{p,s}(E').$$

The above expression defines the function $B(E)$ that we previously introduced, namely:

$$\boxed{B(E) = \tfrac{1}{b(E)} \int^E dE'\ \mathcal{X}^{p,s}(E')}$$

with $b(E) = dE/dt$ the loss term:

$$\begin{aligned} b(E) &\equiv -\frac{dE}{dt} \\ &= b_{\rm IC}(E) + b_{\rm sync}(E) + b_{\rm brem}(E) + b_{\rm coul}(E) \end{aligned}$$

with:

$$\begin{aligned} b_{IC}(E) &\simeq 7\ 10^{-21}\ \gamma^2\ (1+z)^4\ \text{MeV/s} \\ b_{syn}(E) &= 6.6\ 10^{-22}\ \gamma^2 \left(\frac{B}{1\ \mu\text{G}}\right)^2\ \text{MeV/s} \\ b_{Coul}(E) &\approx 8.18\ 10^{-15} \left(\frac{n_e}{\text{cm}^{-3}}\right)\ [75 + \ln(\gamma/n_e)]\ \text{MeV/s} \end{aligned}$$

and $\gamma = \frac{E}{m_e c^2}$. Therefore, if it is possible to neglect the spatial propagation of the cosmic rays, one can write the flux simply as

$$\boxed{\begin{gathered} \tfrac{d}{dE}\phi(E)_{cr} = \phi \times boost \times BR(cr) \times B(E), \\ \text{with} \\ \phi = \sigma v\ \left(\tfrac{\rho_0}{m_{dm}}\right)^2\ \left(\tfrac{r_s}{d}\right)^2 \left[d\ \zeta\ \arctan\left(\tfrac{\sqrt{r_m^2 - d^2\zeta^2}}{d\ \zeta}\right)\right]_{-\delta}^{+\delta} \end{gathered}}$$

2.6.4 Experimental signatures and results

We saw how to compute the flux for the different messengers. One, of course, has to make sure that the dark matter contribution to cosmic ray fluxes is significant enough so that the ratio signal to noise for indirect detection experiments is not too small. For example, the gamma ray flux originating from direct dark matter annihilations into two photons in our galaxy (assuming no boost factor) is about

$$\begin{aligned} \phi_X \quad &\simeq \quad 2.1 \times 10^{-10}/\text{cm}^2/\text{s} \times \left(\frac{\sigma \text{v}}{10^{-26}\text{cm}^3/\text{s}}\right) \left(\frac{\rho_0}{0.3\text{GeV}}\right)^2 \\ &\times \left(\frac{m_{dm}}{100\ \text{GeV}}\right)^{-2} \left(\frac{r_s}{16\text{kpc}}\right)^2 \left(\frac{d}{8.5\text{kpc}}\right)^{-1} \\ &\times \left[\zeta\ \arctan\left(\frac{\sqrt{r_s^2 - d^2\zeta^2}}{d\ \zeta}\right)\right]_{\zeta=-\delta}^{\zeta=+\delta} \end{aligned}$$

where we make use of Eq. 81. Therefore the expected photon flux in a NFW profile is about 10^{-10}photons/cm^2/s for a dark matter particle of 100 GeV, the maximum allowed annihilation cross section in two photons in supersymmetry (namely 10^{-28}cm^3/s) and $r_s = 16$ kpc.

This flux is too low to be detected. Therefore, it is often postulated that our galaxy contains clumps of dark matter particles, i.e. regions where the dark matter is very concentrated. The existence of clumps boost the above flux by an overall factor called "boost" factor which can be very large (assuming no propagation). The existence of boost factors can be modelized but the value of the boost thus generated is still under debate and depends on the type of messengers. The inclusion of a boost factor is much more subtle if one considers propagation. In this case, the boost factors for different messengers can be very different.

Experimentally, no signal in favour of the existence of dark matter particles has been clearly identified. There is a small excess of gamma rays detected by EGRET in the 10-20 GeV range and, perhaps, more importantly in the positron fraction as seen by HEAT and PAMELA. However, it is difficult to reconcile the excess of positrons with the absence of an excess in anti-protons and gamma rays unless the source is already included in the gamma ray background. Therefore the excess of positron could be due to an astrophysical source emitting in gamma rays such as a pulsar. It is important to note, nevertheless, that the fraction of positrons is defined as $r_{e^+} = n_{e^+}/(n_{e^-} + n_{e^+})$. This ratio is therefore very dependent on the number of electrons and an excess in positrons is hard to disentangle from an error on the number of electrons if one does not have the electron and positron fluxes separately (which is the present situation although PAMELA should soon release these fluxes).

2.7 Structure formation

As we have already mentioned if DM is made of particles, it must not be charged. This does not mean that dark matter should not have any interactions. To determine the type of interactions that dark matter can undergo, one has to consider both the free-streaming and self-damping scale.

The free-streaming scale is associated to the free-propagation of the dark matter particles, that is when dark matter stops interacting with other species. The scale on which the primordial matter fluctuations are washed out then depends on the dark matter velocity v_{dm} after its thermal decoupling. This velocity is determined by the temperature at which the dark matter becomes non relativistic and depends, in addition, on whether the Universe is dominated by matter or radiation when this transition happen. Hence the main ingredients to compute the free-streaming length are the temperatures corresponding to [48, 49]:

- the dark matter thermal decoupling (T_{dec}),
- the non-relativistic transition (T_{nr}),
- the matter-radiation equality (T_{eq}).

These are therefore three different times that can be ordered as follows:

- $T_{nr} > T_{dec} > T_{eq}$
- $T_{dec} > T_{nr} > T_{eq}$
- $T_{nr} > T_{eq} > T_{dec}$
- $T_{dec} > T_{eq} > T_{nr}$
- $T_{eq} > T_{nr} > T_{dec}$
- $T_{eq} > T_{dec} > T_{nr}$

defining six distinct types of dark matter particles. For example, the first category ($T_{nr} > T_{dec} > T_{eq}$) corresponds to particles which first become non-relativistic, then decouple and finall pass the equality. This type of dark matter candidate correspond typically to Cold Dark Matter (CDM) candidates because they are "cold" (non relativistic) when they thermally decouple. Examples of CDM are the lightest supersymmetric particle in the Minimal Supersymmetric Standard Model (MSSM), namely the lightest neutralino. The second type ($T_{dec} > T_{nr} > T_{eq}$) corresponds to Hot Dark Matter (HDM) particles because they are hot (relativistic) when they thermally decouple. For example, massive neutrinos with a mass of 10 eV are candidates of HDM. Ordinary neutrinos having a mass of less than 1 eV (and decoupling at $T_{dec} \simeq 1$ MeV) are included in the 4th category ($T_{dec} > T_{eq} > T_{nr}$) and so on.

For each of these categories, it is easy to compute the free-streaming (and self-damping) length of the dark matter candidates and compare it with the size of the smallest fluctuations that have been observed. If the free-streaming length l is greater than the size of the smallest fluctuations which have been observed, the candidate is ruled out. Indeed such a particle would predict the absence of matter fluctuations of size below a size l while such fluctuations exist. If the free-streaming scale l is much smaller than the scale of observations l_{obs}, all fluctuations greater than l exist and the candidate is allowed. If $l \simeq l_{obs}$, then better observations (aiming at probing smaller size fluctuations) will be decisive in saying whether such a candidate is allowed or not. This case is referred to as Warm Dark Matter.

One can report the calculation of the six damping lengths on a graph (interaction rate vs mass). The interaction rate is basically determined by T_{dec} while the mass corresponds to T_{nr}, see Fig. 2.7. The exclusion line separates HDM from CDM (CDM particles are located on the right; HDM on the left of the exclusion line). The particles located on the edge of the exclusion line are examples of WDM particles. One readily sees that WDM or CDM particles can be collisional or collisionless. In some cases, the particles can even have extremely strong "self"-interactions and an acceptable free-streaming length (but one has then to worry about their collisional damping length).

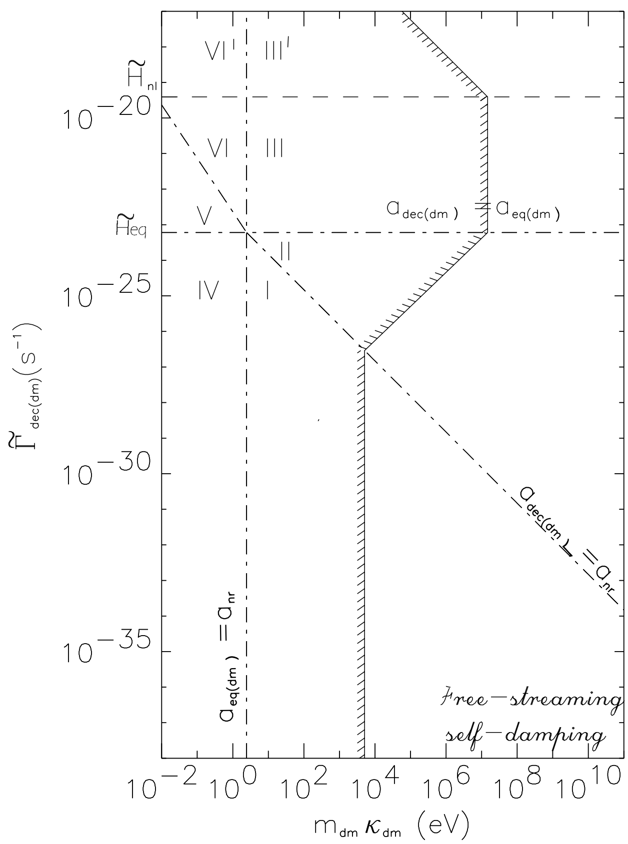

The collisional length is more tricky to compute. It corresponds to the damping that is experienced by dark matter during the time where dark matter is coupled to various species. If the particles to which dark matter is coupled to are relativistic (or semi-relativistic) and if the coupling is significant, dark matter will tend to follow these particles outside the fluctuations. This is called collisional damping. If, in addition, the particle to which dark matter is coupled to is decoupled from all other species and is not tightly coupled to dark matter, it may experience free-streaming. In this case, the dark matter experiences the free-streaming of this particle and dark matter primordial fluctuations are washed out. This is called "mixed" damping as it mixes the dark matter collisional damping with the free-streaming of the particle to which dark matter is coupled to. This case, in fact, illustrates that the interaction rate (cross section times number density) has to be well defined for each particle and is not equal for two particles in interaction since it depends on the number density of the species involved. For example if two species (s_i and s_j) interact, the interaction rate of species s_i, i.e. $\Gamma_{s_i} \simeq (\sigma v)_{ij} \times n_j$ while for s_j, we have $\Gamma_{s_j} \simeq (\sigma v)_{ij} \times n_i$. Here we have, in fact, neglected other factors which correspond to the energy transmitted during the collisions but there are neglected in the above expressions of the collision rate.

Computing the collisional damping scale is not easy but has been done for generic candidates. The most important points are that, even very large dark matter interactions with photons (i.e. cross sections as large as 10^{-30}cm^2) are compatible with structure formation observations and neutrino-dark matter interactions may lead to a large mixed damping effect for MeV particles with weak-strength cross sections. Such a case is in fact the illustration that even "ordinary" WIMPs could experience large damping effects and have a cut-off in their matter power spectra at cosmological scales [50]. This is important to keep in mind since such a cut-off may solve the so-called dark matter crisis (i.e. the discrepancy between CDM numerical simulations which predict many small objects and their non observations, although possible explanation might be that they are to detect since these are "dark" objects). In addition, they show that it may be dangerous to consider that a good dark matter candidate is collisionless. Although, weak interactions cannot be implemented in numerical simulations, the damping that they may generate in the *linear* matter power spectrum should absolutely be considered when computing the non-linear matter power spectrum.

2.8 Conclusion

The nature of dark matter is a fascinating problem. We have no real indication that dark matter is made of new (non-baryonic) particles despite the many experimental efforts to detect either directly or indirectly dark matter particles and some strong phenomenological arguments (such as the Silk damping, CMB observations, BBN predictions and the rotation curves of galaxies). Mean while works on scenarios of modification of gravity progress and seem to describe well (or at least quite well) the physics that we see although, so far, they also fail to overcome the Silk damping at small angular scales. The next few years are going to be very exciting. With the advent of e.g. GLAST, LHC and the already-running experiments (PAMELA and dark matter direct detection experiments) and perhaps new techniques (for example weak gravitational lensing maps of the dark matter distribution in merged clusters), we may perhaps not discover what is the nature of dark matter but we should definitely rule out many possibilities. Whether the parameter space which would be left will correspond to particles (WDM/CDM or thermal/non thermal) or a modification of gravity will be in any case of great interest for the quest of new physics.

3 Dark energy (Julien Lesgourgues)

We have seen that the measurement of the luminosity distance and angular diameter distance versus redhsift relations (using supernovae, CMB and BAO) indicate that the universe is currently accelerating. What does this mean exactly in terms of total density and pressure?

Using the time-derivative of the Friedman equation (3) and the energy conservation equation (4), we see that

$$\frac{\ddot{a}}{a} = -\frac{4\pi\mathcal{G}}{3}(\rho + 3p) \ . \tag{84}$$

Now, let us assume that the universe expansion is affected today both by non-relativistic matter (baryons and dark matter) with energy density ρ_M and zero pressure, and by dark energy with energy density ρ_{DE} and an unknown pressure p_{DE}. Using the last equation, the condition that the universe is accelerating reads

$$\ddot{a} > 0 \qquad \Longleftrightarrow \qquad p_{DE} < -\frac{\rho_M + \rho_{DE}}{3} \ . \tag{85}$$

The energy density ρ_M is positive. So, the above condition implies

$$p_{DE} < -\frac{\rho_{DE}}{3} \ . \tag{86}$$

We see that the Universe can accelerate only if it contains a dark energy component with $p_{DE} < -\rho_{DE}/3$. A positive cosmological constant fulfills this condition, since $p_\Lambda \equiv -\rho_\Lambda < -\rho_\Lambda/3$. In a more general case, let us assume that the universe contains a dark energy fluid obeying to a constant equation of state $p_{DE} = w\,\rho_{DE}$. Using known physical principles, w cannot be arbitrary. General relativity implies a so-called "weak energy condition" stating that for all fluids, $\rho_{DE} \geq 0$ and $(\rho_{DE} + p_{DE}) \geq 0$. This condition might be violated in non-standard physical theories that we will not consider here. The weak energy condition implies that $w \geq -1$. This is compatible with the Universe acceleration: one should simply have a component with pressure

$$-\rho_{DE} \leq p_{DE} < -\frac{(\rho_M + \rho_{DE})}{3} \qquad \Longleftrightarrow \qquad -1 \leq w < -\frac{1}{3}\left(1 + \frac{\Omega_M}{\Omega_{DE}}\right) \ . \tag{87}$$

Let us emphasize that $w = -1$ corresponds to a constant dark energy density, which is identical to a cosmological constant; $w > -1$ corresponds to a slowly diluting dark energy component; while $w < -1$, the situation which violates the weak energy condition, would correspond to a dark energy density increasing with time. As we shall see in section 3.2, the current value of w can be probed by observations, and is already constrained to be very close to -1.

3.1 Possible theoretical models for Dark Energy

3.1.1 Vacuum energy

In the Standard Model (SM) of particles physics, the vacuum energy is defined as the energy density of the fundamental state, which minimizes the Hamiltonian, and in particular, the potential V of the scalar field(s) present in the theory, namely: the Higgs field(s). Actually, the value of the potential at the minimum does not play a role in the SM. Adding a constant to V would not change physical predictions. What really matters in the SM is differences ΔV between the potential energy before and after a phase transition. For instance, during the Electro-Weak (WE) phase transition (responsible for the Higgs mechanism which gives a mass to the quarks), it is well-known that the potential $V(\phi)$ of the (complex) Higgs field ϕ evolves from a quadratic shape to a mexican hat shape; the Higgs field leaves the initial vacuum located at $\phi = 0$ for a new vacuum corresponding to a circle in the complex plane; during this process, in order to have successful predictions concerning particle masses after the EW transition, the vacuum energy should change by $\Delta V \sim M_{EW}^4$, where $M_{EW} \sim 250$ GeV is the EW scale.

Since SM predictions depend only on potential differences, the vacuum energy $V_{\rm min}$ is arbitrary in this model. One could then argue that this value can be easily chosen in such way that today $\Omega_\Lambda = V^0_{\rm min}/\rho^0_c = 0.7$. However, what appears as highly unnatural is that if we fix $V_{\rm min}$ before the EW phase transition, we should fine-tune it with a highly unrealistic precision to a value $V_{\rm min} \sim M_{EW}^4 \sim (250 \text{ GeV})^4$ such that $(V_{\rm min} - \Delta V) \sim \Omega_\Lambda \rho_c^0 \sim (10^{-3}\text{GeV})^4$. In order to ensure such a cancellation, one should play with the 26th digit of $V_{\rm min}$ when fixing it before the transition!!

This problem sounds even more unnatural if we keep in mind that before the EW symmetry breaking, there were other spontaneous symmetry breaking mechanisms at higher energy, e.g. that of the Grand

Unified Theory (GUT). Hence, in the very early universe, the value of $V_{\rm min}$ in the SM should be tuned with incredible precision.

The fact that the vacuum density in the SM can be defined arbitrarily is also related to the structure of Quantum Field Theory. The quantum description of e.g. scalar fields is such that the vacuum energy is obtained by integrating the fundamental energy of a Fourier mode, $\sqrt{k^2+m^2}$, over all Fourier modes, leading to

$$\rho_{vac} = \frac{1}{2}\int_0^{k_{max}} \frac{d^3k}{(2\pi)^3}\sqrt{k^2+m^2} \propto \int_0^{k_{max}} k^3 dk \propto k_{max}^4 \; , \tag{88}$$

where k_{max} is supposed to be the largest k (i.e. the smallest wavelength) to be included in this theory. This is the famous "ultraviolet divergence" of quantum field theory. In the limit $k_{max} \longrightarrow \infty$, the vacuum energy would be infinite; however, it is usually argued that ordinary QFT does not apply to wavelengths smaller than the Planck length λ_P, for which gravity should become a quantum theory. Hence, the cut-off of ordinary QFT is $k_{max} \sim \lambda_P^{-1} \sim M_P \sim 12 \times 10^{19}$GeV, in units where $c = \hbar = k_B = 1$. So, the vacuum energy is naively expected to be of the order of $\rho_{vac} \sim (10^{19}\text{GeV})^4$. If this was true, the universe would contain a huge cosmological constant, at odds with observations (the universe would be dominated by the cosmological constant right from the beginning, there would be no radiation domination, no phase transitions, just nothing...) hence, it is usually argued that one should use normal ordering and introduce counter terms in the theory, in order to cancel the ultraviolet divergence. In order to arrange for a tiny cosmological constant, the counter terms should be tuned to a value close to M_P^4, with an incredible tuning such that $\rho_{vac} \sim (10^{-3}\text{GeV})^4$.

The SM models suffers from divergences not only in the vacuum energy, but also in the mass e.g. of the Higgs field. This was one of the main motivations for introducing an extension of the SM called supersymmetry (SUSY), in which there are cancellations between the contribution of the SM fields to the divergences, and those of symmetric fields called the superpartners of SM fields. As long as supersymmetry is unbroken, the cancellations are exact, leading in particular to zero vacuum energy (i.e., in the fundamental state of the theory, $V_{min} = 0$). Note that in SUSY, V_{min} is not defined up to a constant like in the SM: in supersymmetric frameworks, V_{min} has an absolute meaning. However, supersymmetry should be broken today. Indeed, if it was not, the superpartners would have the same mass as their SM counterparts, and they should be observed today. In order to push up the superpartner masses to values compatible with observational limits ($M \geq$ TeV), while keeping the desirable features of supersymmetry (absence of divergences in the mass of the Higgs field, etc.), it is necessary to assume that supersymmetry is broken is a particular way (called "soft supersymmetry breaking") such that $V_{min} \sim M_{SUSY}^4$, with $M_{SUSY} \sim 10^3$ GeV. Hence, SUSY alleviates the cosmological constant problem in the sense that the cancellation of terms $\rho_{vac} \sim M_P^4$ is ensured by SUSY; however, one still remains with an embarrassingly high value $V_{min} \sim M_{SUSY}^4$ which has to be almost cancelled with incredible fine-tuning in order to obtain $\rho_{vac} \sim (10^{-3}\text{GeV})^4$ today.

It has been thought for many years that the solution could come from supergravity (SUGRA), a more general theory in which supersymmetry is not just a global symmetry, but a local (gauge) symmetry. In this theory, the vacuum energy receives a contribution from different terms, so that the contribution $V_{min} \sim M_{SUSY}^4$ necessary for soft SUSY breaking could be cancelled by other terms, leading to $\rho_{vac} \ll M_{SUSY}^4$. Still, there is no convincing reason for cancelling V_{min} up to one part in 24 in order to obtain $\rho_{vac} \sim (10^{-3}\text{GeV})^4$ today. In summary, with global SUSY, solving the cosmological constant problem is impossible, while in SUGRA it is unnatural.

There are two proposed solutions to this problem:

- either the SM – or its SUSY or SUGRA extension – is a limit of a more general theory, in which some unknown fundamental properties ensures that today the vacuum energy of particle physics is exactly zero; and at the same time the very small value of the observed cosmological constant, which has nothing to do with the energy scales discussed in this section, is explained by a different mechanism, like e.g. the ones that we shall review in the rest of this course. This is a possibility, but such a "fundamental property" is still unknown (for instance, it seems that string theory does not contain naturally such a mechanism).

- or one invokes a so-called "anthropic argument" (see e.g. [51]). In few words, in modern high-energy theories (like string theory), one frequently obtains a very complicated scalar field potential, depending on a large number of degrees of freedom (as if there were many Higgs fields), and with a huge number of local minima. In these theories, the scalar potential is often called "the landscape", because it has a complicated shape with many mountains, valleys and minima, a bit like a mountain range. In which local minimum is Universe trapped? Each minimum corresponds to a given model of particle physics with some symmetry; a fraction of the minima correspond to our known standard model, with the usual gauge symmetries $U(1)_A \times SU(2)_L \times SU(3)_C$. Hence, we have to leave in one of these minima. However, each minimum also corresponds to a different value of V_{min}: in some cases the Universe would have $V_{min} \gg (10^{-3}\text{GeV})^4$, in some others, $V_{min} \ll (10^{-3}\text{GeV})^4$. The question is to estimate the probability for our Universe to have $V_{min} \sim (10^{-3}\text{GeV})^4$, and to understand whether this is an incredible coincidence or a frequent situation. This issue is difficult, but – although this is still controversial – some people argue that one should use an anthropic argument, namely: we can only leave in a Universe in which life can appear. Hence, we should not compute the probability to have $V_{min} \sim (10^{-3}\text{GeV})^4$ among all possible vacua, but only among those vacua leading to a possible development of alive beings. This argument can be interesting, because in any vacuum such that $V_{min} \gg (10^{-3}\text{GeV})^4$, the universe would have $\Omega_\Lambda \gg 1$; so, during the evolution of the Universe, the cosmological constant would dominate very early, much before today, and even much before the time of equality between radiation and matter. However, if there is no matter dominated stage, there cannot be any significant gravitational clustering; the universe would remain forever very homogeneous, consisting in a soup of particles instead of compact objects, without stars (which are responsible for the formation of heavy elements), and without planets (on which, after a long evolution, complicated molecules can form, and life can develop). Hence, according to the anthropic argument, we should calculate the probability to have $V_{min} \sim (10^{-3}\text{GeV})^4$ among all vacua in which the cosmological constant dominates after a sufficiently long matter dominated stage, i.e., in which $V_{min} \leq (10^{-3}\text{GeV})^4 \times$ (a few). When the problem is posed in this way, the probability to have $V_{min} \sim (10^{-3}\text{GeV})^4$ and $\Omega_\Lambda \sim 1$ is not so small.

In this course, we do not want to make a statement on this anthropic argument. The reader should just be aware of it, and know that part of the high-energy physics community considers this as a satisfactory answer, while the other part criticizes this argument, since this is not a physical prediction in the usual sense.

3.1.2 Topological defects

In the rest of the course, we will assume that the vacuum energy of particle physics is exactly zero (for some unspecified reason), and search a model which could explain the observed acceleration of the universe (i.e. a dark energy component with $\Omega_{DE} \sim 0.7$ and $w \sim -1$).

Do we need to introduce some *ad hoc* component, or does the usual SM of particle physics (and its plausible extensions) already contains objects which could potentially accelerate the universe, i.e., with $-1 \leq w < -1/3$? The answer is yes: without introducing any new sector in the theory, we already have objects with $w < -1/3$ at our disposal.

When a symmetry gets spontaneously broken, the scalar field responsible for the breaking rolls towards a degenerate vacuum, i.e. a vacuum consisting of an ensemble of points with a common energy V_{min}. For instance, after the breaking of a Z_2 symmetry $\phi \longrightarrow -\phi$, the new vacuum consists in two points ϕ_{min} and $-\phi_{min}$. After the breaking of a $U(1)$ symmetry $\phi \longrightarrow e^{i\theta}\phi$, the new vacuum consists in a circle $e^{i\theta}\phi_{min}$. However, there is no reason for the universe to choose the same field value in every part of the observable Universe; we know that in the past, the region which corresponds today to the observable universe was divided in several causal patches (for a physical phenomenon on starting during radiation domination, like a phase transition, the quantity playing the role of the causal horizon is the Hubble radius at that time). On distances larger than the Hubble radius, there is no reason for the universe to choose arbitrarily the same vacuum. Hence, after the breaking of e.g. a Z_2 symmetry, the universe will contain several regions with $\phi = \phi_{min}$ and several other regions with $\phi = -\phi_{min}$. These regions will be separated by two-dimensional surfaces on which a large energy density is concentrated (corresponding to $\Delta V = V|_{\phi=0} - V|_{\phi=\phi_{min}}$. These objects are called domain walls. In the case of a $U(1)$ symmetry, the universe will contain several patches with different phases θ, and topologically stable one-dimensional objects concentrating energy, called cosmic string; along any loop in physical space going around a cosmic string, the phase θ describes a circle in field space.

We know that the vacuum energy cannot be diluted. Similarly, the surface density μ of a domain wall does not dilute during the universe expansion. So, if a comoving volume (e.g. a cube of size R) contains some fraction of a domain wall and nothing else, the total energy in the cube is μR^2, while the volume of the cube is R^3; so, the energy density of the cube is μ/R. If the volume expands, we see that the energy density of this volume evolves like a^{-1}. Using equation (4), this corresponds to an equation of state for the domain wall equal to $w = -2/3$. So, domain walls can potentially accelerate the universe. The same reasoning for a cosmic string (assuming a constant linear density) shows that the energy density of a volume containing a piece of cosmic string evolves like a^{-2}, which gives $w = -1/3$: so, cosmic strings cannot accelerate the universe expansion.

There exist some scenarios in which the universe is filled by a large amount of domain walls, forming a kind of crystal (see e.g. [52, 53]). The density and the separation of these walls can be chosen in such way that they would be almost invisible and still undetected today. However, their energy density can dominate the universe expansion today, with $\Omega_{DE} = 0.7$; such a dark energy component would dilute according to $w = -2/3$. This idea is appealing, but now ruled out, mainly because observational constraints on w exclude the value -2/3, as we shall see in section 3.2.

3.1.3 Scalar field (quintessence)

Let us describe the properties of a canonical scalar field (minimally coupled to gravity), with a Lagrangian

$$\mathcal{L} = \frac{1}{2}\partial_\mu\varphi\partial^\mu\varphi - V(\varphi) \ . \tag{89}$$

If we assume that this field is spatially homogeneous, its density and pressure read

$$\rho = \frac{1}{2}\dot{\varphi}^2 + V(\varphi) \ , \tag{90}$$

$$p = \frac{1}{2}\dot{\varphi}^2 - V(\varphi) \ , \tag{91}$$

so that w can vary between -1 (potential energy dominated field), or +1 (kinetic energy dominated field). The condition for the field to be able to accelerate the universe expansion, $w < -1/3$, is simply equivalent to $\dot{\varphi}^2 < V(\varphi)$. The cosmological constant limit $w = -1$ is approached for $\dot{\varphi}^2 < V(\varphi)$. Note that DE domination today requires that $w \simeq -1$ not just precisely now, but for an extended period of time (roughly, between $z \sim 1$ and now, we must have $w \simeq -1$). A quickly oscillating field would satisfy $\dot{\varphi} = 0$ twice per period, but this would not lead to an extended period of dark energy domination and to any acceleration. The condition $\dot{\varphi}^2 < V(\varphi)$ will hold for a while only if the time-derivative of this condition is also fulfilled, i.e., $|2\dot{\varphi}\ddot{\varphi}| < |\dot{\varphi}V'(\varphi)|$, where V' denotes $dV/d\varphi$. In summary, the scalar field can play the role of dark energy provided that

$$\dot{\varphi}^2 \ll V(\varphi) \qquad \text{and} \qquad |\ddot{\varphi}| \ll |V'(\varphi)| \ . \tag{92}$$

These two inequalities are called the first and second Slow-Roll (SR) conditions.

In general, the dynamics of a homogeneous scalar field in the FLRW universe is governed by the Klein-Gordon equation:

$$\ddot{\varphi} + 3H\dot{\varphi} + V' = 0 \ . \tag{93}$$

As long as the second SR condition holds, this equation reduces to a first-order one: $\dot{\varphi} = -V'/(3H)$. Using this result and the Friedmann equation, and after a few lines of calculation, the two SR conditions can be written as

$$\left(\frac{M_P V'}{V}\right)^2 \ll 1 \qquad \text{and} \qquad \frac{M_P^2 V''}{V} \ll 1 \ . \tag{94}$$

A scalar field playing the role of Dark Energy is usually called “quintessence”.

Fine -tuning issues. If we assume that the scalar field plays the role of dark energy, then today

$$\rho_{DE} \simeq V(\varphi_0) \sim (10^{-3}\text{eV})^4 \ , \tag{95}$$

where the field value today is written as φ_0. The effective mass of the field is defined as $m^2 \equiv V''(\phi_0)$ (then, the scalar potential Taylor-expanded in the vicinity of the field value contains a term $\frac{1}{2}m^2(\varphi - \varphi_0)^2$, i.e. a mass term). So, assuming that the field plays the role of dark energy has a second consequence: according to the second slow-roll condition, the effective mass should be as small as

$$m^2 = V''(\varphi_0) \ll \frac{V(\varphi_0)}{M_P^2} \sim (10^{-33}\text{eV})^2 \tag{96}$$

(this is equivalent to saying that the current effective mass of the field must be smaller than the current value of the Hubble radius, which is indeed $H_0 \sim 10^{-33}$eV). So, any quintessence model should address the following question: why are the potential energy and the effective mass of the field so small today?

These problems are usually very difficult to solve in a natural way. In realistic theories, the natural order of magnitude for V and m is usually much larger. A solution to this fine-tuning problems might be to adopt a run-away potential, i.e. a potential $V > 0$ in which $V \longrightarrow 0$ when $\phi \longrightarrow \infty$. In this case, the field rolls forever towards it minimum located at infinity. For whatever value of the parameters of this potential, we can be sure that sooner or later, V and V'' will become smaller than any particular threshold. So, many quintessence models are based on run-away potentials. But even with these potentials, there is still a puzzling issue: although it is clear that quintessence will dominate at some point, is it natural that it starts to dominate now, i.e. soon after the transition between radiation and matter domination? For an arbitrary run-away potential, the time of dark energy domination could occur much earlier or much later. So, with run-away potentials, we avoid to introduce explicitly some unnaturally small parameters in the model, but we introduce another question called the "cosmic coincidence problem".

Scaling solutions. The cosmic coincidence problem could be solved if there was a necessary reason for which the dark energy density is of the same order of magnitude as the matter density today. A solution to this problem has been invented and called "quintessence with a scaling solution" (see e.g. [54, 55]). The idea is that for some particular form of the potential (that we will derive later on), the dynamics of the quintessence field adapts to the background dynamics of the universe, in such way that the field density is always of the same order as the total density. Note that in the early universe, it should remain slightly smaller than the total density, in order not to modify the usual predictions of BBN or CMB models. So, in scaling solutions, there is an attractor solution to the Klein-Gordon and Friedmann equations such that the density of quintessence is just slightly smaller than the total density during radiation domination, and at the beginning of matter domination. With these solutions, we are sure that during matter domination, the quintessence energy has the right order of magnitude; it just should just grow a bit at late time in order to overcome the matter density today. The advantage of these models is that they are insensitive to initial conditions: if we start from a very large or very small value of the field density, we will always reach the attractor.

Before deriving explicitly these scaling solutions, let us mention that these scaling models contain potentially a real improvement with respect to the cosmological constant problem. In the case of static DE (i.e., of a cosmological content), we noticed that in the early universe, we need an incredible amount of fine-tuning in order to have the correct Ω_Λ today; in particular, when we set up initial conditions e.g. at the beginning of radiation domination, the value of ρ_Λ must be incredibly smaller than that of other components. By making dark energy a dynamical quantity obeying to a scaling solution, we can solve this problem: choosing almost whatever initial conditions for the field density, we will end up with the correct order of magnitude during matter domination, i.e. ρ_{DE} a bit smaller than ρ_m. In particular, we can have ρ_{DE} and ρ_m already of the same order of magnitude in the very early universe, which sounds like avoiding any initial fine-tuning. This is very appealing (but we will see soon that some new problems appear in replacement of the previous ones!)

Exact scaling. We will now prove that exact scaling solutions are possible for negative exponential potentials $V(\varphi) \propto e^{-\alpha\varphi}$ with $\alpha > 0$. During radiation domination, we know that the total density scales like $\rho_{tot} \propto a^{-m}$ with $m = 4$; during matter domination, one has $m = 3$. In both cases the law $a(t)$ is found by solving the Friedmann equation; this gives

$$\left(\frac{\dot{a}}{a}\right)^2 \propto a^{-m} \qquad \Longrightarrow \qquad a \propto t^{2/m} \; . \tag{97}$$

Hence, for whatever value of m, one has $\rho_{tot} \propto t^{-2}$.

An exact scaling solution is defined as a solution in which the field density is a constant fraction of the total density, for whatever behavior of the total density, i.e. whatever value of m. Hence, we are looking for attractor solutions such that

$$\rho_\varphi \propto a^{-m} \propto t^{-2} \; . \tag{98}$$

Energy conservation and eqs. (90), (91) give

$$\dot{\rho}_\varphi = -3\frac{\dot{a}}{a}(\rho_\varphi + p_\varphi) = -3\frac{\dot{a}}{a}\dot{\varphi}^2 = -3\left(\frac{2}{mt}\right)\dot{\varphi}^2 \; . \tag{99}$$

On the other hand, we want $\rho_\varphi \propto t^{-2}$, so we need to have $\dot{\rho}_\varphi \propto t^{-3}$. The conclusion is that for scaling solutions, $\dot{\varphi} \propto t^{-1}$, which can be integrated in $\varphi = k \ln t$ (up to a constant which is uninteresting, because we can absorb it in a field redefinition). Finally, this implies that

$$t \propto e^{\varphi/k} \ . \tag{100}$$

Let us consider the Klein-Gordon equation (93), and notice that $\dot{\varphi}$ and H evolve like t^{-1}, while $\ddot{\varphi}$ evolves like t^{-2}. We can conclude that $V' \propto t^{-2}$. Hence, using eq. (100), we find that

$$\frac{\partial V}{\partial \varphi} \propto e^{-2\varphi/k} \qquad \Longrightarrow \qquad V \propto e^{-2\varphi/k} \tag{101}$$

(in the last integration, we could have added a constant to the potential, but this would restore the original cosmological constant problem: let's keep this constant to zero in order to have no small parameter, and a run-away potential with $V \longrightarrow 0$ at infinity). These steps prove that exact scaling solutions can only exist for negative exponential potentials. A more involved analysis – which is beyond the scope of this course, but can be found e.g. in [54, 55] – would lead us to the conclusion that with such a potential, there is indeed an attractor solution, for which the field density divided by the critical density is equal at any time to:

$$\Omega_\varphi(t) = \frac{\rho_\varphi(t)}{\rho_c(t)} = \frac{2\pi m k^2}{M_P^2} \ , \tag{102}$$

where k is the parameter of the potential (fixed once and for all), and m equals 4 (resp. 3) during radiation (resp. matter) domination. So, Ω_φ is always slightly smaller than one provided that k is fixed to a value slightly smaller than the Planck mass (this is a natural choice, it does not invoke any severe fine-tuning). The best constraint on k comes from the observation that during BBN, $\Omega_\varphi(t)$ should be sufficiently small in order not to modify the usual outcome of nucleosynthesis and the abundance of light elements. This implies that $\Omega_\varphi < 0.2$ during radiation domination. Hence, during matter domination, $\Omega_\varphi < 0.15$ (we have multiplied 0.2 by the ratio of the two m values, 3/4). Hence, without introducing any fine-tuned parameter, we have a model in which for whatever initial conditions, we always reach the matter dominated stage with $\rho_{DE} \sim 0.15\rho_m$ (or less if we make k smaller). This is a very nice achievement.

The problem is that this model is incomplete. Indeed, if we don't add a new ingredient, the universe will remain with $\rho_{DE} \sim 0.15\rho_m$ forever: the quintessence energy will never increase with respect to the matter density, and today we will have $\Omega_{DE} \sim 0.1$ at most. Hence, this is a nice starting point, but we need to invent a reason for which the ratio ρ_{DE}/ρ_m would start growing at some point, in such way that today, $(\rho_{DE}/\rho_m) = (\Omega_{DE}/\Omega_m) \sim (0.7/0.3)$. We will see that such a mechanism can be proposed, but usually at the expense or re-introducing a fine-tuning issue.

Approximate scaling. Let m be again the index of the dilution law for radiation or matter, $\rho_{tot} \propto a^{-m}$. If we assume that there is an attractor solution for which ρ_{DE} scales not exactly like a^{-m}, but like a^{-n} with n slightly smaller than m, then the dark energy field can remain subdominant for a long time, and finally reach a point at which ρ_{DE} overcomes ρ_m. We will show now that such solutions can exist for negative power-law potentials $V \propto \phi^{-\alpha}$ with $\alpha > 0$.

If $\rho_\varphi \propto a^{-n}$, we have

$$\frac{\dot{\rho}_\varphi}{\rho_\varphi} = -n\frac{\dot{a}}{a} \ . \tag{103}$$

At the same time, the energy conservation equation reads

$$\dot{\rho}_\varphi = -3\frac{\dot{a}}{a}(\rho_\varphi + p_\varphi) = -3\frac{\dot{a}}{a}\dot{\varphi}^2 \ , \tag{104}$$

so the comparison of the two equations gives

$$\frac{\dot{\varphi}^2}{\rho_\varphi} = \frac{n}{3} \ . \tag{105}$$

This last result means that for our attractor solution, the kinetic energy must be a constant fraction of the total energy of the field during each stage (radiation or matter domination). We assumed that $\rho_\varphi \propto a^{-n}$, so the last result implies that $\dot{\varphi}^2 \propto a^{-n} \propto t^{-2n/m}$, where we used the fact that $a \propto t^{2/m}$ (as shown previously). We infer from this that $\dot{\varphi} \propto t^{-n/m}$, $\varphi \propto t^{-n/m+1}$, $\ddot{\varphi} \propto t^{-n/m-1}$ and $t \propto \varphi^{m/(m-n)}$. Let us now consider the Klein-Gordon equation (93), and notice that $H\dot{\varphi}$ and $\ddot{\varphi}$ both evolves like $t^{-n/m-1}$. We can conclude that $V' \propto t^{-n/m-1}$. Hence, we find that

$$\frac{\partial V}{\partial \varphi} \propto \left(\varphi^{m/(m-n)}\right)^{-n/m-1} \qquad \Longrightarrow \qquad V \propto \varphi^{2n/(n-m)} \tag{106}$$

(in the last integration, we could have added a constant to the potential, but this would restore the original cosmological constant problem: let's keep this constant to zero in order to have no small parameter, and a run-away potential with $V \longrightarrow 0$ at infinity). We mentioned that this model is interesting for n slightly smaller than m, i.e. when the exponent $2n/(n-m)$ is negative. These steps prove that approximate scaling solutions with $\rho_{DE} \propto a^{-n}$, $\rho_{tot} \propto a^{-m}$ and $n < m$ during radiation or matter domination can only exist for negative power-law potentials. A more involved analysis – which is beyond the scope of this course, but can be found e.g. in [54, 55] – would lead us to the conclusion that the solution described here is indeed an attractor solution. Since $\rho_{DE} \propto a^{-n}$ is not diluted as fast as radiation or matter, there will always be a time at which the quintessence density will become dominant – hopefully, during matter domination. For instance, we could choose a potential $V(\varphi) \propto \varphi^{-6}$. In this case, $2n/(n-m) = -6$, i.e. $n = \frac{3}{4}m$. So, during radiation domination, $m = 4$ but ρ_{DE} is diluted like a^{-3}, i.e. like ordinary matter; during matter domination, $m = 3$ but ρ_{DE} is diluted like $a^{-9/4}$.

Let us assume that during matter domination, there is a the time at which $\rho_{DE} \sim \rho_m$. After that time, the solutions written above do not apply anymore, because the expansion is dominated by the quintessence field instead of the component with $\rho_m \propto a^{-3}$. The kinetic energy of the field will not remain a constant fraction of the total field energy. To understand whether the stage of quintessence domination leads or not to accelerated expansion, let us simply evaluate the slow-roll condition (94) for a power-law potential; it is trivial to show that they are both satisfied under a single condition: $\varphi \geq M_P$. If the field reaches such an order of magnitude before or soon after the point at which quintessence dominates, then the universe expansion will accelerate. This requirement can be easily satisfied without any particular fine-tuning.

However, let us study the conditions for dark energy domination to start at the right moment, i.e. soon after matter domination. We write the full potential as

$$V = \lambda M_P^4 \left(\frac{\varphi}{M_P}\right)^{-\alpha} , \tag{107}$$

where λ is a dimensionless factor (a priori, we expect it to be of order one in absence of fine-tuning). We have seen that when quintessence is sub-dominant, the ratio of the kinetic to the total energy of the field is a constant number of order one. Hence, if $\rho_\varphi \simeq \rho_m$ roughly now, when the field value is of φ_0, we have

$$\lambda M_P^4 \left(\frac{\varphi_0}{M_P}\right)^{-\alpha} \sim \rho_\varphi^0 \sim \rho_c^0 \sim M_P^2 H_0^2 \tag{108}$$

so that

$$\lambda \sim \frac{H_0^2}{M_P^2} \left(\frac{\varphi_0}{M_P}\right)^{\alpha} . \tag{109}$$

We know that today $H_0 \sim 10^{-33}$eV $= 10^{-42}$GeV, while $M_P \sim 10^{19}$GeV. So, the dimensionless ratio H_0^2/M_P^2 is of the order of 10^{-122}. This tiny number cannot be compensated by a very large ratio $(\varphi_0/M_P) \gg 1$, because the self-consistency of the theory forbids the field to be larger than M_P by many orders of magnitude. Hence, λ needs to be fine-tuned to ridiculously small values in order to have dark energy domination occurring today (during matter domination), rather than very early (during radiation domination, at very high energy). We conclude that this scaling solution sounds appealing at first sight, because the attractor solution allows to avoid any strong fine-tuning of the initial condition for the DE component, and at the same time, it is guaranteed that DE will dominate sooner or later; however, by requiring the correct order of magnitude for the energy scale at which DE domination starts, we re-introduce a huge amount of fine-tuning.

We have only considered two examples of quintessence models, among the very large number of models proposed so far in the literature; however, this is sufficient for understanding the generic problems of this paradigm. Quintessence is appealing with respect to a cosmological constant only if it solves the issue of fine-tuning of the initial conditions for dark energy; this suggests that there should be an attractor solution, scaling exactly or approximately like the dominant cosmological component. If the scaling is exact, the model has no fine-tuning, but dark energy never dominates; if we cook up a mechanism such that dark energy finally dominates, we need to tune a parameter in order to have this stage occurring at the right moment (some time after radiation/matter equality), which can only be achieved by reintroducing the same amount of fine-tuning that we wanted to avoid at the beginning. Hence, it is fair to conclude that quintessence models do not provide a convincing explanation to the DE problem[3].

[3]Some physicists argue that quintessence is still more natural than a cosmological constant, because fine-tunings issues

There is a second fundamental problem with quintessence models: they assume a scalar field uncoupled with particles, i.e. no terms in the Lagrangian involving both the scalar field and other fields. This is difficult to motivate in the context of particle physics. The only scalar field present in the SM, namely the Higgs field, couples with fermions through some terms called "Yukawa couplings". By definition, the quintessence field has all its Yukawa couplings set to zero, for reasons which are unclear. However, some people have tried to relax this assumption, and have realized that under certain circumstances, assuming a coupling between quintessence and some particular fields can help in solving the coincidence problem.

3.1.4 Scalar field coupled to matter

The general idea of these models is that a coupling term between the scalar field and some other particle can play the role of triggering the stage of dark energy domination at a given time. In this type of scenario, the coupled scalar field is sometimes called the "chameleon field", because its behavior depends on the background, i.e. on the value of other fields in the same point and at the same time.

This idea is particularly interesting if the field is assumed to couple to neutrinos. We know that there are three generations of neutrinos. Neutrino oscillations have been measured by various experiments; they prove that neutrino have a small mass, with at least $m \geq 0.05$ eV for the heaviest neutrino. Other neutrinos could have a comparable mass, or a smaller one. The second heaviest neutrino should satisfy $m \geq 0.008$ eV. Hence, the order of magnitude of neutrino masses is similar to the dark energy scale. Is this a coincidence, or is there a relation between them? All mass scales appearing in the SM and its extensions involve masses of the order of a MeV or greater; the only mass scales of the order of a fraction of eV appear in neutrino masses. Hence, it is very tempting to search for a relationship between neutrinos masses and dark energy.

Let us assume that there is a coupling between neutrinos and a (homogeneous) scalar field playing the role of dark energy; i.e., the Lagrangian contains a term like $m\frac{\varphi}{M_P}\nu\bar{\nu}$, or $m\frac{\varphi^2}{M_P^2}\nu\bar{\nu}$, or something more complicated. Let us write this coupling in a generic way as

$$\mathcal{L}_{coupling} = m(\varphi)\nu\bar{\nu} \tag{110}$$

where $m(\varphi)$ is some function of the field. The energy conservation equations for neutrinos and for the scalar field can be derived from the expression of their energy-momentum tensors. Let us admit that in presence of the coupling, these equations read

$$\dot{\rho}_\nu + 3H(\rho_\nu + p_\nu) = \frac{d \ln m_\nu(\varphi)}{dt}(\rho_\nu - 3p_\nu) \tag{111}$$

$$\dot{\rho}_\varphi + 3H(\rho_\varphi + p_\varphi) = -\frac{d \ln m_\nu(\varphi)}{dt}(\rho_\nu - 3p_\nu) \tag{112}$$

(the term $(\rho_\nu - 3p_\nu)$ on the right hand-side comes from the trace of the neutrino energy-momentum tensor).

Neutrinos are relativistic in the early universe, as long as their temperature T_ν is greater than their mass. Their current temperature is equal to 1.9 K, i.e. approximately of the order of 10^{-4}eV, and in the past this temperature scaled like $T_\nu = (a_0/a)T_\nu^0$. So, if they have masses of the order of $\sim 10^{-2}$eV, they became non-relativistic recently, during matter domination. As long as neutrinos are relativistic, $p_\nu = \rho_\nu/3$, so the right hand-side of equations (111), (112) can be neglected. However, when neutrinos become non-relativistic, the right hand-side can be important and leads to a transfer of energy between the neutrinos and the scalar field or vice-versa. For instance, if we assume for simplicity an exponential coupling with $m(\varphi) \propto e^{\lambda\varphi}$ and $\lambda > 0$, the equations read

$$\dot{\rho}_\nu + 3H(\rho_\nu + p_\nu) = \lambda\dot{\varphi}(\rho_\nu - 3p_\nu) \ , \tag{113}$$

$$\dot{\rho}_\varphi + 3H(\rho_\varphi + p_\varphi) = -\lambda\dot{\varphi}(\rho_\nu - 3p_\nu) \ , \tag{114}$$

leading to two interesting situations:

- if the dynamics of the field is such that φ decreases with time, then the mass decreases, and when neutrinos become non-relativistic, some energy is transferred from the neutrinos to the scalar field.
- if the dynamics of the field is such that φ increases with time, then the mass increases, and when neutrinos become non-relativistic, some energy is transfer-ed from the scalar field to the neutrinos.

are reduced; many other specialists believe that quintessence is even worse, because it is a more complicated model with several parameters, and still, it does not provide a fully natural explanation for the order of magnitude of dark energy and/or for the cosmic coincidence problem.

So, it is crucial to understand the dynamics of the scalar field. Using the general expression of ρ_φ and p_φ, equation (112) leads to a generalized Klein-Gordon equation with a source term:

$$\ddot{\varphi} + 3H\dot{\varphi} + \frac{dV}{d\varphi} = -\frac{d\ln m_\nu(\varphi)}{d\varphi}(\rho_\nu - 3p_\nu) \ . \qquad (115)$$

We immediately see that the evolution of φ can be infer-ed not just from the scalar potential $V(\varphi)$, but from the effective potential

$$V_{eff}(\varphi) = V(\varphi) + [\ln m_\nu(\varphi)]\,(\rho_\nu - 3p_\nu) \ , \qquad (116)$$

since

$$\ddot{\varphi} + 3H\dot{\varphi} + \frac{dV_{eff}}{d\varphi} = 0 \ . \qquad (117)$$

If this effective potential is steep, the field will quickly roll to its minimum; if it is not steep and satisfies the slow-roll conditions, the field moves to the minimum very slowly.

MaVaN scenario. In the so-called Mass Varying Neutrino (MaVaN) scenario, see e.g. [56]), one assumes that $V(\varphi)$ is an arbitrary run-away potential, with no small parameter (slow-roll conditions are not requested). As long as neutrinos are relativistic, $V_{eff} = V$, and the field rolls to its minimum, i.e. to infinity, with some dynamics in which we are not interested. As soon as neutrinos become relativistic, the effective potential receives an extra contribution. For simplicity, let us assume again that $m(\varphi) \propto e^{\lambda\varphi}$ with $\lambda > 0$, so that the effective potential reads

$$V_{eff}(\varphi) = V(\varphi) + \lambda\varphi(\rho_\nu - 3p_\nu) \ . \qquad (118)$$

After the non-relativistic transition, $p_\nu \longrightarrow 0$ and $(\rho_\nu - 3p_\nu) \longrightarrow \rho_\nu$. So, the runaway potential now competes with a linear contribution $\lambda\varphi\rho_\nu$ with positive slope $(\lambda\varphi) > 0$. The minimum is found for some intermediate value of φ. The field will quickly settle in this minimum, and its energy will increase from approximately zero to $V_{min} \sim \lambda\varphi_{min}\rho_\nu$. During this process, $\dot{\varphi} < 0$, so the neutrino masses decrease. In generic models, $\lambda\varphi_{min}$ (which can be found by postulating a given potential $V(\varphi)$ and by minimizing the effective potential) is naturally of order one. Hence, $\rho_{DE} \sim V_{min} \sim \rho_\nu$: this model achieves to establish a relationship between the order of magnitude of ρ_{DE} and the current energy density of neutrinos, which is of the order of $\rho_\nu \sim m_\nu T_\nu^3$, i.e of the order of m_ν^4 since we are close to the non-relativistic transition.

It is possible to compute the equation of state parameter w of dark energy in these models. Indeed, this type of dark energy is not strictly constant in time. The neutrino density ρ_ν decreases (in absence of coupling, it would decrease exactly like a^{-3} in the non-relativistic regime). So, the minimum of the field evolves very slowly: φ_{min} increases, and $V_{\rm min}$ decreases. This evolution can be computed, and w can be related to the parameters of the model (to λ in our example). Hence this model leads to two non-trivial predictions: neutrino mass decrease just after the non-relativistic transition; and w is related to the fundamental parameters of the model.

This scenario is very appealing because it does solve all fine-tuning issues: here, the DE density is predicted to be of the same order as ρ_ν, which is the correct one; and DE domination is predicted to start soon after the non-relativistic transition of neutrinos, which is also correct. Is this a perfect model for DE? Unfortunately not. Soon after this model after was proposed, it realized that it suffers from a problematic behavior. Coupling neutrinos with a scalar field is equivalent to introducing a fifth force for this species. For this reason, neutrinos tend to cluster on the smallest scales, much more than they would under the effect of gravity only. In fact, one can prove that on small wavelengths, spatial perturbations in ρ_ν and ρ_φ blow up just after the non-relativistic transition: they become strongly non-linear, which corresponds physically to the formation of "clumps" made of neutrinos and scalar field (sometimes called neutrino "nuggets"). So, instead of a coherent scale field and a homogeneous distribution of neutrinos, we end up with a distribution of big "particles", which are described by very different equations than what we just presented. Since these big "particles" do not interact significantly with each other, they correspond to a pressureless medium, i.e. to dust with $p = 0$ and $\rho \propto a^{-3}$: instead of leading to accelerated expansion, the clumps will just enhance the distribution of ordinary matter.

Quintessence coupled with neutrinos. The issue of clumps can be avoided by assuming that $V(\varphi)$ is a potential which could play the role of quintessence (for instance, the negative exponential potential or the negative power-law potential studied in previous section), and that the coupling involves a small parameter (for instance, in the case $m(\varphi) \propto e^{\lambda\varphi}$, λ should be small, but not very small). Then, until the neutrino non-relativistic transition, everything proceeds like in a usual quintessence scenario with a scaling solution. Hence, just before the time of the transition, we have ρ_φ slightly smaller than ρ_m. When the non-relativistic transition starts, the effective potential receives like before a new contribution (e.g. $\lambda\varphi\rho_\nu$) leading to the existence of a minimum at φ_{min} such that $V_{min} \sim \lambda\varphi_{min}\rho_\nu$. In realistic models (see e.g. [57]), $V_{\min}$ is slightly smaller than the field density $\rho\varphi$ before the transition. Hence, the role of the correction to the effective potential is to stop the running away of the field: instead of continuing to roll to infinity, φ slows down and settles in the new minimum. Since $\dot{\varphi} > 0$ during the non-relativistic transition, the neutrino mass increases with time in this scenario. We don't have time to enter into details, but the situation described here can occur for natural values of the parameters. Again, in this model, ρ_{DE} is related to ρ_ν, and w can be predicted from the parameters of the model (e.g. from λ). The set up of this scenario is essentially the same as for the MaVaN scenario, excepted that some parameters are chosen differently in order to ensure that the scalar field is in slow roll during the whole cosmological evolution, instead of running at infinity and then moving quickly back to $\varphi_{\min}$. In this model, there are no problems with neutrino nuggets on small scales. Further investigation are still needed in order to understand whether there are other problems with spatial perturbations of neutrinos and of the scalar field, but the situation is promising.

This scenario is appealing because, like MaVaN scenarios, it solves the DE magnitude problem and the cosmic coincidence problem in a convincing way, without suffering from the same instabilities. It can be viewed also as a way to cure the negative exponential quintessence model. As we said before in the last section, this model would be perfect it it didn't lack of a mechanism for DE to dominate at the end. Apart from that, this potential does not require very small parameters or special initial conditions. Here, the mechanism which allows DE to dominate at the end is the coupling with neutrinos, which drives the field away from its perfect scaling solution and triggers DE domination when $T_\nu \sim m_\nu$.

Before claiming that this model is perfectly natural, it would be necessary to carry further investigations concerning the perturbation evolution and the constraints on the coupling term. This is still a topic of research. More generally, some people criticize this model because it invokes a coupling between the scalar field and the neutrinos, but not with other fields. It remains an open question to understand whether this is a natural assumption or not.

3.1.5 Modifications of gravity

Instead of adding a dark energy component to the Universe, some people try to explain the acceleration of the expansion by modifying the laws of gravity. The goal is to find a modification such that gravity is unchanged on small scales, for which Einstein's theory has been thoroughly tested (deviations from general relativity are known to be extremely small); while on very large scale, gravity would take a different form. Then, one may hope that Einstein's theory is relevant for describing all phenomena, excepted the expansion of the universe when the Hubble radius becomes larger than some threshold. If this threshold is chosen to be comparable with the value of the Hubble radius at redshift $z \sim 1$, then a different expansion law might occur at late time (i.e., the Friedmann equation might need to be replaced by something more complicated relation between density and the scale factor at late time).

Many people work on this idea, but it is impossible to summarize the situation at the level of this course; indeed, the various models under investigation go in very different directions, and they are all technically very difficult; in addition, it is not yet clear that any of these theories provides a successful explanation of the acceleration (while being compatible with constraints from the CMB, from large scale structure, from experiments testing gravity, etc.) More years of investigation are needed in order to reach clear and simple conclusions concerning the viability of these paradigms. In few words, Einstein's theory is based on the action

$$S = \int d^3x \sqrt{|g|}\,(R + \mathcal{L}_{matter}) \tag{119}$$

where R is the Ricci scalar (derived from the metric $g_{\mu\nu}$), and $\mathcal{L}_{matter}$ is the Lagrangian describing matter fields. Possible modifications of this theory include: higher-order gravity terms in the action (e.g. R^2), scalar-tensor theories of gravity (with an extra scalar field coupled to all matter fields, unlike quintessence field), theories with extra dimensions (in which gravity propagates in all dimensions, while the matter fields are confined to a lower dimensional sub-space), etc. In some theories, the graviton (i.e. the particle associated to the metric field $g_{\mu\nu}$ in a quantum field theory interpretation) is massive; in other theories, the laws of gravitation change with scales, e.g: gravity can be 4-dimensional on small scales (leading to the usual Newton force in $1/r^2$), and different on large scales due to the role of extra dimensions (then, on large scale, forces are not in $1/r^2$). We refer interested readers e.g. to [58], [59] and references therein.

3.1.6 Non-linear structure formation

Instead of introducing a dark energy component or a modification of gravity, some researchers suggest that we just do not understand properly how to apply usual general relativity to the last stage of evolution of the Universe, and that the acceleration might be explained without introducing anything new. This idea is of course the most appealing and economical one might think of, but it is far from obvious that it could work, and this direction remains very controversial.

The Friedmann equation is derived from the Einstein equation

$$G_{\mu\nu} = 8\pi\mathcal{G}T_{\mu\nu} \tag{120}$$

which is non-linear in the metric $g_{\mu\nu}$ (since $G_{\mu\nu}$ contains quadratic and quartic terms in the metric). The universe expansion and the scale factor are supposed to describe the average dynamics of the universe. Hence, they should be inferred from the Einstein equation averaged over large scales:

$$\langle G_{\mu\nu}\rangle = 8\pi\mathcal{G}\langle T_{\mu\nu}\rangle \; . \tag{121}$$

However, the FLRW model does not consist in solving the latter equation. Instead, the logic of the FLRW approach is to define an average metric $\langle g_{\mu\nu}\rangle = \mathrm{diag}(1, -a^2, -a2, -a^2)$, an average density and pressure, and to compute the Einstein equation for these averages:

$$G_{\mu\nu}(\langle g_{\mu\nu}\rangle) = 8\pi\mathcal{G}T_{\mu\nu}(\langle\rho\rangle, \langle p\rangle) \; . \tag{122}$$

This leads to the Friedmann equation, but clearly, eq. (122) is not equivalent to eq.(121) because of the non-linear structure of $G_{\mu\nu}$.

A usual argument is that the current universe, although it contains non-linear structures, can be described by a perturbed metric which is very close to the average metric: we know that metric perturbations should be of the order of $(v/c)^2$, where v stands for typical velocities in our current universe, i.e. a few hundreds of km/s; hence metric perturbations are small, of the order of 10^{-5}, and the exact metric of our universe is very close to the average metric used in the FLRW model. Does this mean that Eq. (122) provides a very good approximation of Eq. (121)? This is not so obvious, because $G_{\mu\nu}$ contains time derivatives and spatial derivatives of $g_{\mu\nu}$; hence, it is possible that $g_{\mu\nu}$ is very close to $\langle g_{\mu\nu}\rangle$ while, at the same time, $G_{\mu\nu}$ is significantly different from $\langle G_{\mu\nu}\rangle$. Hence, it might be necessary to employ the average of the exact Einstein tensor, instead of the Einstein tensor corresponding to the average of the exact metric.

The effect described here can be safely neglected before the time of equality between radiation and matter, because it is clear that the universe is nearly homogeneous before that time. When structures like galaxies form and density perturbations become non-linear, the exact Einstein equation becomes very difficult to compute, and people use various approximations based on Newtonian gravity. A majority of cosmologist believes that the standard approach, which consists in applying the Friedman law for the global evolution of the universe, and in using Newtonian N-body simulations for structure formation on small scales, provides a good approximation to the real universe. A few experts challenge this picture (see e.g. [60, 61]) and try to compute structure formation in a fully relativistic way, with a proper use of averages. Their motivations is to find an average expansion which would differ from the one predicted by the Friedmann equation, possibly with an acceleration at late times. This problem is technically so difficult that nobody has a definite answer yet.

3.2 Cosmological tests for DE models

In section 1.4.11, we have presented current measurements of the cosmological constant density today, parametrized by Ω_Λ. In order to discriminate between various DE model, and to check whether this DE is equivalent or not to a cosmological constant, one should fit cosmological observations assuming a time-dependent density $\rho_{DE}(t)$ (or $\rho_{DE}(a)$ or $\rho_{DE}(z)$).

The simplest approach consists in assuming a constant equation of state parameter w, i.e. to work in the approximation in which ρ_{DE} is diluted like a power-law: $\rho_{DE} \propto a^{-3(1+w)}$. In this case, the two parameters to be measured are Ω_{DE} (the density today) and w. If the value $w = -1$ could be excluded by the data, the case of a cosmological constant (and presumably, also that of a vacuum energy) would be excluded.

Of course, the evolution might be more complicated than $\rho_{DE} \propto a^{-3(1+w)}$, but it is useless to introduce a lot of freedom in the function $\rho_{DE}(a)$ as long as the data is not accurate enough for discriminating between different functions. However, people are already trying to work in the next order approximation, in which the redshift dependence of w is parametrized as $w(z) = w_0 + \frac{z}{1+z} w_a$: then, the three DE parameters are Ω_{DE} (the density today), w_0 (the equation of state parameter today) and w_a (the difference between the equation of state parameter at high redshift, $z \gg 1$, and the one today).

3.2.1 Current measurements of $\Omega_{DE}(z)$

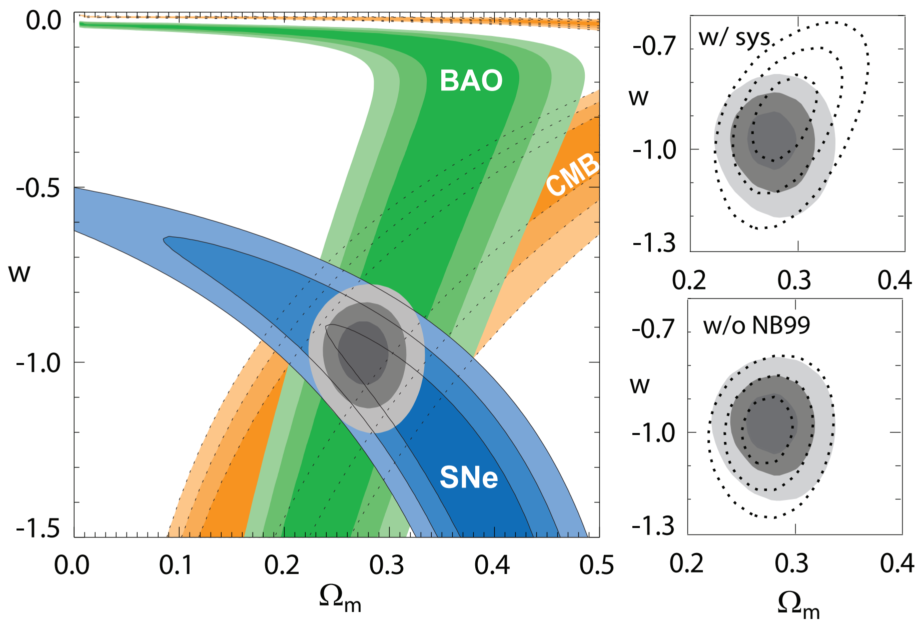

Figure 19: *(Left)* Constraints on a model with CDM, dark energy and no spatial curvature, assuming that the DE component has a constant equation of state parameter w. The contours correspond to the regions preferred at the 68.3%, 95.5% and 99.7% confidence level in the (Ω_m, w) plane, using recent supernovae data (blue solid lines), baryon acoustic oscillations (green dashed), or the measurement of CMB peak positions. *(Right)* Zoom on the region allowed by the combination of all experiments, using different assumptions concerning systematic errors in supernovae data. *Plots taken from arXiv:0804.4142 [astro-ph] by M. Kowalski et al.*

In figure 19, we see the best current constraints on DE parameters, assuming a model with a constant equation of state parameter w. This model is taken to be flat, so that $\Omega_\Lambda = 1 - \Omega_m$. The experimental techniques used here have been explained in section 1.4: estimate of $d_A(z \sim 1100)$ with the angular scale of CMB peaks; of $d_L(z)$ in the range $0.4 < z < 1.4$ with the luminosity of supernovae; and, roughly, of $d_A(z \sim 0.2)$ with the angular scale of BAOs in galaxy redshift surveys. The functions $d_L(z)$ and $d_A(z)$ are always integrated over redshift, starting from today. Hence, they are sensitive to the evolution of the scale factor at low redshift ($0 < z < 1$), when DE plays a role, and they can be used to measure any parameter describing the evolution of $\rho_{DE}(z)$, including w or even its derivative.

Note that the plot starts from the value $w = -1.5$. The region $w < -1$ is known to be unphysical (at least in the framework of currently understood theories); however it can be included in the analysis, because the functions $d_L(z)$ and $d_A(z)$ can always be computed, even with a DE density growing with time. In addition, it is important to keep the region $w < -1$ in the analysis for two reasons. First, the weak energy principle might be wrong; the data could show that $w < -1$, and force us to reconsider our understanding of first principles. Second, there exist some models in which each component obeys to the weak energy principle, but because of some non-trivial coupling between these components, the model "looks" like ΛCDM with $w < -1$. Note that $w < -1$ means that ρ_{DE} grows with time, but not necessarily that $\rho_{DM} + \rho_{DE}$ grows with time. If our distinction between a DM and a DE component is wrong, then the case $w < -1$ might describe a situation in which the density of the total DM+DE fluid decreases, obeying to the weak energy principle, but what we artificially identify as the DE component seems to grow.

The main conclusion from figure 19 is that current data are perfectly compatible with $w = -1$, i.e. with a cosmological constant or a constant vacuum energy. This proves, at least, that current data do not have the sensitivity to detect any departure from ΛCDM.

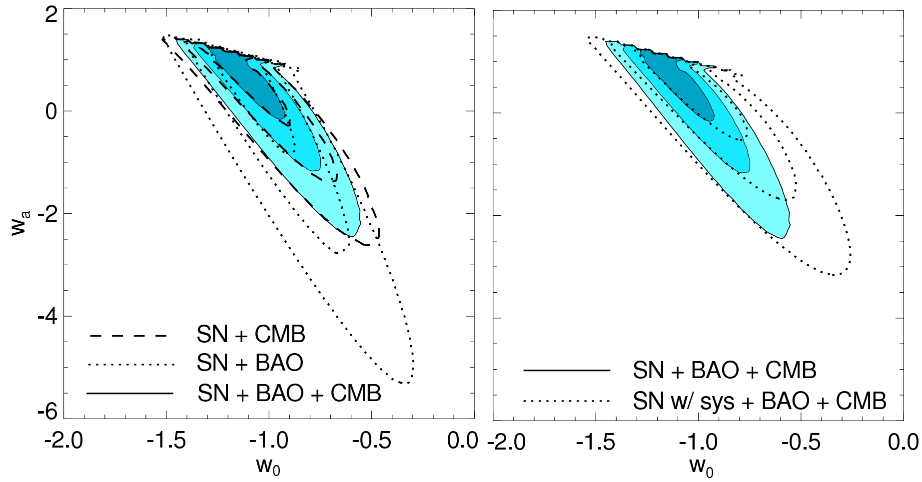

Figure 20: *(Left)* Constraints on a model with CDM, dark energy and no spatial curvature, assuming that the DE component has an equation of state parameter $w(z) = w_0 + \frac{z}{1+z} w_a$. The contours correspond to the regions preferred at the 68.3%, 95.5% and 99.7% confidence level in the $(w_0,\ w_a)$ plane, using recent supernovae data (SN), baryon acoustic oscillations (BAO), and/or the measurement of CMB peak positions. In order to have matter domination before DE domination, one should have $w < 0$ at large z, i.e. $(w_0 + w_a) < 0$: this constraint is visible in the plot, it cuts the allowed region from above. *(Right)* same with different assumptions concerning systematic errors in supernovae data. *Plots taken from arXiv:0804.4142 [astro-ph] by M. Kowalski et al.*

In figure 19, the next level of complexity is assumed, i.e. $w(z) = w_0 + \frac{z}{1+z} w_a$. Again, the case of a cosmological constant (i.e. $(w_0, w_a) = (-1, 0)$) provides a good fit to observations.

If we do not measure any departure from $w = -1$, it will be particularly difficult to discriminate between a cosmological constant and other DE models. Indeed, many of these model can have w arbitrarily close to -1 when their parameters are chosen appropriately. For instance, in quintessence model, one can usually tune the scalar potential slope to a very small value, so that the kinetic energy of the field becomes arbitrarily small, and $w \longrightarrow -1$. However, for some DE models, w cannot be made smaller than a given value, and some of these models are already excluded. For instance, we have seen that DE consisting in a network of domain walls predict $w = -2/3$. This is already in conflict with observations. So, the motivation for measuring w with increasing precision is two-fold; either we will finally observe that $w = -1$ is excluded, ruling our the case of a cosmological constant; or the upper limit on $(w + 1)$ will become closer and closer to zero, allowing to rule out more and more alternative DE models.

3.2.2 Future measurements of $\Omega_{DE}(z)$

There are essentially two ways of improving current measurements of the DE density and of its time evolution:

- we can improve our measurement of the geometrical quantities $d_L(z)$ and $d_A(z)$ at various redshifts. This can be achieved with better CMB data (e.g. from the future Planck satellite, to be launched in 2009 by ESA); by accumulating more observations of luminosity and light-curve of supernovae, with a dedicated supernovae satellite (like the project SNAP of NASA); or by probing the BAO scale at various redshift, using larger galaxy redshift catalogues (many projects have been proposed).

- we can use a new technique, namely, the study of the time-evolution of the linear matter power spectrum $P(k)$ described in section 1.4.7. We have mentioned that during DE domination, gravitational potential wells decay on all scales. This means that the overall amplitude of $P(k, z)$ evolves as a function of z in a way which depends on the function $\rho_{DE}(z)$. This overall amplitude is called the linear growth factor. With current redshift surveys, the matter power spectrum has been measured only at small redshifts $z < 0.1$; we need data at much larger scales in order to estimate $P(k, z)$ at various redshifts, and infer $\rho_{DE}(z)$ and $\Omega_{DE}(z)$.

On experimental technique is very promising; namely, the study of galaxy deformations through weak lensing. The image of galaxies is deformed by lensing effects, caused by intervening matter along the line of sight. With involved statistical studies, one can reconstruct the three-dimensional distribution of total matter (baryonic plus dark matter) needed in order to explain the observed lensing patterns. Once this is done, one obtains a three-dimensional map of total matter inhomogeneities. The latter can be expanded in Fourier modes, in order to reconstruct $P(k, z)$ at various redshifts. This technique works already very well on small scales. Many projects, based on ground-based or spatial telescopes (LSST, PanStar, DES, SNAP, JDEM, etc.), aim at measuring these weak lensing distortions up to very high redshift, in order to be able to reconstruct $P(k, z)$ up to $z \sim 1$. These measurements are expected to provide spectacularly precise measurement of Ω_{DE}, w and its derivatives.

3.3 Conclusion

In this section, we presented an overview of possible models for explaining the acceleration of the universe. Let us stress that this short review was very incomplete: there have been many more proposals than those mentioned here. We arbitrarily decided to pick up a few possibilities, hoping that that this choice is sufficient for understanding the main directions of research, and the typical problems to which theorists are confronted.

We should mention that people working in observational cosmology and astrophysics tend to consider that there is only one model around: quintessence. This is probably because quintessence is the only dark energy model for which one can present a short, well-defined set of equations, which are easy to solve in order to make observable predictions (on w today, and on its possible time-dependence). It is doubtful that quintessence has further merits than that... as we saw, it does not have any deep motivations (this scalar field is added "ad hoc", just for the purpose of explaining one observation, and it cannot make other predictions), and it probably cannot even solve fine-tuning issues.

Quintessence has however a practical advantage: this model contains enough freedom for describing any possible dynamics for dark energy (or modifed gravity); in other words, even if the acceleration of the universe has nothing to do with a scalar field, the true model can probably be described effectively by a scalar field mimicking its properties. Hence, when observers try to constrain quintessence models, they implicitely provide general constrains, which will be useful anyhow.

The study of DE models is interesting provided that we can keep some hope of probing experimentally which model is the correct one. Discriminating between different models is difficult, because there might be very few observables accessible to experiment in this field: maybe just Ω_{DE} and its time evolution, parametrized in first approximation by w. The motivation for measuring w with increasing precision is two-fold; either we will finally observe that $w = -1$ is excluded, ruling our the case of a cosmological constant; or the upper limit on $(w + 1)$ will become closer and closer to zero, allowing to rule out more and more alternative DE models. However, in any case, it is not obvious that knowing w (and eventually its time derivative) with high precision will be sufficient for deciding which model is the good one. This information will be, of course, a very useful indication, but we should hope that the correct DE framework will lead to independent, testable predictions. For instance, scenarios with modified gravity might be tested with specific laboratory experiments searching for particular deviations from gravity (although no such deviations have been identified so far); models with mass-varying neutrinos could be tested by various neutrino experiments, or even by looking at the consequences of a time-varying neutrino mass on cosmological observables; etc. Let us hope that the correct model for DE is not such that no independent test can ever be done; although such an uninteresting situation is possible in principle (e.g. for a cosmological constant or for many models of quintessence). However, let's not be too pessimistic; after all, nobody has proposed yet a really convincing model, able to explain the apparent universe acceleration without any kind of fine-tuning or any ad hoc assumption. When a such a convincing model will finally be presented, its validity might become obvious for reasons that we cannot even think of at the moment...

References

[1] F. Zwicky, Helv. Phys. Acta **6**, 110 (1933).

[2] F. Zwicky, Helvetica Physica Acta **6**, 110 (1933).

[3] S. Smith, APJ **83**, 23 (1936).

[4] H. W. Babcock, Ph.D. thesis, AA(UNIVERSITY OF CALIFORNIA, BERKELEY.) (1938).

[5] J. H. Oort, APJ **91**, 273 (1940).

[6] H. I. Ewen and E. M. Purcell, Nature **168**, 356 (1951).

[7] C. A. Muller and J. H. Oort, Nature **168**, 357 (1951).

[8] V. C. Rubin and W. K. Ford, Jr., in *The Spiral Structure of our Galaxy*, edited by W. Becker and G. I. Kontopoulos (1970a), vol. 38 of *IAU Symposium*, pp. 61–+.

[9] V. C. Rubin and W. K. J. Ford, APJ **159**, 379 (1970b).

[10] D. H. Rogstad and G. S. Shostak, APJ **176**, 315 (1972).

[11] M. S. Roberts and A. H. Rots, AAP **26**, 483 (1973).

[12] E. M. Burbidge and G. R. Burbidge, *The Masses of Galaxies* (Galaxies and the Universe, 1975), pp. 81–+.

[13] M. S. Roberts, *Radio Observations of Neutral Hydrogen in Galaxies* (Galaxies and the Universe, 1975), pp. 309–+.

[14] V. C. Rubin, N. Thonnard, and W. K. Ford, Jr., APJ Letters **225**, L107 (1978).

[15] P. C. van der Kruit and A. Bosma, AAP **70**, 63 (1978).

[16] A. Bosma and P. C. van der Kruit, AAP **79**, 281 (1979).

[17] J. P. Ostriker, P. J. E. Peebles, and A. Yahil, APJ Letters **193**, L1 (1974).

[18] R. V. Wagoner, APJ **179**, 343 (1973).

[19] J. Silk, Nature **215**, 1155 (1967).

[20] R. Massey et al., Nature **445**, 286 (2007), `astro-ph/0701594`.

[21] D. Tytler, J. M. O'Meara, N. Suzuki, and D. Lubin, Phys. Scripta **T85**, 12 (2000), `astro-ph/0001318`.

[22] K. A. Olive, D. N. Schramm, M. S. Turner, J. Yang, and G. Steigman, APJ **246**, 557 (1981).

[23] P. J. E. Peebles, APJ **146**, 542 (1966).

[24] C. W. Misner, NATURE **214**, 40 (1967).

[25] P. J. E. Peebles, APJ **142**, 1317 (1965).

[26] C. Bœhm, A. Riazuelo, S. H. Hansen, and R. Schaeffer, PRD **66**, 083505 (2002), `arXiv:astro-ph/0112522`.

[27] M. Milgrom, Astrophys. J. **270**, 365 (1983).

[28] R. H. Sanders (2005), `astro-ph/0509532`.

[29] J. D. Bekenstein, Phys. Rev. **D70**, 083509 (2004), `astro-ph/0403694`.

[30] C. Skordis, D. F. Mota, P. G. Ferreira, and C. Boehm, Phys. Rev. Lett. **96**, 011301 (2006), `astro-ph/0505519`.

[31] M. I. Vysotskii, A. D. Dolgov, and I. B. Zeldovich, ZhETF Pis ma Redaktsiiu **26**, 200 (1977).

[32] S. Tremaine and J. E. Gunn, Physical Review Letters **42**, 407 (1979).

[33] C. Pryor, M. Davis, M. Lecar, and E. Witten, in *Bulletin of the American Astronomical Society* (1980), vol. 12 of *Bulletin of the American Astronomical Society*, pp. 861–+.

[34] J. R. Bond, G. Efstathiou, and J. Silk, Physical Review Letters **45**, 1980 (1980).

[35] V. F. Shvartsman, Soviet Journal of Experimental and Theoretical Physics Letters **9**, 184 (1969).

[36] P. Hut, Physics Letters A **69**, 85 (1977).

[37] B. W. Lee and S. Weinberg, Physical Review Letters **39**, 165 (1977).

[38] G. Steigman, K. A. Olive, and D. N. Schramm, Physical Review Letters **43**, 239 (1979).

[39] C. L. Bennett et al. (WMAP), Astrophys. J. Suppl. **148**, 1 (2003), `astro-ph/0302207`.

[40] C. Boehm and P. Fayet, Nucl. Phys. **B683**, 219 (2004), `hep-ph/0305261`.

[41] C. Boehm, A. Djouadi, and M. Drees, Phys. Rev. **D62**, 035012 (2000), `hep-ph/9911496`.

[42] J. L. Feng, K. T. Matchev, and F. Wilczek, Phys. Lett. **B482**, 388 (2000), `hep-ph/0004043`.

[43] R. Bernabei et al. (2003), `astro-ph/0311046`.

[44] R. Lemrani (EDELWEISS), Phys. Atom. Nucl. **69**, 1967 (2006).

[45] J. Yoo (CDMS) (????), fERMILAB-CONF-07-606-E.

[46] W. Westphal et al., Czech. J. Phys. **56**, 535 (2006).

[47] J. F. Navarro et al., Mon. Not. Roy. Astron. Soc. **349**, 1039 (2004), `astro-ph/0311231`.

[48] C. Bœhm, P. Fayet, and R. Schaeffer, Physics Letters B **518**, 8 (2001), `arXiv:astro-ph/0012504`.

[49] C. Boehm and R. Schaeffer, AAP **438**, 419 (2005), `arXiv:astro-ph/0410591`.

[50] C. Boehm, H. Mathis, J. Devriendt, and J. Silk (2003), `astro-ph/0309652`.

[51] L. Susskind, arXiv:hep-th/0302219.

[52] R. A. Battye, M. Bucher and D. Spergel, arXiv:astro-ph/9908047.

[53] R. A. Battye, B. Carter, E. Chachoua and A. Moss, Phys. Rev. D **72**, 023503 (2005) [arXiv:hep-th/0501244].

[54] E. J. Copeland, A. R. Liddle and D. Wands, Phys. Rev. D **57**, 4686 (1998) [arXiv:gr-qc/9711068].

[55] E. J. Copeland, M. Sami and S. Tsujikawa, Int. J. Mod. Phys. D **15**, 1753 (2006) [arXiv:hep-th/0603057].

[56] R. Fardon, A. E. Nelson and N. Weiner, JCAP **0410**, 005 (2004) [arXiv:astro-ph/0309800].

[57] C. Wetterich, Phys. Lett. B **655**, 201 (2007) [arXiv:0706.4427 [hep-ph]].

[58] G. Dvali, Prog. Theor. Phys. Suppl. **163**, 174 (2006).

[59] R. Durrer and R. Maartens, arXiv:0811.4132 [astro-ph].

[60] T. Buchert, Gen. Rel. Grav. **40**, 467 (2008) [arXiv:0707.2153 [gr-qc]].

[61] S. Rasanen, arXiv:0811.2364 [astro-ph].